Adhesion of critical interfaces in microelectronics

Mag. Andreas Kleinbichler

Being a thesis in partial fulfilment of the requirements for the degree of a
Doktor der montanistischen Wissenschaften (Dr. mont.)
at the Montanuniversität Leoben

Erich Schmid Institute of Materials Science
of the Austrian Academy of Sciences,
Jahnstrasse 12, 8700 Leoben, Austria

Affidavit

I declare in lieu of oath that I wrote this thesis and performed the associated research myself, using only literature cited in this volume.

Leoben, May 2018

Andreas Kleinbichler

This work was jointly funded by the Austrian Research Promotion Agency (FFG: Project No. 846579) and the Carinthian Economic Promotion Fund (KWF, contract KWF-1521/26876/38867) further financial support by the Austrian Federal Government (837900) within the framework of the COMET Funding Program is appreciated.

Copyright © 2018 by Andreas Kleinbichler. All rights reserved.

KAI - Kompetenzzentrum Automobil- und Industrieelektronik GmbH

Technologiepark Villach

Europastraße 8

9524 Villach

Austria

https://www.k-ai.at

Acknowledgements

The past three years of my PhD studies were full of challenges and personal growth. For that I want to express my deepest gratitude to all people at ESI in Leoben and KAI in Villach who made this thesis possible.

First and foremost, I want to thank Dr. Megan Cordill for her excellent guidance throughout the entire duration of my PhD studies. Without her careful supervision and tremendous support, the transition to the field of material science would have been much harder. I am grateful for having the opportunities to learn, travel and widen my horizon. Her encouragement for trying new ideas and looking more closely made this thesis a success.

Secondly, I want to thank Dr. Johannes Zechner from KAI for his supervision, fruitful discussions and help with all matters of company issues over the past years. Without his commitment to my work, it would not have been possible.

I am grateful for all the people at ESI who were terrific colleagues and have become good friends. Especially, DI Markus Alfreider, Dr. Ruth Konetschnik and Dr. Reinhard Fritz for their constant assistance with FIB, Claus Trost for frequent help with the wafer curvature experiments, Dr. Juraj Todt for his assistance with XRD and DI Manuel Pfeifenberger for being a great laser buddy. Finally, Dr. Thomas Schöberl for his detailed introduction to AFM.

Special thanks goes to my office mate DI Katharina Schwarz, for constant but welcome distractions. She was the best mentor to ESI a Carinthian could have.

Additional thanks go to DI Elisabeth Jäger for all her help at KAI and always making me feel welcome in Villach. Furthermore, I would like to express my gratitude to DI Josef Fugger at KAI for all the support and approval he offered.

I also want to thank Dr. Stefan Wöhlert and Dr. Tiphaine Pelisset of Infineon Technoilogies AG Villach for providing me with samples.

Last but not least, I want to thank my parents Franz and Christine, my sister Teresa and my girlfriend Marlene for all their support and love they have given, making me the person I am today.

"… when you have eliminated the impossible, whatever remains, however improbable, must be the truth?"

Sherlock Holmes, The Sign of the Four by Sir Arthur C. Doyle (1890)

Abstract

In modern microelectronic devices a wide variety of thin film materials are utilized such as metals, ceramics and glasses in specially tailored structures to fulfill and enhance the device performance. The adhesion of the individual thin film layers is crucial for the longevity and reliability of the integrated circuits. Especially the interfaces between the isolating layers, e.g. doped silica glass, and the metallization can be a critical due to their different bonding types. As adhesion is affected by many factors such as thermal treatments or film stresses it is important to evaluate the critical interfaces in these devices quantitatively.

In the course of this thesis, residual compressive stresses, nanoindentation and scratch testing were utilized to produce defined areas of delamination, called buckles. The materials' response to the used techniques was investigated via focused ion beam (FIB) cross-sectioning to determine the cause for the delamination, thereby furthering the understanding and applicability of the methods. Three different interfaces exemplary for today's microelectronic devices have been tested ranging from metal/polymer to ceramic/glass.

In a first step, the effect of residual stress and a tantalum (Ta) interlayer on the adhesion in a gold-polyimide system was investigated. It was found that spontaneous buckles formed in the Au film without the interlayer after deposition, while external loading is required to delaminate the Au film with the Ta adhesion layer indicating a higher adhesion energy.

Secondly, the three techniques, residual stress, nanoindentation and scratch test were utilized to induce interface delamination of a tungsten-titanium (WTi) film on two different borophosphosilicate glass (BPSG) films. Although buckles induced by compressive stress and nanoindentation have been extensively investigated over the last decades, the scratch test is usually regarded as a semi-quantitative method but is, under the right conditions, capable to induce buckles suited for adhesion evaluation. The comparison of the results calculated from the buckles induced by compressive stress and scratch testing were in good agreement for the two types of BPSG. However, FIB cross-sectioning of the nanoindentation buckles revealed that additional fracture events in the BPSG led to incorrect adhesion energies in both cases. The fracture events following indentation are a serious concern when utilizing nanoindentation for adhesion measurement.

To further analyze these fracture events, cross-sectional investigation of indentation buckles on a silicon nitride (Si_3N_4) film on a BPSG film with a compressively stressed WTi overlayer was performed to illustrated that the fracture paths are very sensitive to the applied loads. In a narrow load range two types of buckles were produced by indentation. While type one of the

buckles were the result of through-thickness cracks, type two were representative of the Si_3N_4/BPSG interface.

The scratch test on the other hand, does not result in BPSG fracture under the buckled region because the scratch induced stresses lead to initial delaminations parallel to the scratch trace which acted as points of origin for spontaneous buckles. Therefore, the scratch test was chosen to investigate the effects of annealing duration, from 30 minutes to 2 hours, at 400°C on the adhesion of the WTi film on BPSG. As the annealing duration increased, the adhesion energy increased to about double the value of the unannealed WTi film.

The study illustrates the applicability of nanoindentation and scratch testing in compressively stressed film systems for quantitative adhesion measurement. Special emphasis was put on the investigation of the failure modes responsible for buckle development in nanoindentation and scratch testing, thereby furthering the understanding of buckle formation. The methods allow for the evaluation of thin film adhesion without sample preparation and give quantitative adhesion energies with good statistics.

Zusammenfassung

In modernen mikroelektronischen Bauteilen wird in komplexen Strukturen eine Vielzahl an dünnen Schichten aus verschiedensten Materialien wie Metallen, Keramiken und Gläser eingesetzt um die Leistungsfähigkeit zu verbessern. Die Haftung der einzelnen Schichten zu einander ist ausschlaggebend für die Zuverlässigkeit und Lebensdauer von integrierten Schaltungen. Aufgrund ihrer unterschiedlichen Bindungsarten sind die Grenzflächen zwischen isolierenden Schichten wie z.B. dotierten Silikatgläsern und der Metallbeschichtung von besonderer Bedeutung.

In dieser Dissertation wurden kompressive Schichtspannungen, Nanoindentation und der Scratchtest eingesetzt um gezielt Bereiche lokaler Delamination, genannt Buckles, zu erzeugen. Der Einfluss der Methoden auf das Probenmaterial wurde mittels fokussierten Ionenstrahl (FIB) Querschnitts untersucht um die Ursachen der Delaminationen auf den Grund zu gehen und dadurch das Verständnis der und die Anwendbarkeit der Methoden zu verbessern. Drei verschiedene Grenzflächen die exemplarisch für heutige Mikroelektronische Bauteile sind wurden getestet.

In einem ersten Schritt wurden die Auswirkungen von Schichtspannungen und einer Tantal (Ta) Zwischenschicht auf ein Gold-Polyimid Schichtsystem untersucht. Während sich Spontane Buckles in der Goldschicht ohne Zwischenschicht bildeten, wies die Ta-Schicht eine höhere Haftung zum Polyimid auf und es wurde eine externe Kraft benötigt um die Schichten abzulösen.

Im zweiten Schritt wurden die drei Methoden, Schichtspannungen, Nanoindentation und der Scratchtest genutzt um Delaminationen zwischen einer Wolfram-Titan (WTi) Schicht und zwei verschiedenen Borphosphorsilikatgläsern (BPSG) zu erzeugen. Anders als Druckeigenspannungen und Nanoindentation gilt der Scratchtest nur als semi-quantitative Methode, die aber unter geeigneten Bedingungen Buckles erzeugen konnte welche zur Haftungsbestimmung herangezogen wurden. Die Haftungswerte der WTi-Schicht, berechnet aus den Spannungs- und Scratch-induzierten Buckles, zeigten gute Übereinstimmung für beide BPSG-Schichten. FIB Querschnitte der Indentierungs-Buckles zeigten hingegen, dass zusätzliche Risse in der BPSG-Schicht auftraten die zur inkorrekten Berechnung von Haftungsenergien führen.

Daraufhin wurden Indentierungs Buckles in einem WTi, Siliziumnitrid (Si_3N_4) und BPSG Schichtsystem mittels FIB Querschnitten analysiert um den Einfluss der aufgebrachten Last auf die Ausbreitung der Risse in den Schichten zu untersuchen. In einem kleinen Lastbereich

wurden zwei Arten von Buckles erzeugt. Die erste Buckleart war das Resultat von Rissen durch die Schichten und daher nicht geeignet um die Haftung zu bestimmen. Die zweite Art entstand aus Rissen entlang der Si_3N_4/BPSG Grenzflächen woraus Haftungsenergien für diese Grenzfläche berechnet werden konnten.

Der Scratchtest hingegen führte nicht zu Rissen in der BPSG-Schicht unter den Buckles. Die durch den Scratch induzierten Spannungen erzeugen erste Delaminationen parallel und entlang der Scratchfurche die den Ausgangspunkt für spontane Buckles bilden. Aus diesem Grund wurde der Scratchtest gewählt um die Auswirkungen von 30 Minuten bis 2 Stunden langen Glühbehandlungen bei 400°C auf die Haftung einer WTi- auf einer BPSG-Schicht zu untersuchen. Mit zunehmender Glühdauer stieg die Haftung im Verglich mit der nicht geglühten WTi-Schicht um das Doppelte.

Die Untersuchungen verdeutlichen die Eignung von Nanoindentation und Scratchtest für quantitative Haftungsuntersuchungen in Schichtsystemen unter Druckeigenspannungen. Besondere Aufmerksamkeit wurde auf die Untersuchung der Ursachen für die Delamination bei Nanoindentation und Scratchtest gelegt, was zu einem besseren Verständnis der Bucklebildung führte. Mit den vorgestellten Methoden lassen sich die Haftungsenergien von Schichtsystemen quantitativ und ohne vorherige Probenpräparation bewerten.

Contents

1. **Introduction** 1

2. **Film Stress Characterization** 3

2.1 Wafer Curvature 3

2.2 X-Ray Diffraction 5

3. **Interface Fracture Mechanics** 7

3.1 Work of Adhesion 7

3.2 Interface Fracture 10

3.3 Buckling Response 12

4. **Inducing Buckles** 16

4.1 Spontaneous buckles 16

4.2 Nanoindentation Buckles 19

4.3 Scratch Induced Buckles 27

5. **Summary of Key Results** 34

References 40

Publication I 47

Publication II 62

Publication III 79

Publication IV 99

Publication V 117

1. Introduction

Thin films are a widespread and integral part of everyday life due to their unique properties. They can be found in a wide variety of applications, such as decorative items, mirrors or as wear protective coatings on sun glasses or drill bits and as corrosion protection films on car planes and hulls of ships. But probably the most important area of application is in microelectronics, where the large technological progress in the last century would not have been possible without the utilization of thin films [1,2]. Modern microchips incorporate a wide range of thin film materials, for instance metals for electric and thermal conductivity, ceramics and dielectrics for gate materials or semiconductors and polymers for passivation and environmental protection, each with different electrical and mechanical properties. Although, chip-design is mainly driven by electrical considerations tailored to increase computational performance, the increasing intricacy of chip-architecture makes the mechanical stability of the involved films and interfaces one of the most important factors for chip reliability.

Critical interfaces in microchips arise especially between the semi-conductors (front-end of line) and the conductive metallization (back-end of line) where transition metals like tungsten, tungsten-titanium or titanium nitride, but also isolators like silicon nitrides are used as barrier layers. These barrier layers fulfill important electrical functions and provide the device with chemical as well as mechanical stability. Chemical stability mainly means the prevention of silicon diffusion into the power metallization thereby tarnishing the electrical properties of the power metal.

Mechanical stability connotes the absence of delamination or fracture of thin film systems and is mainly governed by film stress and interface adhesion. Film stress can be determined by well-established methods like wafer curvature [3] or X-ray diffraction [4]. Adhesion, on the other hand, cannot be determined so easily and testing techniques are not as straight forward. Many different experimental methods have been developed over the last decades to determine the interface strength of thin films [5–8]. The techniques can be divided into two categories: qualitative and quantitative. Qualitative techniques mostly give a general pass or fail result on the adhesion of a film or coating. Examples are the tape test where the film is removed by a standardized adhesive tape and the results can be differentiated by the amount of film area that was removed. Another example is the scratch testing, a technique usually used to determine a critical load for coating detachment which has to be carefully examined. Quantitative methods on the other hand provide a measure of the adhesion energy

of an interface. These methods include micromechanical techniques like four point bending (4PB) or micro-cantilevers where a pre-crack is forced along an interface by bending [9–13]. Extensive sample preparation is needed for these methods including heat treatments and focused ion beam milling. Other methods of adhesion testing utilize lasers to spall films or induce delamination [14,15]. Another class of techniques is based on nanoindentation where the indenter tip induces compressive stress into a film causing it to deflect away from the substrate and form a buckle [6,16–19]. The same can be achieved using a compressively stressed overlayer [20–22]. The tests can be performed in the as deposited condition but the thickness of the sample layers is limited to a range where the compressive stresses can reach the interface of interest.

The aim of this thesis is to investigate the adhesion of metal and ceramic films on doped silicate glass. Utilizing residual compressive stress, nanoindentation and scratch testing, controlled areas of delamination, called buckles, are produced which can be used to quantitatively determine the adhesion energy of an interface. The utilized methods will be closely investigated by cross sectioning in order to characterize the failure mechanisms of the interfaces and shed new light on the development of buckles. The results of the techniques are compared to values calculated from other experimental methods performed on the same materials. Additionally, the interplay of stress and adhesion will be investigated. The characterization of film stress utilized in the course of this thesis will be discussed in Chapter 2. Chapter 3 will provide an overview on interface fracture mechanics and a derivation of the model used for the evaluation of buckles for adhesion calculation. Chapter 4 presents the three different experimental methods used to induce buckling and failure modes involved to critically evaluate their potential for future use. Finally Chapter 5 will summarize the key findings of the thesis.

2. Film Stress Characterization

Thin films deposited by physical or chemical vapor deposition on a substrate are usually in a state of stress. Residual stress in a thin film can be imagined by considering a free standing relaxed film which has to change its in-plane dimensions by the application of pressure to be bonded on a substrate of a different size. The origin of film stress can be classified into two main categories: growth stresses and extrinsic stresses [1,4,23]. Growth or intrinsic stresses arise due to the growth process of the film which is strongly dependent on the material that is deposited, the substrate and the process parameters such as gas pressure or substrate temperature [24]. Extrinsic or induced stresses mostly come from a mismatch of the coefficient thermal expansion of film and substrate which results in different relaxation of the respective materials when cooling to room temperatures but can also come from electrical and chemical effects [1,23]. In general the stress in a homogeneous film is a combination of growth related and thermal mismatch stresses. Several techniques have been developed to determine the stress of thin film systems [25–28]. The most prominent and widely utilized methods are wafer curvature [29] and X-ray diffraction (XRD) [4].

2.1 Wafer Curvature

Macroscopic stress can manifest itself through bending of the sample or curvature, as depicted in Figure 2.1. The curvature κ of the film and substrate can be related to the bending moment which is exerted on the plate sample by

$$\kappa = \frac{1}{R} = \frac{12M}{h^3} z, \qquad (2.1)$$

with M being the bending moment of the plate, R the radius of curvature, h the thickness of the plate and z the direction of the deflection. The stresses in the interface plane are assumed to be equi-biaxial, $\sigma_{xx}=\sigma_{yy}=\sigma$ with no stress component perpendicular to this plane and the moment, M, generates small deflections of the film compared to the sample thickness which leads to the approximation to an elastic beam bending possible. The bending moment of the plate sample can be related to the stress in the film through $M = -\sigma h_f h_s/2$ which leads to the well-known Stoney formula [29],

$$\sigma = \frac{E_S}{6(1-\nu_S)} \frac{{h_S}^2}{h_f} \frac{1}{R}, \qquad (2.2)$$

with h_s being the substrate thickness, E_s the elastic modulus and v_s the Poisson's ratio of the substrate, h_f the film thickness and R the radius of the curvature as depicted in Figure 2.1.

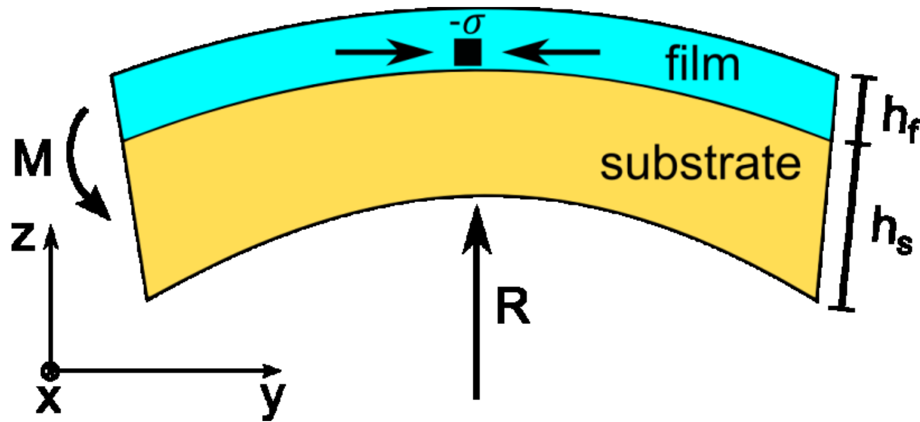

Figure 2.1: Schematic of a radius of curvature induced by the bending moment, M, as a result of a compressively stressed (-σ) film on a thicker substrate.

The Stoney formula has certain requirements which must be fulfilled in accordance with the elastic approach. For instance, the film and substrate must be isotropic materials, the thickness of the film has to be $h_f << h_s$ and the lateral dimensions of the entire sample have to be much larger than the substrate thickness, resulting in $R>>h_f+h_s$. Additional basic assumptions and limitations of this model can be found in Suresh and Freund [1]. This method is of special interest for microelectronics with one of the most important applications of wafer curvature systems being to investigate the thermal behavior of stresses in thin films from room temperature up to 1000°C [3,23]. The change in stress in the film due to temperature is of high importance to the reliability of thin film systems. Elevated temperatures can lead to a relaxation of residual stresses due to grain growth or through thickness crack formation [3,30,31]. The curvature is, in most cases measured by a grid of laser points which are reflected off the film, where the change of distance between the points is related to the change in curvature [3]. Many investigations have been directed towards the extension of the Stoney formula towards multilayered films, the influence of sample geometry and thickness ratio of film and substrate [32–34]. The macroscopic response to the stresses in subsequent layers can influence each other which may have important implications when designing layered structures [35–37]. For instance a combination of compressively and tensile stressed layers can lead to an overall stress free multilayer stack.

2.2 X-Ray Diffraction

X-ray diffraction (XRD) is a widely used method in materials science for phase analysis or the determination of crystal structures of materials. XRD can be used to determine the stress state in a thin film is the $\sin^2\psi$ method [4]. This technique measures the elastic strain of a material under applied or residual stress. These elastic strains are measured from the atomic planes in the crystal lattice due to the change in the interplanar lattice spacing, *d*. The change of *d* can be determined with Bragg's law,

$$n\lambda = 2d\, sin\theta, \tag{2.3}$$

with λ as the wavelength of the incident X-ray beam, *n* the integer multiple and the Bragg scattering angle, θ. As a consequence of the changed lattice spacing caused by the residual stress the diffraction peak, for a given *hkl*-reflection, will shift to a different angle θ, dependent on the direction of the stress. The elastic lattice strain in the film can be found by using the relation $\varepsilon_{\phi\psi} = (d_{\phi\psi}-d_0)/d_0$, where d_0 is the unstressed and $d_{\phi\psi}$ is the measured lattice spacing. The strains $\varepsilon_{\varphi\psi}$ can be measured as a function of ψ for fixed values of ϕ by the shift of the diffraction peak. Figure 2.2 illustrates that by tilting the sample through a range of ψ angles, the planes that are at the angles ϕ and ψ to the surface normal are brought into a position where they fulfill Bragg's law.

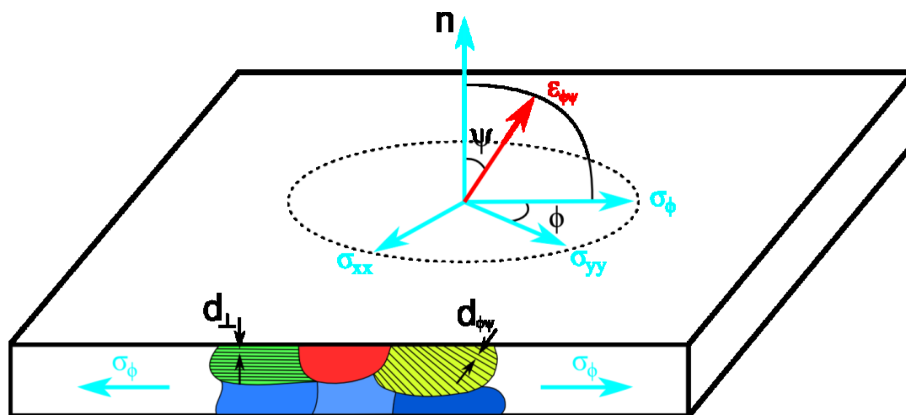

Figure 2.2: Schematic of the $\sin^2\psi$ stress measurement showing the lattice planes parallel to the surface with the corresponding lattice spacing, $d_\perp$, and at the in-plane angle ϕ and out of plane angle ψ with $d_{\varphi\psi}$ (redrawn from [38]*).*

In thin films the biaxial stress state, $\sigma_{xx} = \sigma_{yy}$, $\sigma_{zz} = 0$ can be assumed, therefore the principal equation for the $\sin^2\psi$ strain measurement can be written as,

$$\frac{d_{\phi\Psi} - d_0}{d_0} = \frac{1}{2} s_2 \sigma_\phi \sin^2(\Psi) - s_1(\sigma_{xx} + \sigma_{yy}), \tag{2.4}$$

where the X-ray elastic constants s_1 and s_2 are related to the elastic constants E and v of the film and σ_ϕ the in-plane stress. Equation 2.4 predicts a linear behavior of d against $\sin^2\Psi$ and σ_ϕ can be directly obtained from the slope of the d vs. $\sin^2\Psi$ curve. It should be noted that for most materials, the difference between d_0 and $d_\perp$ is about 0.1%. Therefore, in practice d_0 is often replaced by $d_\perp$ causing a negligible error in the stress calculation. A more detailed derivation with basic assumptions and definitions of the method can be found in Noyan and Cohen [4]. Often used for $\sin^2\psi$ measurement is a synchrotron source due to the higher intensity and brilliance of the radiation which is more suited for the characterization of thin films [39,40].

More sophisticated methods have been developed to investigate inhomogeneity of stress on the nanoscale and achieve higher depth resolution, such as grazing incidence X-ray [4] or nano-beam diffraction [41,42]. In the case of a film with unknown X-ray elastic constants a procedure proposed by Eiper et al. [43] can be employed to determine them experimentally if the film is deposited on a silicon substrate with the orientation (100). XRD is also frequently used for in-situ tensile testing of thin films on compliant substrates to determine the stress development in the film due to loading [44,45].

3 Interface Fracture Mechanics

In the following section the mathematical basis for the buckle analysis in the context of adhesion is derived as presented by Hutchinson and Suo in 1991 titled "Mixed mode cracking of layered materials". For a more detailed exploration of the topic the interested reader is referred to their works [16,46].

3.1 Work of Adhesion

By thermodynamic definition the true work of adhesion, W_A, is the amount of energy necessary to create two new surfaces from the interface. This energy depends solely on the type of bonding between the two involved materials and is a constant for a given interface, written as,

$$W_A = \gamma_f + \gamma_s - \gamma_{fs}, \tag{3.1}$$

with γ_f and γ_s being the specific surface energies of the film and substrate respectively and γ_{fs} the energy of the interface [6]. The true work of adhesion can be determined experimentally by contact angle measurements [47] of metallic particles bonded to a substrate as depicted in Figure 3.1.

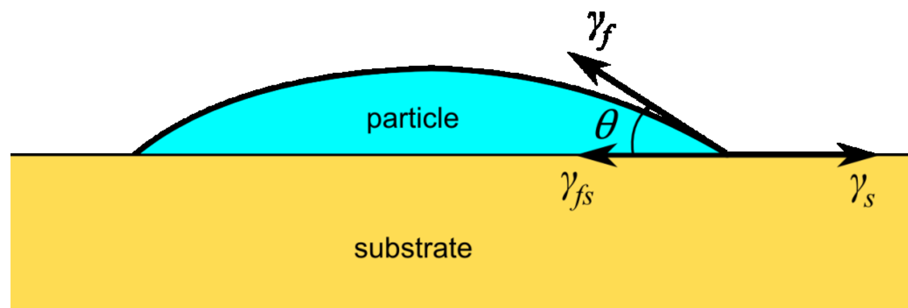

Figure 3.1: Schematic of the contact angle measurement (redrawn from [6]*)*

Given the particle and substrate are in thermal equilibrium, the true work of adhesion can be calculated, when the surface energy of the particle is known, using the Young-Dupré equation,

$$W_A = \gamma_f (1 + cos\theta), \tag{3.2}$$

where θ is the contact angle in Figure 3.1. While this method works well for metal particles on ceramic films it is not a very practical approach and doesn't work for materials which

cannot be deposited as droplets. For real thin film systems other experimental testing techniques have been developed which are based on the removal of the film from its substrate by some mechanical means. During the process of delamination the film system can experience other forms of energy dissipation that can be summarized in the practical work of adhesion,

$$W_{A,P} = W_A + U_f + U_s + U_{fric}, \tag{3.3}$$

with U_f and U_s being energy contributions from plastic deformation of the film and substrate, respectively and U_{fric} represents energy loss due to friction [48].

In a fracture mechanics approach to adhesion the crack driving force is regarded as a measure of the practical work of adhesion. The resistance to the crack advance, Γ, has to be surpassed in order to separate the interface and create new surfaces by fulfilling the Griffith criterion [49],

$$G(b) \geq \Gamma(\psi). \tag{3.4}$$

Here G is the energy release rate, a measure of the crack driving force in linear elastic fracture mechanics, depending on the crack length b and Γ which is a function of the angle ψ depending on the loading mode. The loading conditions at a crack tip can be divided into three different modes or combinations of them, depicted in Figure 3.2.

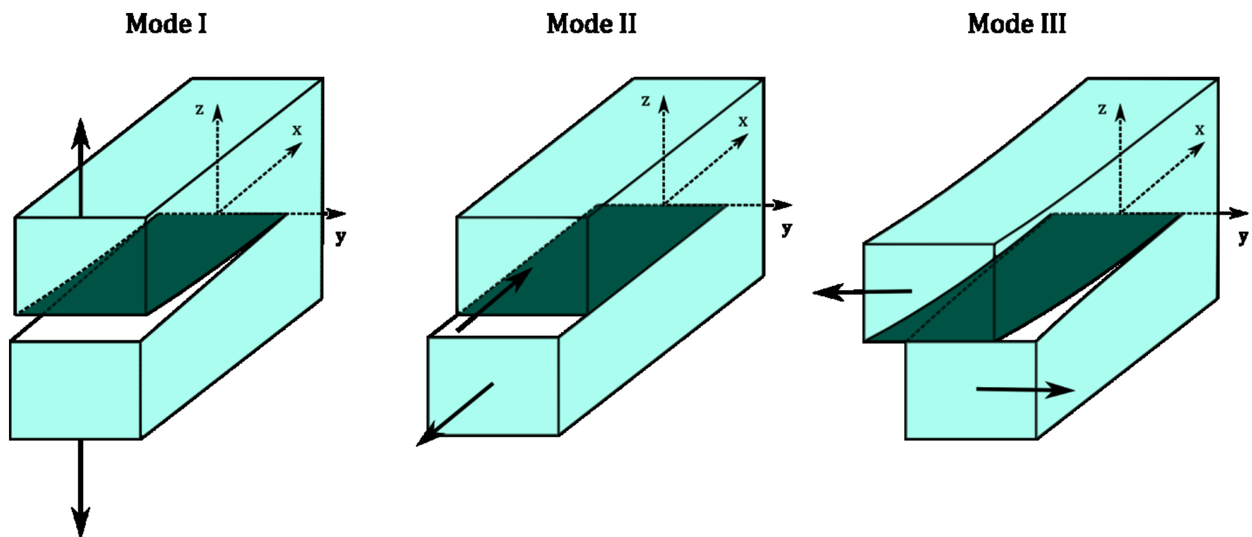

Figure 3.2: Crack opening modes (redrawn from [50]*)*

Mode I, called normal or opening mode, corresponds to crack extension perpendicular to the loading direction and parallel to the crack plane. Mode II, the shear mode loading, is

directed along the crack extension and Mode III corresponds to loading of the sample perpendicular to the crack extension and parallel to the crack plane. For crack tip advance in a thin film system only Mode I and II will be considered in the following. In Equation 4 it is stated that the interface fracture resistance depends on the phase angle of loading, ψ, which is a measure of the amount of shear and normal stress components acting at the crack tip. The fracture resistance strongly depends on the phase angle, shown in Figure 3.3, where more energy is dissipated and a higher fracture resistance is present when the crack tip is in pure shear at 90° compared to pure normal crack opening at 0°. Through the knowledge of the phase angle the fracture energy under pure mode I loading, Γ_{IC}, can be calculated which can be regarded close to the true work of adhesion or the fracture toughness of the interface.

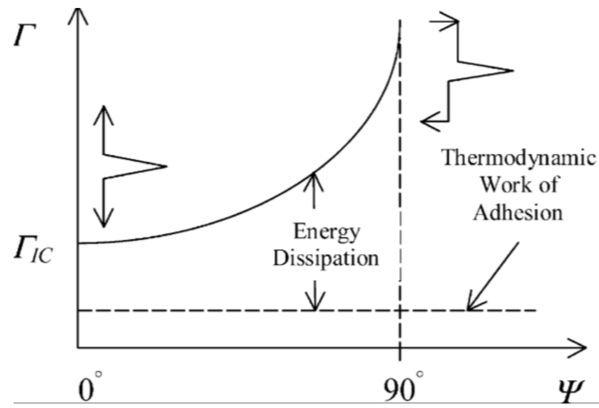

Figure 3.3: Mode dependence of the interfacial toughness (taken from [6]*).*

The crack driving force can also be described in terms of Irwin's fracture condition which postulates that the amplitude of the singular stress field at the crack tip, called the stress intensity factor *K*, is related to the fracture resistance, by assuming purely elastic behavior [51]. The stress field of an interface and sub-interface crack have been described by Hutchinson et al. [52]. The stress intensity factors depend on the loading modes shown in Figure 3.2 and can be written as,

$$K_I = \lim_{r \to 0} \sqrt{2\pi r}\, \sigma_{zz}(r, 0), \quad (3.5)$$

$$K_{II} = \lim_{r \to 0} \sqrt{2\pi r}\, \sigma_{xz}(r, 0), \quad (3.6)$$

with σ_{zz} and σ_{xz} the normal and shear components, respectively. The energy release rate can be written in terms of the stress intensity factors to be,

$$G = \frac{1-\nu^2}{E}({K_I}^2 + {K_{II}}^2), \tag{3.7}$$

where E and ν are the elastic modulus and Poisson's ratio of the fractured material, or film in the case of thin films. This illustrates that there exists a critical stress, σ_c, to advance a crack. Finally, the phase angle can be represented in terms of the Equation 3.5 and 3.6 as,

$$\psi = arctan\left[\frac{K_{II}}{K_I}\right]. \tag{3.8}$$

The phase angle ranges from 0° to 90°, as illustrated in Figure 3.3. It has to be noted that all the above relations can be modified for the case of plasticity at the crack tip [49].

3.2 Interface Fracture

To drive a crack along an interface between two different materials and delaminate a portion of the film, the Griffith criterion in Equation 3.4 must be satisfied. A film of thickness, h_f, is attached to a substrate which is much thicker than the film and both the film and substrate materials are linear elastic with the film in a state of residual stress σ_m due to a physical mismatch with the substrate, depicted in Figure 3.4.

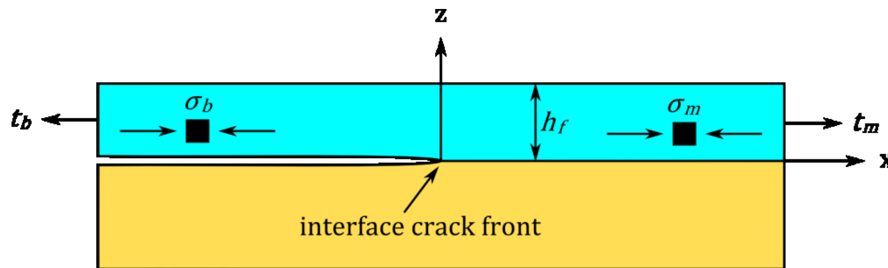

Figure 3.4: Schematic of a partially delaminated film.

It has to be noted that the residual stress can either be tensile or compressive. A delamination is propagating along the interface in x-direction, the stress far behind the crack front compared to h_f, is relaxed to a stress, σ_b, with the stress far in front of the crack front still being σ_m. The traction forces on the edges of the film are $t_b=\sigma_b h_f$ and $t_m=\sigma_m h_f$ behind and in front of the crack, respectively. In the case that the interface cracks, it extends over the whole sample width, the stress behind the front is assumed to be completely relieved, with $\sigma_b=0$. The reduction of the potential energy due to crack propagation is the driving force of the delamination and when defined per unit area of separated interface it is called the energy release rate which can be written as,

$$G = \frac{1-\nu_f^{\,2}}{2E_f}(\sigma_m - \sigma_b)^2 h_f, \tag{3.9}$$

with E_f and ν_f being the Young's modulus and the Poisson's ratio of the film, respectively and plane strain conditions are assumed. The value G is the energy which is stored in the film available for crack advance given by equation 3.4. It has to be noted here that in the case of film buckling the part of the film behind the crack front is not free of stress but has a traction force proportional to the partially relaxed residual stress and the bending due to the deflection of the film. Due to this Equation 3.9 will become a combination of the stress in the unbuckled part, the traction in the buckled part and the bending of the film.

The case of interface separation accompanied by buckling is depicted in Figure 3.5, with $\Delta t_b = t_b - t_m$ being the stress resultant per unit thickness of the film which is the result of the residual stress and the traction from the stress due to buckling and m_b is the bending moment per unit thickness. A detailed derivation from a more general loading condition can be found in Suo and Hutchinson [46].

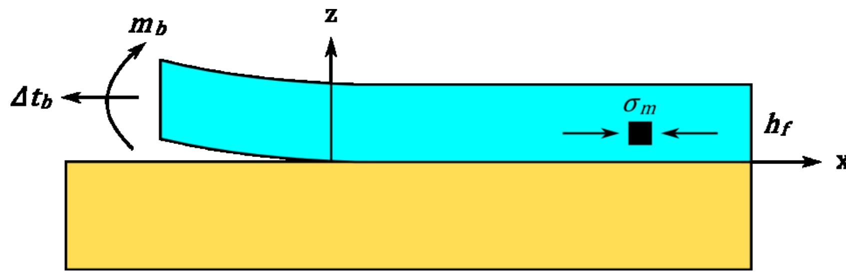

Figure 3.5: Schematic of an interface crack with buckling of the delaminated film (redrawn from [16]*).*

At a distance behind the edge of the delamination zone, on the order of h_f, the deformation of the film is the result of pure bending and extension. With the values of Δt_b and m_b fixed at a point behind the crack front the delamination leads to a reduction in potential energy. The energy release rate can now be written in terms of the bending and extension,

$$G = \frac{1}{2\bar{E}_f h_f}\left(\Delta t_b^{\,2} + 12\frac{m_b^{\,2}}{h_f^{\,2}}\right), \tag{3.10}$$

where $\bar{E}_f = E_f/(1-\nu_f^2)$ is the reduced elastic modulus in plain strain conditions. The consequence of this relation is that the energy involved in interface separation can be related to the behavior of the film in the buckled region.

3.3 Buckling Response

To quantitative the out of plane deflection of the film an analysis of the forces in close proximity to the crack front has to be conducted in terms of linear elastic fracture mechanics. It has to be noted that the process of buckling is not entirely linear elastic, rather around the crack tip the deformation is regarded as geometrically linear elastic [53]. In the following the residual stress in the film is taken to be compressive, $\sigma_m<0$ and the substrate is assumed to be rigid and therefore unaffected by the buckling. However, it has been shown that under certain conditions the buckle can exert forces on the substrate leading to additional deformation [54]. The deflection of the film is balanced by the reduction in the strain energy in the material due to relaxation of the stress and bending of the film due to the formation of the buckle which in turn increases the strain energy of the film. If the total energy of the film is negative the film will buckle and if it is positive it will stay flat even if debonded. The stress discontinuity at the edge of the buckled region causes a stress concentration which can affect the size and continued growth of the buckle. In the course of the following discussion a section of the film is not bonded to the substrate over the range $-b<x<b$ and a buckle is formed that extents infinitely in the y-direction. The displacements of the sections of the unbonded film experience a displacement due to the buckling which depends on their position in the unbuckled condition. The displacement component in the interface plane direction is $u(x)$ and the deflection out-of-plane is $w(x)$, illustrated in Figure 3.6.

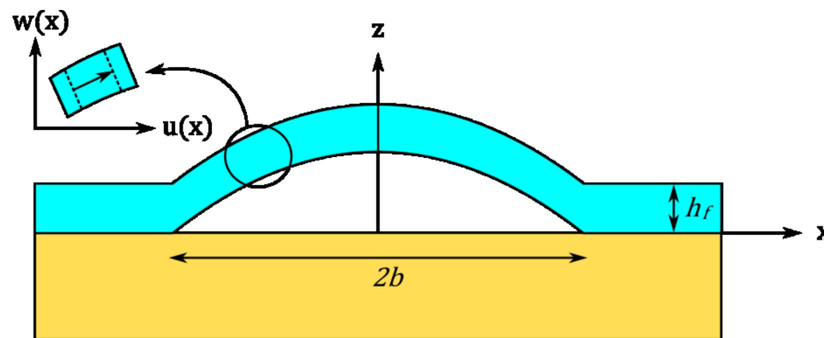

Figure 3.6: Schematic of the buckle deflection and the following displacement components of a section of the buckled film. (redrawn from [1]).

The stress resultant $t_x(x)$ and the bending moment $m_x(x)$ can be determined from deformation induced by the buckling using nonlinear von Kármán theory of elastic thin plates with the boundary condition of fully rigidly clamped edges at $x=\pm b$ [55]. A detailed derivation and approach to more involved considerations around buckling can be found in

Suresh and Freund [1]. The relation between the resulting stress and the bending moment in terms of the displacement can be written as follows,

$$t_x(x) = \bar{E}_f h_f \left[\varepsilon_m(1+\nu_f) + u'(x) + \frac{1}{2}w'(x)^2\right], \tag{3.11}$$

$$m_x(x) = \frac{\bar{E}_f {h_f}^3}{12} w''(x), \tag{3.12}$$

with ε_m being the uniform residual mismatch strain in the film. If no buckling occurs $u(x)=w(x)=0$ and Equation 3.11 reduces to $t_x(x)=\sigma_m h_f$ and Equation 3.12 results in $m_x(x)=0$. For the film to be in equilibrium the potential energy has to be minimized in the buckled region, hence the elastic deformations must satisfy the differential equations,

$$\left[u'(x) + \frac{1}{2}w'(x)^2\right]' = 0, \tag{3.13}$$

$$w''''(x) - \frac{12}{\bar{E}_f {h_f}^3} w''(x) t_x(x) = 0. \tag{3.14}$$

The consequence of Equation 3.13 it is that $t_x(x)=t_b$ is a constant taken at the edge of the buckling zone $x=\pm b$. Utilizing the clamped boundary conditions $w(\pm b)=0$ and $w'(\pm b)=0$ the eigenvalue problem in Equation 3.14 can be solved and following from the constraint that the compression in the film is relaxed due to buckling leads to,

$$\sigma_c = -\frac{\pi^2 \bar{E}_f}{12}\left(\frac{h_f}{b_c}\right)^2, \tag{3.15}$$

which states that there exists a critical buckle size, meaning that for given compressive stress σ_c a debonded zone of the size $b<b_c$ does not form a buckle. In turn this means that the stress in the film has to exceed the critical buckling stress, σ_c for a delaminated region of size b_c for deflection to occur. The minus sign in Equation 3.15 means that the stress has to be compressive to induce buckling. The stress resultant can now be expressed in terms of b_c,

$$\Delta t_b = |t_m|\left(1 - \frac{{b_c}^2}{b^2}\right). \tag{3.16}$$

The shape of the buckle can also be derived from Equation 3.14 and is described as,

$$w(x) = \frac{1}{2}w_0\left[1 + cos\left(\frac{\pi x}{b}\right)\right], \tag{3.17}$$

with $w_0=w(0)$ being the deflection in the center of the buckle. Together with Equation 3.13, integration over the buckled region and the condition $u(\pm a)=0$,

$$w_0{}^2 = \frac{16a^2}{\pi^2}\frac{\Delta t_b}{h_f \bar{E}_f}. \qquad (3.18)$$

Inserting Equation 3.16 into Equation 3.18 gives the relation between the deflection in the buckle center and the residual stress in the film resulting in,

$$\sigma_m = \sigma_c\left(\frac{3}{4}\frac{w_0{}^2}{h_f{}^2} - 1\right). \qquad (3.19)$$

Equation 3.19 states that the residual compressive stress in the film σ has to exceed the critical buckling stress σ_c to form a buckle with amplitude w_0. Finally, the edge bending moment can be determined from Equation 3.12 with $m_x(b)=m_b$ to be,

$$m_a = \frac{|t_m|h_f}{\sqrt{3}}\frac{b_c{}^2}{b^2}\sqrt{\frac{b^2}{b_c{}^2} - 1}. \qquad (3.20)$$

With these values derived, Equation 3.10 can be expressed in terms of the residual compressive stress and the critical buckling stress and making the total driving force for the edge crack as,

$$G(b) = \left[\frac{(1-\nu_f{}^2)h_f\sigma_m{}^2}{2E_f}\right]\left(1 - \frac{\sigma_b}{\sigma_m}\right)\left(1 + \frac{3\sigma_b}{\sigma_m}\right), \qquad (3.21)$$

with the term in the square brackets being the strain energy stored in the film and available for crack advance. Recall that Equation 3.4 connects the expression in Equation 3.21 to the practical work of adhesion which can now be calculated from the measurements of the buckle size, b_c, and the height of the buckle, w_0. However, Equation 3.4 also postulates that for any particular material system the delamination resistance of the interface depends on the loading mode at the crack tip expressed by the phase angle, ψ. As illustrated in Figure 3.3 the loading mode can have a rather large effect on the energy required to separate an interface. The local stress distributions in normal and shear modes at the crack tip are related to the stress intensity factors of Equations 3.5 and 3.6. Combining Equation 3.4 with 3.21 the phase angle can be written in terms of w_0, leading to,

$$\psi = tan^{-1}\left[\frac{4\,cos(\omega) + \sqrt{3}\,w_0/h\,sin(\omega)}{-4\,sin(\omega) + \sqrt{3}\,w_0/hcos(\omega)}\right], \qquad (3.22)$$

where the angle ω depends on the Dundur's parameters between the film and substrate. Dundur postulated two dimensionless parameters which combine the elastic mismatch between the two dissimilar materials comprising the interface [56]. The angle ω has been calculated for many different material systems [52,57]. Equations 3.21 and 3.22 hold for straight sided buckles which are assumed to be infinite in y-direction but a similar derivation can be made for a circular crack path which leads to a very similar result and can be found in Hutchinson and Suo [16]. Using the phase angle the Mode I contribution of the energy release rate in Equation 3.21 can be calculated from,

$$\mathrm{G(b)} = \Gamma(\psi) = \Gamma_{Ic}[1 + tan^2(\lambda\psi)], \qquad (3.23)$$

with λ is a parameter usually between 0.7 and 0.8, describing the influence of the phase angle on the delamination resistance [57]. The mode I energy release rate, Γ_{IC} can be regarded as the true work of adhesion or the fracture toughness in the case of a brittle interface.

In an ideal film system with brittle interface fracture, when no compliance of the substrate, no fracture events in film or substrate this approach holds up quite well compared with other methods [1,57]. Of course most systems are far from ideal and caution has to be exercised when analyzing buckles for adhesion assessment. Many aspects of buckle delamination have been investigated and additions the original model have been proposed, for instance the effect of the compliant substrate [54,58] of plasticity [59] and fracture events [60] in the deflected films as well as for multilayered film systems [61].

4 Inducing Buckles

To utilize the model derived in the previous section and calculate adhesion, controlled areas of delaminations have to be produced on the sample under investigation. The three techniques used will be discussed in the following section. Special emphasis will be put on how the delamination is caused in different film systems ranging from metal and ceramic films on silicon glass to metal on polyimide. All film systems presented below are deposited on 725 µm thick silicon wafer. The surface characterization has been done with either atomic force microscopy (AFM) or confocal laser scanning microscopy (CLSM) and the interface cross-sections have been prepared with focused ion beam (FIB) milling in scanning electron microscope (SEM).

4.1 Spontaneous buckles

Residual stresses can affect the mechanical of behavior thin film structures in positive or negative ways. There are two ways to relieve the stress in the film, it can crack under tensile stress or buckle under compressive stress, as depicted in Figure 4.1. In tensile stressed films through thickness cracks can occur, which can lead to spallation of a weakly adherent part of the film. When attempting to measure the adhesion of the thin film the buckling is the more interesting failure mode. Buckling based techniques are ideal for adhesion measurement, because fracture and plastic deformation are minimized and buckle delamination is well understood [6,18,46]. The Buckles in a thin film system are defined by the residual compressive stress and the adhesion to the substrate or subsequent layers. As described in Chapter 3, for buckling to occur the compressive stress must exceed the critical stress, σ_c, which depends on the strength of the interface. From an initial debonded path the film can deflect away from the substrate in order to relieve the strain energy in the film. The initial debonded path can be caused by an interface defect or develops at the film edge. The buckles grow and propagate to relieve the stress in the film until the residual stress has been relieved to a point where it is lower than the critical buckling stress.

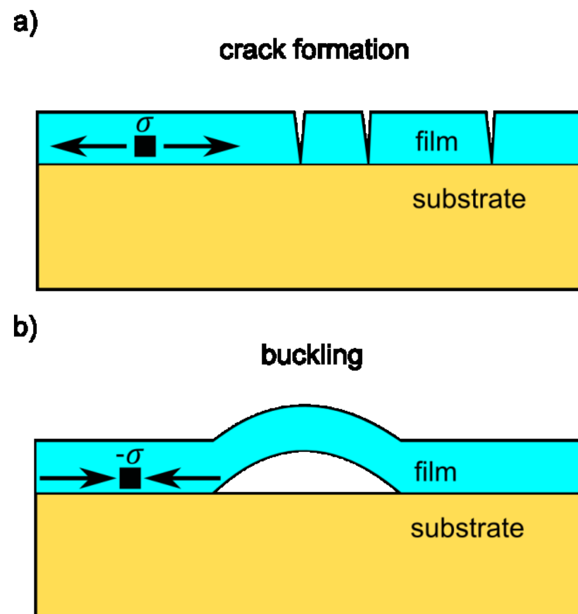

Figure 4.1: Failure modes of thin films under stress. Tensile stress leads to through thickness crack formation (a) and compressive stress leads to buckling of the film (b).

Various shapes of spontaneous buckles can develop, with the most prominent circular blisters, straight sided and telephone cord buckles [16,21,62–64]. The morphologies of buckles, especially telephone cords, are still a subject great interest since it is not completely clear why they take this kind of shape. It has been well established that the interface strength, due to the non-linear coupling of buckling and fracture, strongly depends on the relation of normal and shear mode at the interface crack tip [16,62]. Many investigations have been directed towards the question why buckles form in these specific shapes and the stability of the respective morphologies [62,65]. Some have pointed at the anisotropy of stress distribution in a film as a possible cause [64], others to a connection to the Poisson’s ratio of the film material [66]. Another possibility is the dependence on adhesion for the deflection of the interface crack [63].

Telephone cords have been observed on many systems and to investigate the phenomenon more closely many ways to induce spontaneous buckling have been developed. The most obvious way is to vary the deposition parameters to induce higher compressive stress or change the thickness of the films [2,6]. The most prominent examples are compressively stressed overlayers of a material with a high elastic modulus which can induce the necessary stress to cause delamination. A more sophisticated technique is sputtering a overlayer with a thickness gradient across a film system thereby identifying the thickness needed for delamination [67,68]. Other techniques are utilizing a global force on a film system to induce buckling in a part of the sample that is far away from the point of force

application. Wide spread methods include global tension [44,60,69] and compression [58,62,65].

An example for spontaneous buckles induced by residual stress is shown in Figure 4.2. The spontaneous buckle that developed in the telephone cord shape due to the distribution of the compressive residual stress of about 1.5 GPa in a 300 nm tungsten-titanium (WTi) film on a 800 nm borophosphosilicate glass (BPSG) film [70]. Telephone cords have a main direction of propagation and small sinusoidal deflection around the propagation direction (Figure 4.2a). Telephone cord buckles are modeled as straight sided buckles and measured from straight wall to straight wall as indicated by the white line in Figure 4.2a and the corresponding profile is shown in Figure 4.2b, if measured at any other point additional geometric correction factors have to be taken into account [20,21].

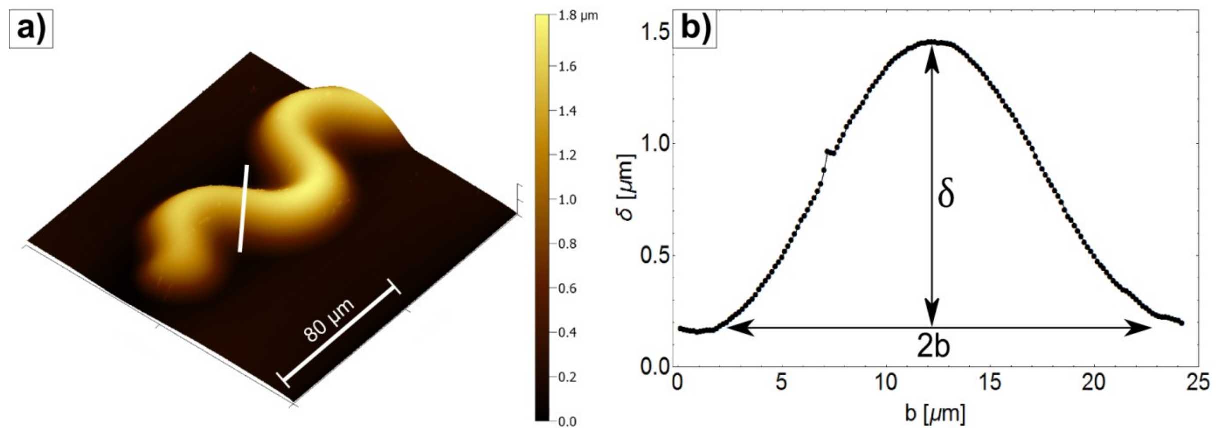

Figure 4.2: a) AFM height image of a spontaneous buckle of a 300 nm WTi film on an 800 nm BPSG layer. The white line indicates where the profile has been taken. The buckle profile is shown in b) and the height and width measures for adhesion calculation are depicted.

Spontaneous buckling normally does not occur on polymer substrates because the substrate can accommodate for the film stress by macroscopically bending unlike a rigid substrate. However, in some cases, if the substrate is stiff enough and substrate bending is avoided, the stress can be relieved via buckling, as shown in Figure 4.3 for a gold (Au) film on a polyimide (PI) film [69]. The film system was deposited on the PI which was attached on a glass slide and later removed after deposition. The glass slide most likely prevented the deformation and bending of the PI due to the stress in the Au film causing the stress to be relieved by buckling. The image illustrates that the delamination starts as single straight-sided buckles, but then continues to propagate as telephone cord buckles. This is a common

delamination process in bi-axially stressed films with spontaneous buckles because of the large amount of shear stresses.

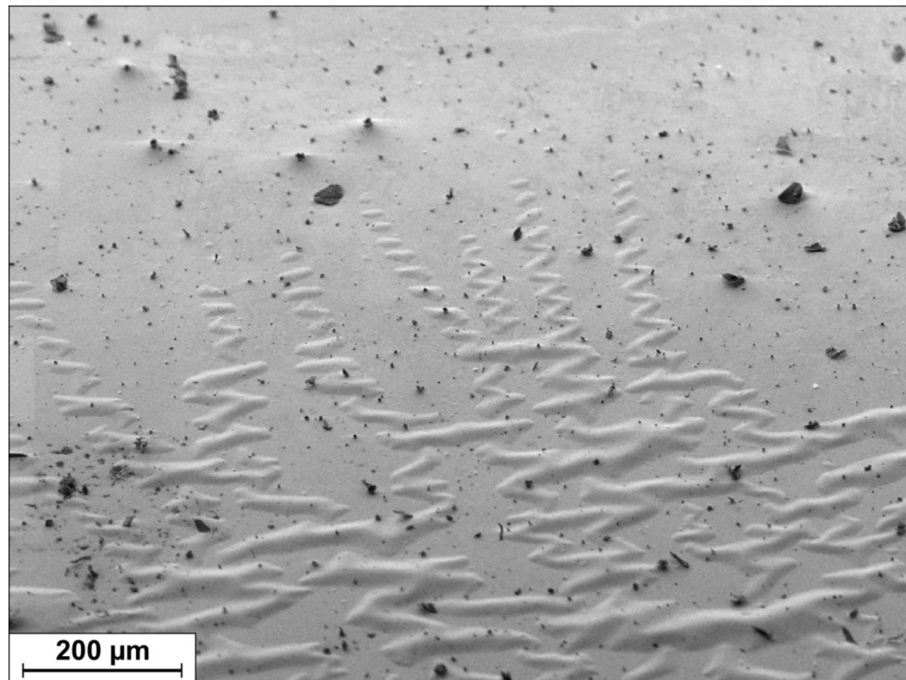

Figure 4.3: SEM image of spontaneous buckles in a gold film on a polyimide substrate. The evolution of the buckle morphology from small and straight to telephone cords can be observed.

Spontaneous buckles are the preferred way to assess the adhesion of thin films because they are usually not accompanied by fracture or plastic deformation of the film, which are an additional form of energy dissipation affecting the measured adhesion energy. All other buckling inducing techniques are compared to spontaneous buckles for their accuracy.

4.2 Nanoindentation Buckles

Nanoindentation is an important tool usually used in the determination of material properties such as hardness and elastic modulus [71]. By driving a sharp micrometer sized tip of known properties into a material, its elastic modulus and hardness can be calculated from the load-displacement response using the Oliver and Pharr method [72]. In the case of thin films, these material properties are not so easily determined due to unintentional probing the substrate properties. Indentation measurements of thin films mainly run into two basic difficulties, the rounding of the indenter-tip, generally in the range of 50-100 nm, and the often strong dissimilarity of the film and substrate properties [73]. Therefore, it is common to restrict the

maximum depth of penetration in a test to no more than 10% of the film thickness, which leads to serious challenges and sometimes the impossibility of property determination when the film thickness becomes less than 100 nm. However, as described in Chapter 3, the elastic modulus and the Poisson's ratio play a crucial role in the buckling behavior of the film and the calculation of the adhesion energy [1,16]. Additionally, the presence of discontinuities in the load-displacement response reveals information about fracture, delamination, and plasticity in the film and substrate [17,71,74].

Nanoindentation has also become a popular technique for adhesion measurements over the last decades. Typically the method works well when using an indenter capable of applying high loads (on the order of hundred millinewtons and higher) and for films made of hard materials which respond with little plasticity. An early indentation-induced interfacial fracture test was developed by Marshall and Evans [75,76] which was based on the change in strain energy in the film due to residual and indentation stresses. In brief, the Marshall and Evans model required that the indent volume remains within the film, as shown in Figure 4.4a, and the stress induced to create the indent is used in the model and works well for thick films (5-10 µm) on hard and stiff substrates. The stress induced by the indenter tip can be calculated through the indenter load and the volume of the imprint left by the indent. It is important that the volume of the indent remains within the film thickness because this implies that the substrate does not deform under the indent, nor does the formation of pile-ups around the indent occur. When the film thickness is reduced to a few 100 nm, causing a delamination where the indent remains in the film is difficult. Improvements and updates to the original models of Marshall and Evans [75] and Hutchinson and Suo [16] were added by Kriese et al. [61] and Cordill et al. [17]. By adding a stressed overlayer of a material with a high elastic modulus, as performed by Kriese et al. [61] and sketched in Figure 4.4b, the depth of the indent and the possibility of blister formation could be increased as a result of a compressive stress in the overlayer. It also allows for soft materials and films without residual compressive stress to be tested. The work of Cordill et al [17] helped determine when an indentation delamination had a pinned or unpinned circular blister geometry, as illustrated in Figure 4.4c and d, and when the indent volume can be ignored as a result of substrate deformation. It has also been shown that the load-displacement curves indicated the occurrence of a pinned or unpinned geometry. The tip geometry is also an important factor to be taken into account when indenting in general but especially for the purpose of adhesion measurement. To induce buckles in a film the conical shape is the tip of choice because of the homogenous stress field

induced into the film [75]. Tips with sharp edges like Berkovich or cube-corner indenter often lead to increased radial cracking [77].

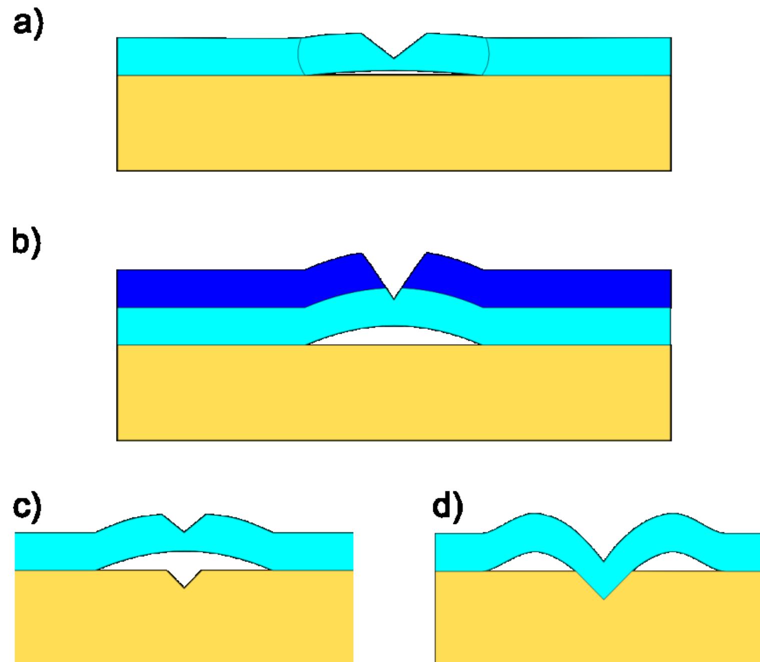

Figure 4.4: Nanoindentation-induced delamination models by (a) Marshall and Evans, (b) Kriese et al. with a stressed overlayer, and Cordill et al. with (c) unpinned and (d) pinned buckle geometries.

The first examples shown in Figure 4.5 are 300 nm WTi films on 800 nm of BPSG which were indented with conical tips and circular indentation blisters were produced [70]. The WTi had a residual compressive stress of about 1.5 GPa. Both forms of blisters, pinned (4.5a) and unpinned (4.5b), were observed at maximum loads around 300 mN [16,17]. Pinned indentation blisters (4.5c) exhibit a torus-like form because the center of the delamination is held at the center of the indent imprint, while the unpinned blisters (4.5d) resemble a more cone like-shape and the centers are not "pinned" at the indent imprint. Unpinned blisters often had extensive radial cracking and therefore are not considered in the adhesion calculation. This is due to the fact that cracks represent another form of energy dissipation which can change the calculated adhesion energy [22]. Some of these delaminations were not completely symmetric, but were included in the adhesion calculation. It should be noted here, that for a pinned blister its diameter has to be much larger than the residual indentation imprint to be used in order to avoid plastic deformation effects which can influence the adhesion calculation [17].

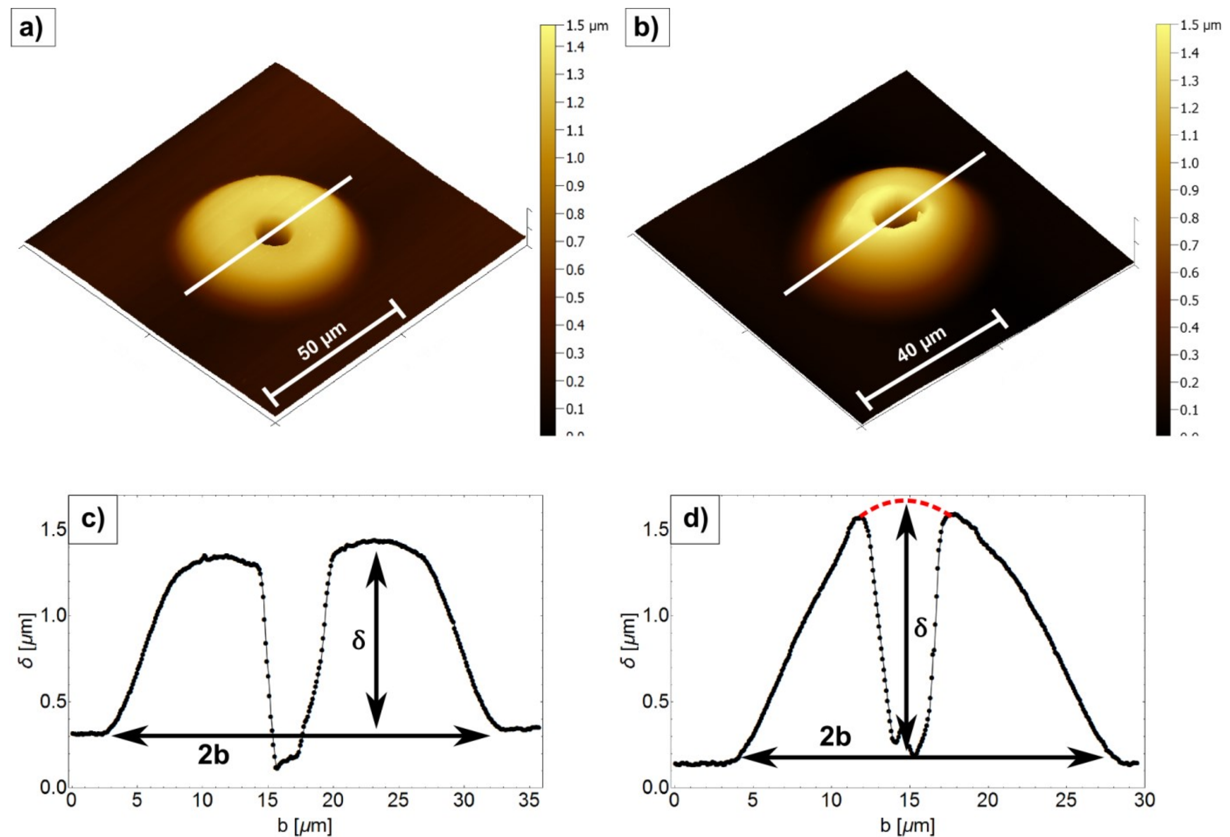

Figure 4.5: AFM height *images and profiles of indentation blisters. (a) A pinned indentation blister produced by a maximum load of 300mNwith a 5 µm conical tip. (b) An unpinned blister produced at a maximum load of 300 mN using a 1 µm conical tip. The difference in the geometry is observed in thein the profiles of the (c) pinned and (d) unpinned blister indicated by the white lines in (a) and (b). The red dashed line in (d) shows* the form of the buckle without the imprint.

When taking a closer look at the delaminating interfaces of the indentation blisters in Figure 4.5a via FIB cross-sectioning, they showed considerable fracture of the BPSG substrate around the tip imprint and the origin of the interface crack at the BPSG-Si interface. The crack then kinks upwards to the WTi-BPSG interface as seen in Figure 4.6. This type of multiple interface fracture under a nanoindent has been previously observed [78,79]. When more than one interface is failing as seen in Figure 4.6, the buckle is no longer characteristic for one single interface and the measured adhesion energy will contain errors due to the change in buckle geometry.

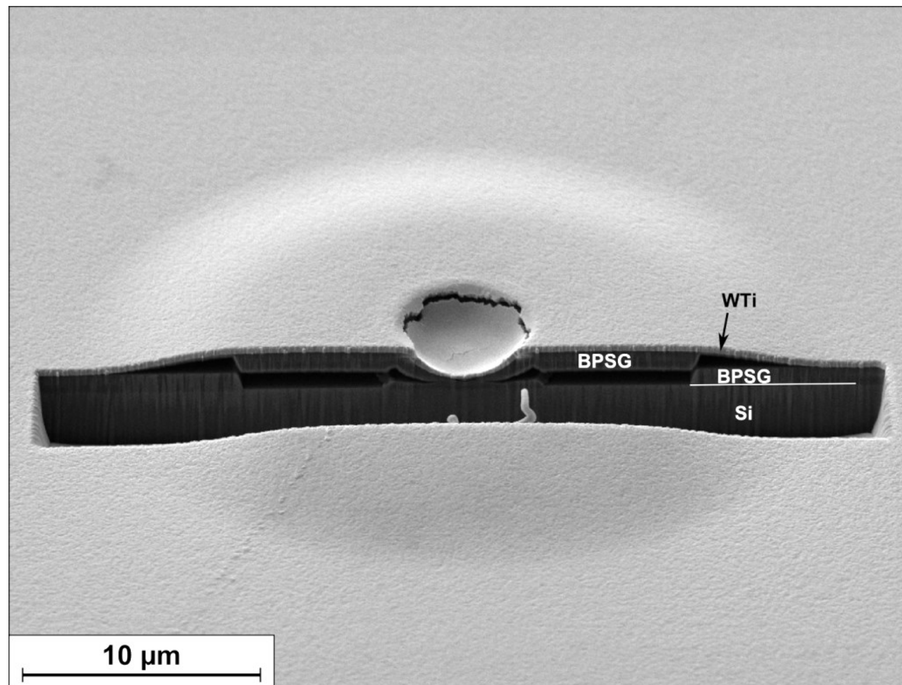

Figure 4.6: FIB cross section of the pinned blister in Figure 4.5a. The actual fracture path is revealed to be the BPSG and Si interface with the crack kinking upwards after more than the blister radius.

A more extreme example is shown in Figure 4.7, where a 300 nm Cu on a BPSG film was indented with a 2 µm conical tip and a load of 400 mN. When looking at the surface of the sample after the indent in Figure 4.7a the indent seems to have induced a buckle with unpinned geometry. However, the FIB cross section in Figure 4.7b revealed the extensive fracture in the BPSG and even the Si substrate underneath the Cu film. The entire buckle is the result of the fracture through the individual layers and not the separation of any interface. It is possible that due to the tensile stress in the Cu film of 400 MPa the fractured pieces where pulled up and formed the structure resembling a buckle similar to metal strips that curl due to their stress [80]. This sort of fracture of the BPSG and Si substrate could also cause problems at higher loads, hindering the formation of blisters if the crack also kinks through to the top film.

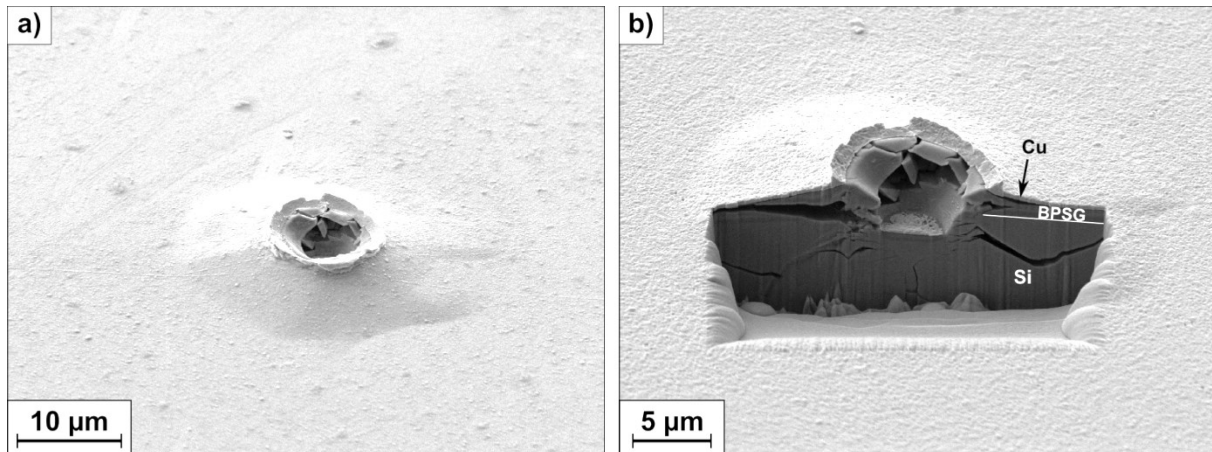

Figure 4.7: SEM image (a) and cross section (b) of an indent made with 400 mN. The whole buckle is the result of fracture which is unseen from the surface.

Following the observations of multiple interface fracture in Figure 4.6 and 4.7, it is clear that a simple surface characterization of the buckles is not enough to determine the adhesion of thin films, especially when more layers are involved. Most of the fracture events cannot be observed using in-situ indentation in the SEM because they occur under the indent. Utilizing cross-sectioning with the FIB is an efficient method to use for the observation of the failing interface as well as any interface or substrate fracture events that can result in pop-ins in the load–displacement curves which allows a better interpretation of the load–displacement curve. Film and substrate deformation of the indent as well as the pinned/unpinned buckle geometry can also be assessed better with FIB cross-sectioning. Interpretation of adhesion energies is enhanced with knowledge of how the film and substrate are deforming or fracturing.

Such an analysis has been performed on a 400 nm silicon nitride (Si_3N_4) on an 800 nm BPSG film. By using a 300 nm (WTi) stressed overlayer (1.5 GPa compressive residual stress) combined with nanoindentation, indentation blisters were produced, shown in Figure 4.8 [74]. In this particular system, the WTi film is helping to control the delamination of the Si_3N_4 layer as well as supporting this brittle film to prevent it from spalling from the BPSG. Indentations with loads between 300 mN and 500 mN in the WTi/Si_3N_4/BPSG film system produced delaminations. At higher loads (400–500 mN), the buckles partially or completely spalled from the substrate. Buckles usable for adhesion measurements were produced in the load range of 300–350 mN. Indents with loads lower than 250 mN did not produce buckles. The buckles often exhibited significant radial cracking at loads higher than 300 mN, and indents made with lower loads showed almost no radial cracking. By investigating the spallation areas of the indents in the CLSM images it was determined that the failing interface is the Si_3N_4/BPSG.

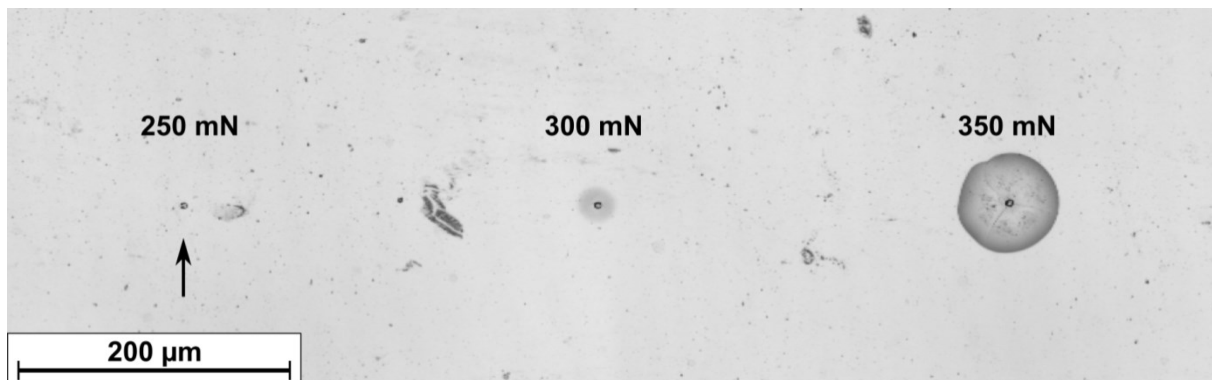

Figure 4.8: Indentation buckle overview in a load range of 250–350 mN made with a CLSM. Indents made with 250 mN did not produce buckles (indicated by arrow). At 300 mN small buckles of about 30 µm of width were produced. Loads of 350 mN resulted in either large circular buckles or film spallation.

The FIB cross sections shown in Figure 4.9 revealed that during indenting, multiple forms of cracking occurred in the film stack. In Figure 4.9a, the indents at the 250 mN interface, no delamination was produced and the cross-section shows no observable interface fracture. Nevertheless, cracks in the Si_3N_4 film can be observed directly under the indent (white arrows in 4.9a). Also of interest is that the indent deforms the underlying BPSG layer and the WTi and Si_3N_4 thicknesses remain constant under the indent. At 300 mN, multiple interfaces have separated as shown in Figure 4.9b. It can be seen from the cross section that the small buckle is mostly a result of the Si_3N_4-BPSG and BPSG-Si interfaces separating and the kinking of the crack rather than a single, well defined interface separation. Interface cracks develop between the Si_3N_4 and the BPSG as well as between the BPSG and Si and afterwards extend for about 30 µm in a cone-like pattern to become a small buckle (white arrows in 4.9b). The interface crack between BPSG and Si originates directly under the indenter tip, extends for a few micrometers, and eventually kinks up to the Si_3N_4 interface. This type of fracture under the indenter is similar to the fracture observed in Figure 4.7b. When the load has been increased to 350 mN the interface crack has kinked and it propagates along the Si_3N_4-BPSG interface for about 70 µm into a large buckle due to the additional force as seen in Figure 4.9c, until it kinks through the Si_3N_4 film and arrests in the WTi film. The resulting single interface separation can be used for adhesion calculation. The fracture of the BPSG and Si resulting from the indent (white arrows in 4.9c) is no longer affecting the buckle because the Si_3N_4 film was lifted off completely from the BPSG.

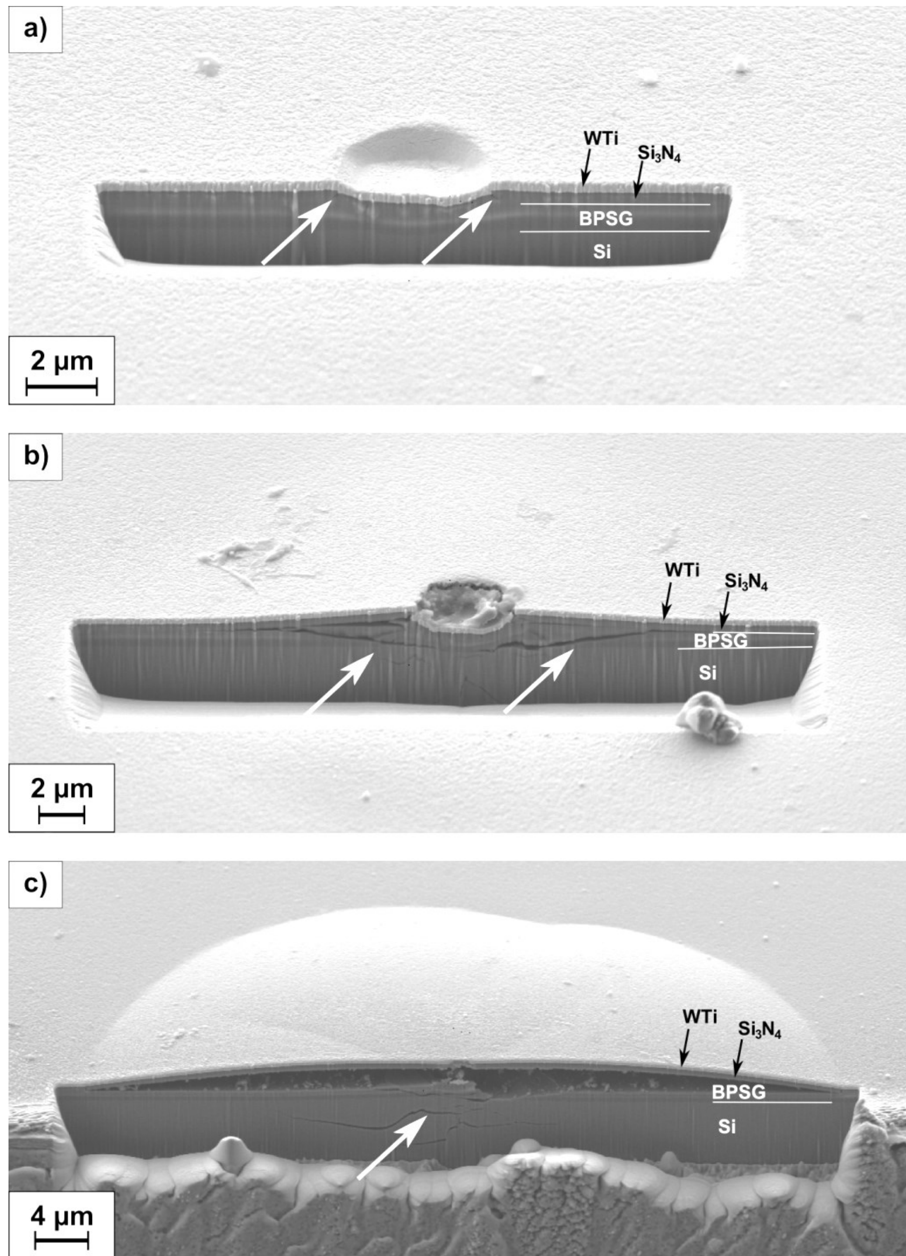

Figure 4.9: FIB cross sections of indents made with loads of (a) 250 mN, (b) 300 mN and (c) 350 mN of Figure 4.8. The cross sections show the development of the interface crack and the fracture underneath the indenter with increasing load. Arrows indicate cracks of interest discussed in the text.

Figure 4.9 illustrates that determining adhesion of thin films from nanoindentation is not as straight forward as it may seem. When selecting indentation blisters on a new film system, it has to be done with a great deal of care because substrate fracture is not obvious and may have a strong impact on the results. On the other hand, fracture of the substrate can also be

advantageous for the development of buckles, however not all film-substrate systems will behave in such a manner and should be carefully characterized.

4.3 Scratch Induced Buckles

Scratch testing has been a well-known method to assess the wear resistance and the fracture of thin films and coatings. However, the results are mainly qualitative by revealing the critical load a film detaches from its substrate. Usually a scratch test is performed in a way that the tip is first brought into contact with the surface with a very small load (micro-newton range) after which the tip is drawn across the surface with increasing load up to a defined maximum load. Following the scratch, the trace is inspected using microscopy for signs of film failure which can then be linked to the specific load at which it occurred. It has been shown that for a better understanding of the scratch test a careful evaluation of the failure mode of the coating in response to the scratch is necessary as proposed by Bull et al. [81–83]. These failure modes depend on a large range of parameters such as the hardness and elastic modulus of the film in relation to the substrate, the scratch load, tip shape and size as well as film thickness and residual stress. The two failure modes generally associated with the adhesion of the film to the substrate are spallation, where a segment of the coating is detached and lifted away from the substrate ahead of the scratch tip, and buckling, where the film deflects away from the substrate as a result of the stress induced around the moving scratch tip [81]. An example for the buckling mode is shown in Figure 4.10 on a Si_3N_4-BPSG film system with a WTi overlayer, where the scratch made with a maximum load of 500 mN produced spallation areas along the trace and resulted in the formation of a circular blister at the very end of the trace. The blister most likely formed in front of the moving tip due to the compressive stress in the film due to scratching. This kind of stress is very hard to model because it depends on a large variety of parameters like scratch velocity, material properties of the whole system and tip shape as well as on the variables like load and displacement. The spallation areas along the trace have circular geometries which suggests a classical buckling failure where the buckle forms in front of the tip but is then crushed as the tip moves ahead and thereby spalling the brittle Si_3N_4 film [81]. Due to the brittle Si_3N_4 film crushed buckles are spalled off the BPSG. Both of these failure modes, spallation and buckling, can be used to quantitatively assess the adhesion energy of an interface. The spallation failure can be quantified under certain conditions as demonstrated by Venkataraman et al. [84] by using the geometry of the spalled

area, the width of the scratch trace and the critical load of spallation to calculate the scratch induced stress and the adhesion energy.

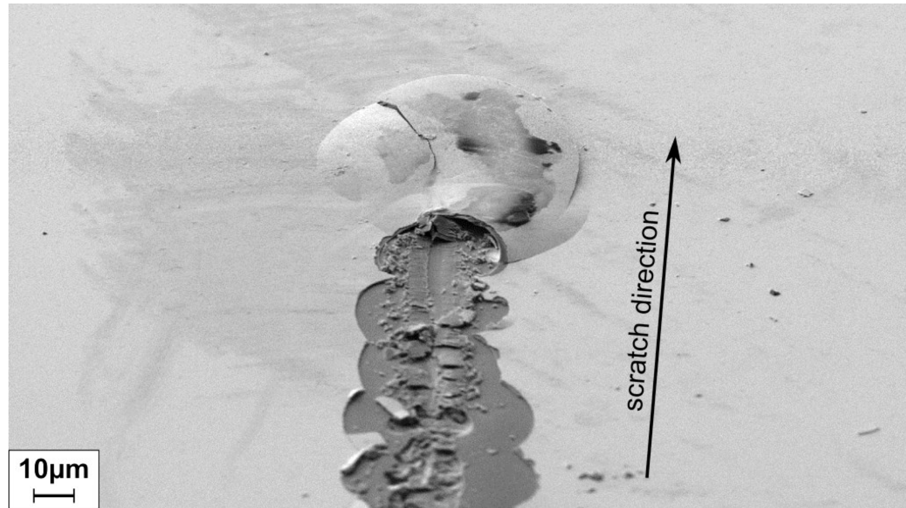

Figure 4.10: Circular blister forming at the end of the scratch trace as a result of induced compressive stress. The circular form of the spallation around the trace suggests that blisters were about to form along the trace but were crushed by the passing tip.

However, spallation usually occurs on systems with very brittle film and the geometry of the spalled areas is rarely well defined. Moody et al. [85] showed that a scratch can trigger a uniform width buckle at the side of the scratch trace which could be used to assess the adhesion of a thin film. In the course of this study buckling is the most desirable failure mode because it can easily be compared to indentation induced and spontaneous buckles.

Using a Berkovich tip with the sharp side of the tip as the scratch front and a range of maximum loads of 100-500 mN scratch tests were performed on a variety of different interfaces. Figure 4.11a shows a WTi/BPSG and 4.11b a WTi/Si_3N_4/BPSG system where buckles parallel to the scratch trace formed, as well as spontaneous telephone cord buckles originating from the scratch trace. On both systems the buckles developed in a load range between 300-500 mN with buckling occurring below 300mN. These buckles could develop either on one or on both sides of the trace, as seen in Figure 4.11a and b, respectively. This could be caused by non-uniformities of the scratch tip which have a large influence on the scratch test [83,86]. Parallel buckles mostly formed immediately after scratching but also could emerge several hours after testing. Spontaneous buckles originated from the parallel buckles and propagated as telephone cords according to the film stress distribution after several hours or even a few days after testing [62]. Spontaneous buckles emerged randomly along the parallel buckles, probably at locations with an interface defect located close to the

parallel buckles. The scratches on the WTi/BPSG system showed no sign of the tip piercing the film or fracture on the surface in the whole range of maximum loads. The scratches on the WTi/Si_3N_4/BPSG system had spallation occurring at the end of the trace at maximum loads of 300 mN (4.11b) and as the maximum load was increased to 400 and 500 mN, the spallation occurred earlier in the trace.

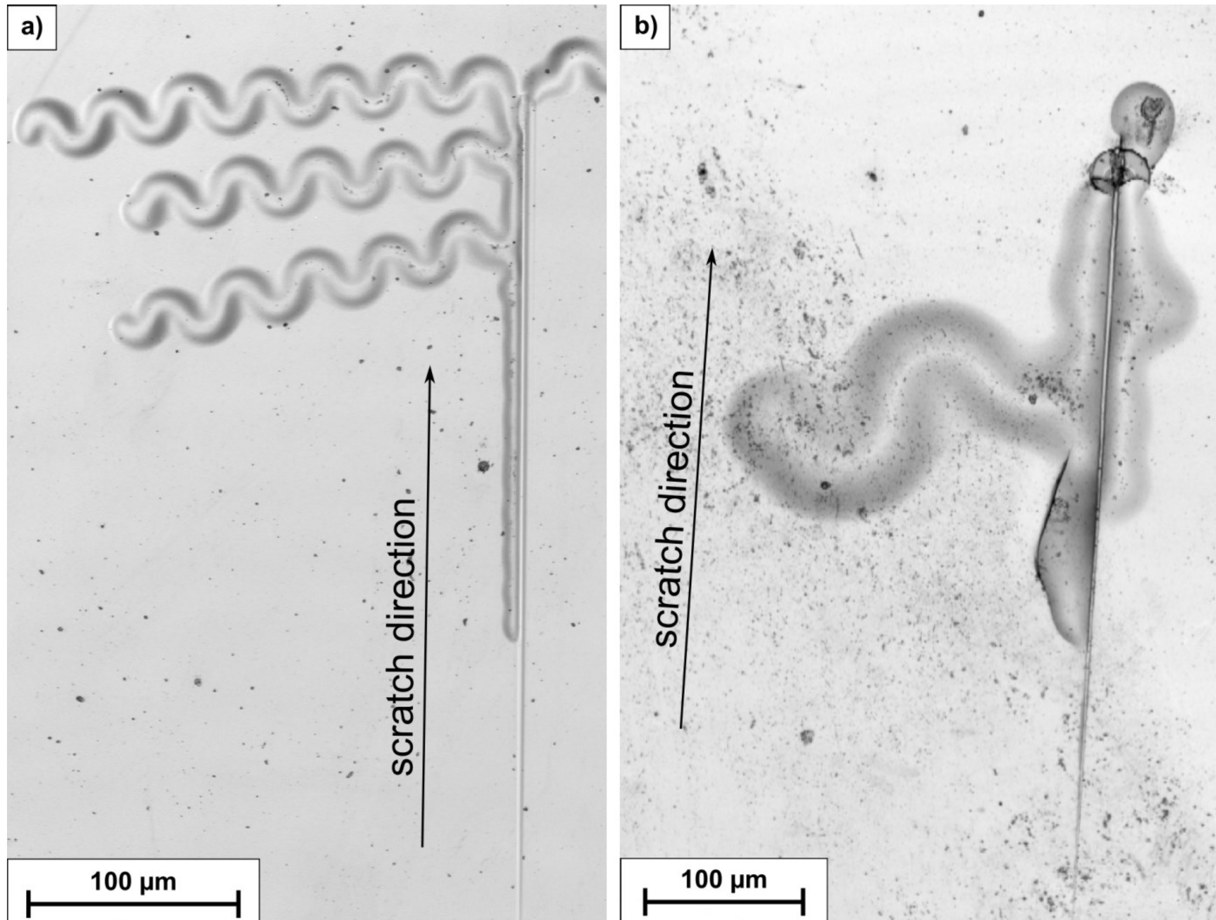

Figure 4.11: CLSM laser images of buckles developed from scratch traces with maximum loads of (a) 500 mN on a WTi/BPSG system and (b) 300 mN on a WTi/Si_3N_4/BPSG system, both made with the sharp side of the Berkovich pyramid as the scratch front. Both scratches show buckles propagating parallel to the trace and away from the trace as telephone cords.

The spalled areas showed that the WTi and the Si_3N_4 film were removed from the BPSG film suggesting that the Si_3N_4/BPSG interface is the weakest interface as previously seen with nanoindentation experiments [74].

As an example, a surface profile of the scratch buckles from the WTi/Si_3N_4/BPSG system was measured using CLSM and is shown in Figure 4.12a. When using the spontaneous buckles for the adhesion calculation, it is also necessary to measure the buckles far enough away from the parallel buckles where they originated. This distance depends on

many factors such as material properties of the film and substrate, distribution of film stress, adhesion and extension of the scratch trace. The spontaneous buckles were again modelled as straight buckles according to the Hutchinson and Suo model [57] and an example profile is shown in Figure 4.12b. The cross-section profile of the parallel buckles in Figure 4.12c suggests that the model of the pinned circular buckles can be applied to this kind of buckle [16]. It should be noted here, that for a pinned blister its diameter has to be much larger than the residual indentation imprint to be used to avoid plastic deformation effects which can influence the adhesion calculation [17]. The same condition should be applied to the parallel buckles if modelled in this way.

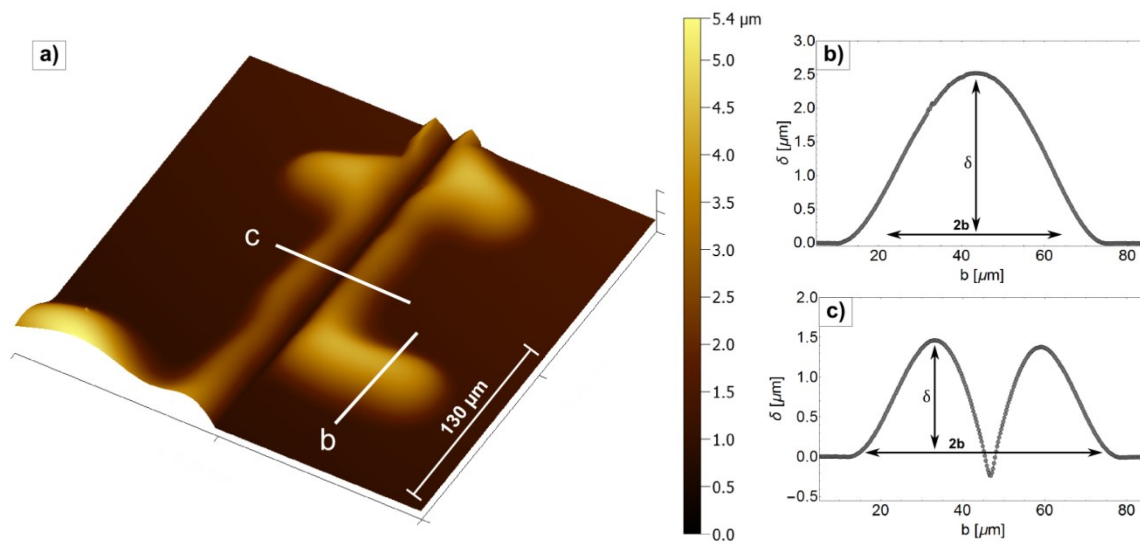

Figure 4.12: (a) AFM height image of scratch on the WTi/Si_3N_4/BPSG system made with 400 mN load with parallel and spontaneous buckles. The white lines indicate the where the profiles for (b) spontaneous and (c) parallel buckles have been taken.

The cross-sections of parallel buckles on the WTi/BPSG system is shown in Figure 4.13 as an example, to illustrate how the interface crack propagated and is influenced by the scratch trace. The WTi film is completely detached from the BPSG and the parallel buckles were always attached to the trace. In contrast to indentation, the scratch test did not show signs of fracture underneath the buckles. However, it can be observed that the BPSG is denser under the trace which involves a shear stress at the interface in the trace and causes of the parallel buckles and their propagation along the trace. Similar behavior was observed in the WTi/Si_3N_4/BPSG system (detailed investigation in Publication *V*).

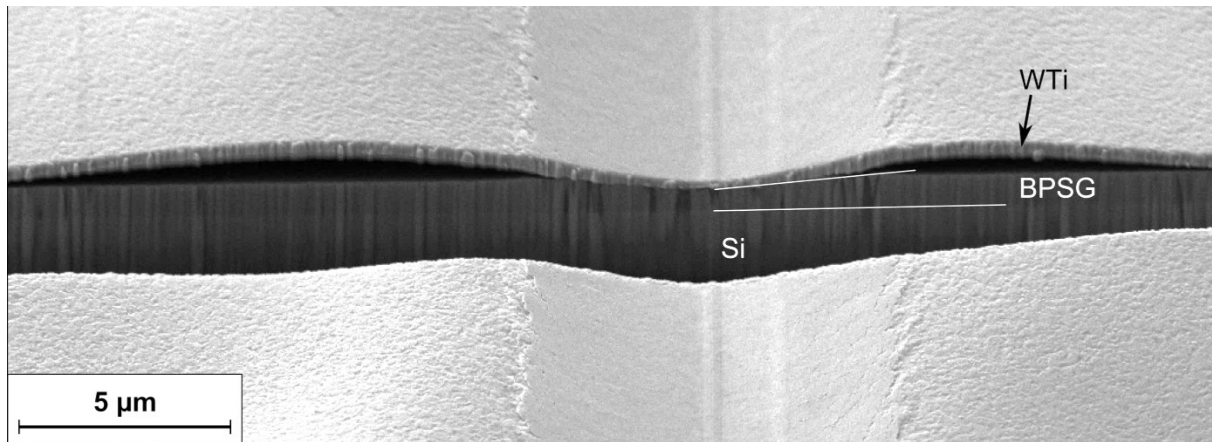

Figure 4.13: Cross-section of parallel buckles on the WTi/BPSG system showing the densification of the BPSG under the trace. The white lines indicate the orientation of the interfaces.

Another investigated system is a 300 nm copper film on 800 nm of BPSG with a compressively stressed (1 GPa) molybdenum overlayer (Mo/Cu/BPSG). The scratch tests resulted in buckle development along the trace in the whole used range of maximum loads 100-500mN, as shown in Figure 4.14. The morphology of the buckles on the side of the trace, shown in Figure 4.14a, suggests that the delamination followed the classical scratch buckling mode proposed by Bull et al. [81] since it appears that a buckle formed in front of the tip but was crushed by the tip moving over it which repeated several times along the trace. The FIB cross-section in Figure 4.14b shows clear delamination on the side of the trace and strong deformation of the Mo and Cu film in the trace but no densification or fracture of the BPSG.

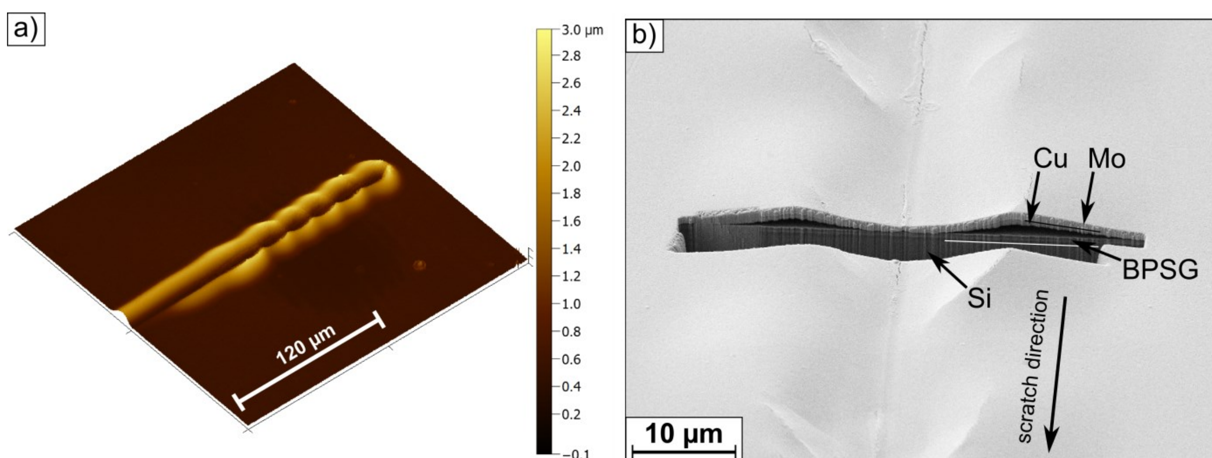

Figure 4.14: (a) CLSM height image of buckles on the Mo/Cu/BPSG system as the result of a scratch made with maximum load of 100 mN. (b) FIB cross-section of the same buckle showing the no densification or fracture of the BPSG under the trace rather deformation is contained within the Mo/Cu films.

The tip orientation is also an important factor for scratch testing since the tip radius and shape together with the load and scratch speed determines the induced stress field [86]. Using a Berkovich tip, two orientations of the tip are frequently chosen, the sharp and the broad side. The results of the sharp side on the WTi/BPSG system were shown in Figure 4.11 and 4.15 shows a scratch made with a 500 mN load and using the broad side of the Berkovich tip as the scratch front. With this tip orientation it was possible to induce a larger amount of buckles, especially for better adhering films [87]. However, it also resulted in more spallation of the film which can lower the amount of measurable buckles.

Additionally, the significant amount of wear the tip experiences during the scratch tests is another important factor to consider. Bull et al. [86] has demonstrated that the tip radius has large influence on the failure modes of the scratch test and Steinmann et al. [83] showed that a significant amount of wear of the scratch tip that changes the geometry will impact the critical load of coating detachment. This is supported by the fact that the scratches exhibited a decreasing number of buckles after continuous use of a tip up to a point where the scratch tip was no longer able to produce parallel buckles on the same sample and under the same scratch conditions. Further examination on tip wear and scratch testing is currently underway.

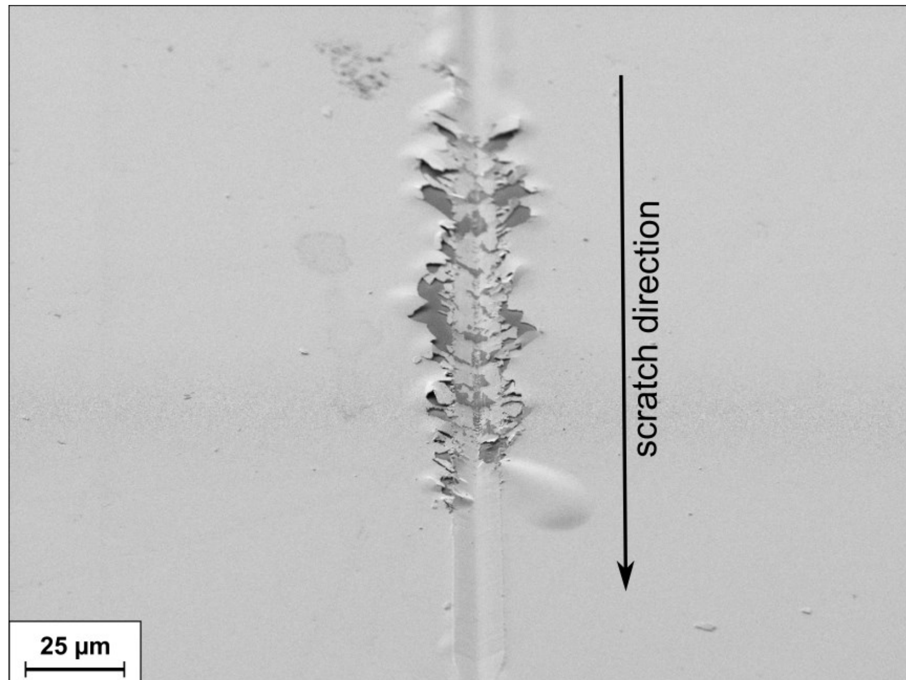

Figure 4.15: Scratch made with 500 mN and the broad side of the tip. This tip orientation results in more delaminations but also more spallation of the film.

The buckles following the scratch test can be an ideal source for adhesion calculation, especially when spontaneous buckles are induced. In the cases presented in this section the

scratch tests provided a large number of buckles useable for adhesion calculation which yields good statistics. The combination of scratch testing and stressed overlayers has proven to be useful in inducing delamination as it has been for nanoindentation. However, many factors can affect the scratch test and each system has to be evaluated cautiously.

5 Summary of Key Results

In the course of this thesis film stress and nanoindentation based techniques for quantitative adhesion measurement were investigated for a better understanding of the buckling behavior and interpretation of the failure mechanisms involved in thin film systems. The findings improve and increase the applicability of the studied techniques to many interfaces in microelectronics and protective coatings. A number of different model interfaces have been investigated ranging from metal on polymer to ceramic on glass showing the applicability of the techniques to a wide variety of material systems.

In Publication *I* the adhesion of an Au film on a flexible PI substrate with and without a Ta interlayer was investigated, utilizing spontaneous and tensile induced buckles. The respective buckles and the comparison of their profiles are shown in Figure 5.1. The Au/PI film system showed a low adhesion while the Ta film heavily promoted the adhesion between Au and the PI as the difference in buckles height, shown in Figure 5.1c, would suggest. The mixed mode adhesion energy of the Au film to the PI was calculated to be $\Gamma(\Psi)$=0.8±0.3 J/m² which is in agreement with results from 4PB [88]. The addition of the Ta interlayer increased the adhesion energy to $\Gamma(\Psi)$=11.7±2.2 J/m² which is much higher than the results of 4PB on the same system (2-3 J/m²) [88]. The reason for the difference in the case of the interlayer is most likely due to large amount of plastic deformation the film undergoes during tensile testing and which the Hutchinson and Suo [16] model does not account for.

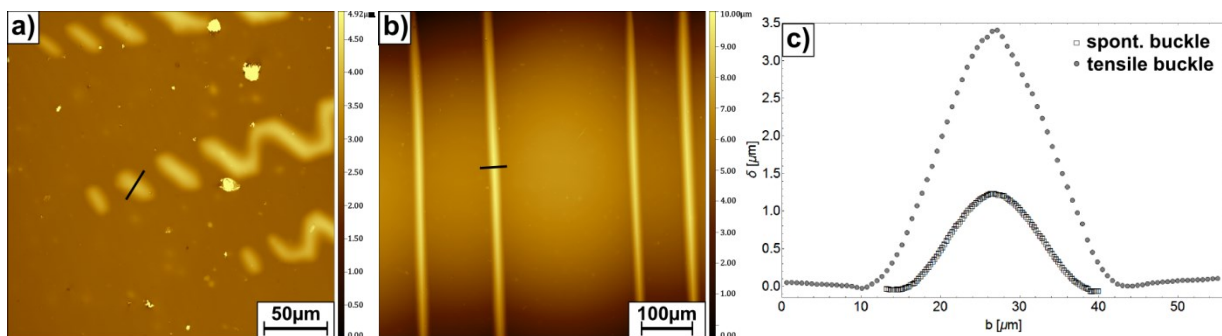

Figure 5.1: CLSM height image of spontaneous buckles forming in the Au film with no interlayer (a) and the tensile induced buckles for the case of the Ta interlayer in (b). The comparison of the profiles of the buckles of each system is shown (c) and the location where the profiles have been take is indicated in (a) and (b) by the black lines.

The focus of Publication *II* was the comparison of the adhesion energies from nanoindentation and scratch testing to spontaneous buckles on two WTi-BPSG systems, one with annealed and one with unannealed BPSG. Figure 5.2 show examples of the delaminations induced by the three different techniques. The results, shown in Table I,

illustrated that the adhesion calculation from the spontaneous and scratch induced buckles matched each other well. The buckles induced by scratch testing were of spontaneous nature and thus this technique is an ideal source for determining the adhesion energies of thin films. The blisters caused by nanoindentation included additional delamination of the BPSG and fracture of the underlying Si leading to lower adhesion values due to the multiple interfaces which fractured. The comparison of the calculated adhesion energies of the WTi film on the BPSGs to results measured from other techniques illustrated that they are very similar to the adhesion energies of pure W on glass-like substrates [10,11,17]. Additionally, the results show little difference between the two samples and thus little influence on the adhesion due to the annealing of the BPSG.

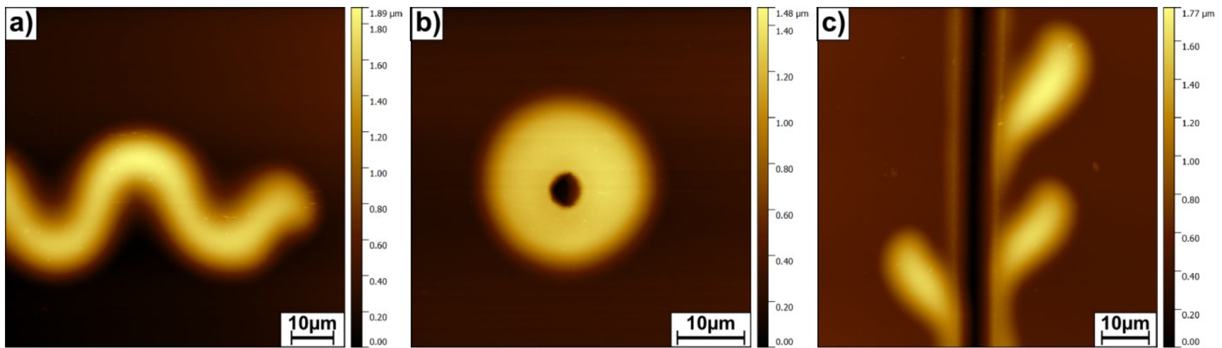

Figure 5.2: AFM images of (a) spontaneous, (b) indentation induced and (c) scratch induced buckles on the WTi-BPSG film system.

Table I: Summary of the calculated adhesion energies for the WTi film on unannealed and annealed BPSG using three different buckle geometries.

Sample	Unannealed BPSG		Annealed BPSG	
	$\Gamma(\psi)$ $[J/m^2]$	Γ_I $[J/m^2]$	$\Gamma(\psi)$ $[J/m^2]$	Γ_I $[J/m^2]$
Spontaneous buckles	*2.48±0.36*	*0.51±0.08*	*2.59±0.62*	*0.54±0.13*
Scratches	*2.72 ±0.74*	*0.66±0.19*	*3.14±0.85*	*0.65±0.17*
Indents	*1.91 ±0.43*	*0.77±0.27*	*2.1±0.5*	*0.87±0.24*

Further investigation of fracture events caused by nanoindentation was conducted in Publication *III*, where a Si_3N_4 on BPSG film with a WTi stressed overlayer was indented to induce delamination and buckling. Depending on the load, different types of buckles were produced as shown in Figure 5.3. By utilizing FIB and laser cross-sectioning the delamination process for this system was revealed which would otherwise be concealed under the surface. The small buckles were the result of an engulfed fracture path not distinctive for any interface

while the large buckles were mainly the result a single interface separation between the Si_3N_4 and the BPSG.

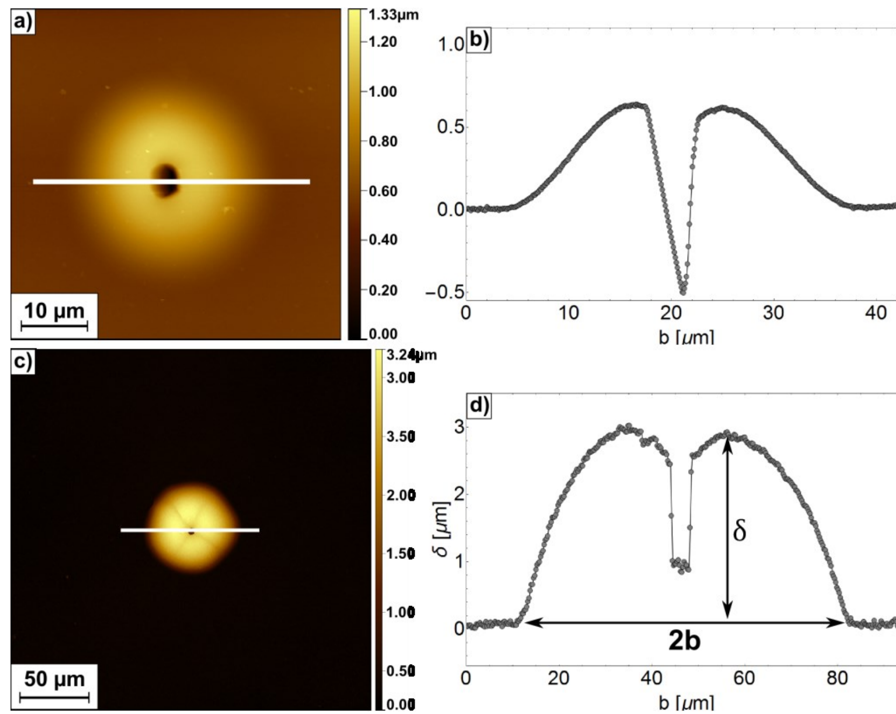

Figure 5.3: Images of indentation buckles produced from loads of 300 mN, with the white line indicating where the buckle profile is measured. (a) AFM image of a small buckle and (b) the according profile displaying an unpinned geometry. (c) Large buckle imaged with CLSM with the corresponding profile (d).Figure taken from [74].

The adhesion energies are shown in Table II and demonstrate how the buckle size affects the adhesion calculation. Due the cross-sectioning of the two buckle types it can be concluded that the small buckles do not represent a distinct interface failure and the adhesion cannot be calculated. The values from the large buckles are reasonable for ceramic-ceramic interfaces and agreed well with other results where adhesion energy of a Si_xN_y/SiO_2 interface was reported to be 1.2-1.8 J/m² [89]. Additionally, it was found that the half buckles which were not fully circular, due to radial cracking of the Si_3N_4 film, could also be used for adhesion calculation and Table II illustrates that the results of the full and half buckles are equivalent for this system. It also demonstrated that the WTi overlayer supported the brittle Si_3N_4 film and provided the necessary compressive stress which made the buckling possible in the first place and allowed the calculation of the adhesion energy.

Table II: Summary of half buckle widths (b), buckling stresses (σ_b), and mixed mode adhesion energies ($\Gamma(\Psi)$) from the buckles produced by nanoindentation shown in Figure 5.3.

Buckle Type	$b[\mu m]$	$\sigma_b[MPa]$	$\Gamma(\Psi)$ $[J/m^2]$
Small (Figure 5.3a)	15.8±1.7	525.7±115	1.13±0.31
Large (Figure 5.3c)	31.7±2.8	128.9±23	1.35±0.28
Half	30.9±4.2	138.1±32	1.36±0.16

Publication *IV* demonstrated the effect of annealing duration at 400°C on the film stress and adhesion of a WTi/BPSG system using scratch induced buckles. The buckle size and amount decreased significantly as the annealing times were increased and the calculated film stresses were in good agreement with the stresses measured with laboratory XRD and wafer curvature. From the scratch induced buckles the adhesion energy of the WTi film to the BPSG substrate was calculated and showed the increase of interface strength with annealing time up to two hours, as shown in Figure 5.4. The results for the 1 hour anneal compares well to energies measured form other methods [9,11]. The increase of adhesion energy with annealing time is due to the segregation of the Ti atoms from the WTi film towards the WTi-BPSG interface where they form a new film which a few atom layers thick, a behavior reported before [9].

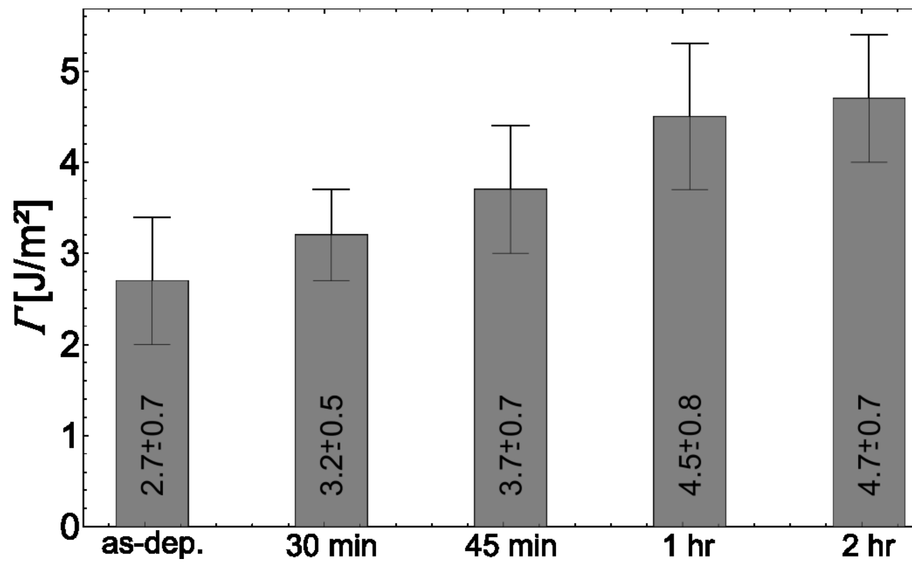

Figure 5.4: The mixed mode adhesion energies, $\Gamma(\Psi)$, for the as-deposited and the annealed WTi films. The adhesion energy increases continuously with the annealing time up to approximately 1-2 hours. Figure taken from [87].

Finally, in Publication *V* the development and mechanisms behind the scratch induced buckles were studied on two sample systems, WTi/BPSG and WTi/Si3N4/BPSG. Two types

of delaminations occurred from the scratch test: parallel buckles along the trace and spontaneous buckles originating from the parallel buckles. Delaminations parallel to the trace were produced as direct result of the scratching through a combination of the deformation and fracture of the films induced by the scratch and residual stresses. The initial parallel delaminations were the point of origin for the spontaneous telephone cord buckles which developed and propagated away from the scratch trace. Adhesion was calculated by modeling the spontaneous buckles as straight sided buckles and the parallel buckles as pinned blisters, with the results matching each other well and shown in Table III.

Table III: Mixed mode adhesion energies ($\Gamma(\Psi)$) from the spontaneous and parallel buckles produced by scratch testing.

Sample	WTi/BPSG	WTi/Si3N4/BPSG
	$\Gamma(\Psi)$ $[J/m^2]$	
Spontaneous buckles	2.7±0.6	1.54±0.3
Parallel buckles	2.1±0.2	1.54±0.2

The lower adhesion energy calculated from the parallel buckles on the WTi/BPSG system is due the geometry change of the buckle because of the amount of plastic deformation of the films resulting from the scratch. On the WTi/Si_3N_4/BPSG system the results for the parallel buckles match the spontaneous well because the here the deformation due to scratching is small compared to the buckle size. Additionally, the scratch buckles exhibit less fracture on the buckle surface compared to the indentation buckles which had radial cracking, suggesting that less energy is dissipated by fracture on the scratch buckles and the calculated adhesion energy is more accurate. It was also shown that the scratch test can be combined with stressed overlayers in order to produce buckles on brittle ceramic films (WTi/Si_3N_4/BPSG system). The technique works well for thin films with thickness in the range of a few hundred nanometers where nanoindentation has problems with substrate fracture. Moreover, it should be noted that one scratch is able to induce a large amount of buckles on both systems which provide better statistics for adhesion calculations compared to other methods.

However, the techniques used and presented in the course of this study are limited by film thickness due to the fact that the stresses induced by an indent or scratch in a film that is very thin (< 100 nm) or thick film (> 1 µm) may not reach the interface to cause delamination or the state of compressive stress is not high enough for buckling to occur. In many cases an

additional compressively stressed overlayer can compensate for these problems. In conclusion, buckle induced delamination has proven to be a very useful tool to assess the adhesion of thin films and can be a good source for reliable measurements given a careful post-buckling characterization.

References

[1] L.B. Freund, S. Suresh, Thin Film Materials, Cambridge University Press, Cambridge, 2004. doi:10.1017/CBO9780511754715.

[2] W.W. Gerberich, M.J. Cordill, Physics of adhesion, Reports Prog. Phys. 69 (2006) 2157–2203. doi:10.1088/0034-4885/69/7/R03.

[3] P.A. Flinn, Principles and applications of wafer curvature techniques for stress measurements in thin films, Mat Res Soc Symp Proc. 130 (1989) 41–51. doi:10.1557/PROC-130-41.

[4] I.C. Noyan, J.B. Cohen, Residual stress: measurement by diffraction and interpretation, Springer-Verlag, Berlin, 1987.

[5] K.L. Mittal, Adhesion Measurement of Thin Films, Electrocompon. Sci. Technol. 3 (1976) 21–42. doi:10.1155/APEC.3.21.

[6] A.A. Volinsky, N.R. Moody, W.W. Gerberich, Interfacial Toughness Measurements for Thin Films on Substrates, Acta Mater. 50 (2002) 441–466. doi:10.1016/S1359-6454(01)00354-8.

[7] J. Chen, S.J. Bull, Approaches to investigate delamination and interfacial toughness in coated systems: an overview, J. Phys. D. Appl. Phys. 44 (2011) 1–19. doi:10.1088/0022-3727/44/3/034001.

[8] H. Ollendorf, D. Schneider, A comparative study of adhesion test methods for hard coatings, Surf. Coatings Technol. 113 (1999) 86–102. doi:10.1016/S0257-8972(98)00827-5.

[9] B. Völker, W. Heinz, K. Matoy, R. Roth, J.M. Batke, T. Schöberl, et al., Interface fracture and chemistry of a tungsten-based metallization on borophosphosilicate glass, Philos. Mag. 6435 (2014) 1–15. doi:10.1080/14786435.2014.913108.

[10] B. Völker, W. Heinz, K. Matoy, R. Roth, J.M. Batke, T. Schöberl, et al., Mechanical and chemical investigation of the interface between tungsten-based metallizations and annealed borophosphosilicate glass, Thin Solid Films. 583 (2015) 170–176. doi:10.1016/j.tsf.2015.03.047.

[11] K. Matoy, T. Detzel, M. Müller, C. Motz, G. Dehm, Interface fracture properties of thin films studied by using the micro-cantilever deflection technique, Surf. Coatings Technol. 204 (2009) 878–881. doi:10.1016/j.surfcoat.2009.09.013.

[12] P.G. Charalambides, H.C. Cao, J. Lund, A.G. Evans, Development of a test method for measuring the mixed mode fracture resistance of bimaterial interfaces, Mech. Mater. 8 (1990) 269–283. doi:10.1016/0167-6636(90)90047-J.

[13] P.G. Charalambides, J. Lund, A.G. Evans, R.M. McMeeking, A Test Specimen for Determining the Fracture Resistance of Bimaterial Interfaces, J. Appl. Mech. 56 (1989) 77. doi:10.1115/1.3176069.

[14] M.R. Miller, M.C. Mello, Laser spallation adhesion metrology for electronic packaging development, 52nd Electron. Components Technol. Conf. 2002. (Cat. No.02CH37345).

(2002) 192–198. doi:10.1109/ECTC.2002.1008094.

[15] J. Wang, N.R. Sottos, R.L. Weaver, Thin Film Adhesion Measurement by Laser Induced Stress Waves, (n.d.).

[16] J.W. Hutchinson, Z. Suo, Mixed Mode Cracking in Layered Materials, Adv. Appl. Mech. 29 (1991) 63–191. doi:10.1016/S0065-2156(08)70164-9.

[17] M.J. Cordill, D.F. Bahr, N.R. Moody, W.W. Gerberich, Recent Developments in Thin Film Adhesion Measurement, IEEE Trans. Device Mater. Reliab. 4 (2004) 163–168. doi:10.1016/j.msea.2006.08.027.

[18] A.G. Evans, D.B. Marshall, on the Mechanics of Delamination and, Int. J. Solids Struct. 20 (1984) 455–466.

[19] A.G. Evans, J.W. Hutchinson, On the mechanics of delamination and spalling in compressed films, Int. J. Solids Struct. 20 (1984) 455–466. doi:10.1016/0020-7683(84)90012-X.

[20] M.J. Cordill, D.F. Bahr, N.R. Moody, W.W. Gerberich, Adhesion measurements using telephone cord buckles, Mater. Sci. Eng. A. 443 (2007) 150–155. doi:10.1016/j.msea.2006.08.027.

[21] M.W. Moon, H.M. Jensen, J.W. Hutchinson, K.H. Oh, A.G. Evans, The characterization of telephone cord buckling of compressed thin films on substrates, J. Mech. Phys. Solids. 50 (2002) 2355–2377. doi:10.1016/S0022-5096(02)00034-0.

[22] S. Faulhaber, C. Mercer, M.W. Moon, J.W. Hutchinson, A.G. Evans, Buckling delamination in compressed multilayers on curved substrates with accompanying ridge cracks, J. Mech. Phys. Solids. 54 (2006) 1004–1028. doi:10.1016/j.jmps.2005.11.005.

[23] W.D. Nix, Mechanical properties of thin films, Metall. Trans. A. 20 (1989) 2217–2245. doi:10.1007/BF02666659.

[24] D.M. Mattox, Handbook of Physical Vapor Deposition (PVD) Processing, 2nd Edition, William Andrews, Oxford, 2010. doi:10.1016/B978-0-8155-2037-5.00025-3.

[25] R. Schöngrundner, R. Treml, T. Antretter, D. Kozic, W. Ecker, D. Kiener, et al., Critical assessment of the determination of residual stress profiles in thin films by means of the ion beam layer removal method, Thin Solid Films. 564 (2014) 321–330. doi:10.1016/j.tsf.2014.06.003.

[26] K. Sasaki, M. Kishida, T. Itoh, The accuracy of residual stress measurement by the hole-drilling method, Exp. Mech. 37 (1997) 250–257. doi:10.1007/BF02317415.

[27] N. Sabaté, D. Vogel, A. Gollhardt, J. Keller, C. Cané, I. Gràcia, et al., Residual stress measurement on a MEMS structure with high-spatial resolution, J. Microelectromechanical Syst. 16 (2007) 365–372. doi:10.1109/JMEMS.2006.879701.

[28] A.M. Korsunsky, M. Sebastiani, E. Bemporad, Focused ion beam ring drilling for residual stress evaluation, Mater. Lett. 63 (2009) 1961–1963. doi:10.1016/j.matlet.2009.06.020.

[29] G.G. Stoney, The Tension of Metallic Films Deposited by Electrolysis, Proc. R. Soc. A

Math. Phys. Eng. Sci. 82 (1909) 172–175. doi:10.1098/rspa.1909.0021.

[30] S. Bigl, W. Heinz, M. Kahn, H. Schoenherr, M.J. Cordill, High-Temperature Characterization of Silicon Dioxide Films with Wafer Curvature, Jom. 67 (2015) 2902–2907. doi:10.1007/s11837-015-1600-8.

[31] S. Bigl, S. Wurster, M.J. Cordill, D. Kiener, Advanced characterisation of thermo-mechanical fatigue mechanisms of different copper film systems for wafer metallizations, Thin Solid Films. 612 (2016) 153–164. doi:10.1016/j.tsf.2016.05.044.

[32] C.A. Klein, How accurate are Stoney's equation and recent modifications, J. Appl. Phys. 88 (2000) 5487–5489. doi:10.1063/1.1313776.

[33] J.M. Pureza, M.M. Lacerda, A.L. De Oliveira, J.F. Fragalli, R.A.S. Zanon, Enhancing accuracy to Stoney equation, Appl. Surf. Sci. 255 (2009) 6426–6428. doi:10.1016/j.apsusc.2009.01.097.

[34] G.C.A.M. Janssen, M.M. Abdalla, F. van Keulen, B.R. Pujada, B. van Venrooy, Celebrating the 100th anniversary of the Stoney equation for film stress: Developments from polycrystalline steel strips to single crystal silicon wafers, Thin Solid Films. 517 (2009) 1858–1867. doi:10.1016/j.tsf.2008.07.014.

[35] G.H. Olsen, M. Ettenberg, Calculated stresses in multilayered heteroepitaxial structures, J. Appl. Phys. 48 (1977) 2543–2547. doi:10.1063/1.323970.

[36] V. Teixeira, Mechanical integrity in PVD coatings due to the presence of residual stresses, Thin Solid Films. 392 (2001) 276–281. doi:10.1016/S0040-6090(01)01043-4.

[37] C.H. Hsueh, Thermal stresses in elastic multilayer systems, Thin Solid Films. 418 (2002) 182–188. doi:10.1016/S0040-6090(02)00699-5.

[38] Q. Luo, A.H. Jones, High-precision determination of residual stress of polycrystalline coatings using optimised XRD-sin2ψ technique, Surf. Coatings Technol. 205 (2010) 1403–1408. doi:10.1016/j.surfcoat.2010.07.108.

[39] P.J. Withers, H.K.D.H. Bhadeshia, Residual stress. Part 1 – Measurement techniques, Mater. Sci. Technol. 17 (2001) 355–365. doi:10.1179/026708301101509980.

[40] G.S. Schajer, C.O. Ruud, Overview of Residual Stresses and Their Measurement, in: Pract. Residual Stress Meas. Methods, John Wiley & Sons, Ltd, Chichester, UK, 2013: pp. 1–27. doi:10.1002/9781118402832.ch1.

[41] J. Keckes, M. Bartosik, R. Daniel, C. Mitterer, G. Maier, W. Ecker, et al., X-ray nanodiffraction reveals strain and microstructure evolution in nanocrystalline thin films, Scr. Mater. 67 (2012) 748–751. doi:10.1016/j.scriptamat.2012.07.034.

[42] M. Bartosik, R. Daniel, C. Mitterer, I. Matko, M. Burghammer, P.H. Mayrhofer, et al., Cross-sectional X-ray nanobeam diffraction analysis of a compositionally graded CrNxthin film, Thin Solid Films. 542 (2013) 1–4. doi:10.1016/j.tsf.2013.05.102.

[43] E. Eiper, K.J. Martinschitz, I. Zizak, N. Darowski, J. Keckes, X-ray elastic constants determined by the combination of sin2 ψ and substrate-curvature methods, Zeitschrift Für Met. 96 (2005) 1069–1073.

[44] D.C. Agrawal, R. Raj, Measurement of the ultimate shear strength of a metal-ceramic interface, Acta Metall. 37 (1989) 1265–1270. doi:10.1016/0001-6160(89)90120-X.

[45] O. Glushko, M.J. Cordill, Electrical Resistance of Metal Films on Polymer Substrates Under Tension, Exp. Tech. 40 (2014) 303. doi:10.1111/ext.12082.

[46] Z.G. Suo, J.W. Hutchinson, Interface Crack between 2 Elastic Layers, Int. J. Fract. 43 (1990) 1–18. doi:Doi 10.1007/Bf00018123.

[47] D.M. Lipkin, D.R. Clarke, A.G. Evans, Effect of interfacial carbon on adhesion and toughness of gold-sapphire interfaces, Acta Mater. 46 (1998) 4835–4850. doi:10.1016/S1359-6454(98)00071-8.

[48] M.L. Jokl, V. Vitek, C.J. McMahon, Microscopic Theory of Brittle Fracture in Deformable Solids: a Relation Between Ideal Work To Fracture and Plastic Work., Acta Metall. 28 (1980) 1479–1488. doi:10.1016/0001-6160(80)90048-6.

[49] T.L.Anderson, Fracture mechanics : fundamentals and applications, 2004.

[50] D. Gross, T. Seelig, Fracture Mechanics, 2nd ed., Springer Berlin Heidelberg, Berlin, Heidelberg, 2011. doi:10.1007/978-3-642-19240-1.

[51] G. R. Irwin, Analysis of Stresses and Strains Near the End of a Crack Traversing a Plate, J. Appl. Mech. (1957).

[52] J.W. Hutchinson, M.E. Mear, J.R. Rice, Crack Paralleling an Interface Between Dissimilar Materials, J. Appl. Mech. 54 (1987) 828. doi:10.1115/1.3173124.

[53] J.W. Hutchinson, Stresses and failure modes in thin films and multilayers, in: Notes a Dcamm Course, Lyngby, 1996: p. 45.

[54] H.H. Yu, J.W. Hutchinson, Influence of substrate compliance on buckling delamination of thin films, Int. J. Fract. 113 (2002) 39–55. doi:10.1023/A:1013790232359.

[55] and E.M.L. Landau, Lev D., Theory of Elasticity, Pergamon Press, Oxford, 1986.

[56] J. Dundurs, Edge-Bonded Dissimilar Orthogonal Elastic Wedges Under Normal and Shear Loading, J. Appl. Mech. 36 (1969) 650. doi:10.1115/1.3564739.

[57] Z. Suo, J.W. Hutchinson, Interface crack between two elastic layers, Int. J. Fract. 43 (1990) 1–18. doi:10.1007/BF00018123.

[58] G. Parry, J. Colin, C. Coupeau, F. Foucher, A. Cimetière, J. Grilhé, Effect of substrate compliance on the global unilateral post-buckling of coatings: AFM observations and finite element calculations, Acta Mater. 53 (2005) 441–447. doi:10.1016/j.actamat.2004.09.039.

[59] M.J. Cordill, N.R. Moody, D.F. Bahr, The effects of plasticity on adhesion of hard films on ductile interlayers, Acta Mater. 53 (2005) 2555–2562. doi:10.1016/j.actamat.2005.02.013.

[60] F. Toth, F.G. Rammerstorfer, M.J. Cordill, F.D. Fischer, Detailed modelling of delamination buckling of thin films under global tension, Acta Mater. 61 (2013) 2425–2433. doi:10.1016/j.actamat.2013.01.014.

[61] M.D. Kriese, W.W. Gerberich, N.R. Moody, Quantitative adhesion measures of multilayer films: Part I. Indentation mechanics, J. Mater. Res. 14 (1999) 3007–3018. doi:10.1557/JMR.1999.0404.

[62] J.W. Hutchinson, M.D. Thouless, E.G. Liniger, Growth and configurational stability of circular, buckling-driven film delaminations, Acta Metall. Mater. 40 (1992) 295–308. doi:10.1016/0956-7151(92)90304-W.

[63] J.-Y. Faou, G. Parry, S. Grachev, E. Barthel, How Does Adhesion Induce the Formation of Telephone Cord Buckles?, Phys. Rev. Lett. 108 (2012) 116102. doi:10.1103/PhysRevLett.108.116102.

[64] D. Nir, Stress relief forms of diamond-like carbon thin films under internal compressive stress, Thin Solid Films. 112 (1984) 41–50. doi:10.1016/0040-6090(84)90500-5.

[65] G. Parry, A. Cimetière, C. Coupeau, J. Colin, J. Grilhé, Stability diagram of unilateral buckling patterns of strip-delaminated films, Phys. Rev. E - Stat. Nonlinear, Soft Matter Phys. 74 (2006) 1–7. doi:10.1103/PhysRevE.74.066601.

[66] B. Audoly, Stability of straight delamination blisters, Phys. Rev. Lett. 83 (1999) 4124–4127. doi:10.1103/PhysRevLett.83.4124.

[67] S.J. Yu, Y.J. Zhang, H. Zhou, P.G. Cai, M.G. Chen, Buckle morphologies of wedge-shaped Fe films quenched by silicone oil during deposition, Appl. Surf. Sci. 256 (2009) 909–915. doi:10.1016/j.apsusc.2009.08.084.

[68] S.Y. Grachev, A. Mehlich, J.D. Kamminga, E. Barthel, E. Søndergård, High-throughput optimization of adhesion in multilayers by superlayer gradients, Thin Solid Films. 518 (2010) 6052–6054. doi:10.1016/j.tsf.2010.06.049.

[69] A. Kleinbichler, M. Bartosik, B. Völker, M.J. Cordill, Thin Film Adhesion of Flexible Electronics Influenced by Interlayers, Adv. Eng. Mater. 19 (2017) 1600665. doi:10.1002/adem.201600665.

[70] A. Kleinbichler, J. Zechner, M.J. Cordill, Buckle induced delamination techniques to measure the adhesion of metal dielectric interfaces, Microelectron. Eng. 167 (2017) 63–68. doi:10.1016/j.mee.2016.10.020.

[71] A.C. Fischer-Cripps, Nanoindentation, Springer New York, New York, NY, 2004. doi:10.1007/978-1-4757-5943-3.

[72] W.C. Oliver, G.M. Pharr, An improved technique for determining hardness and elastic modulus using load and displacement sensing indentation experiments, J. Mater. Res. 7 (1992) 1564–1583. doi:10.1557/JMR.1992.1564.

[73] J.L. Hay, M.E. O'Hern, W.C. Oliver, Tie Importance of Contact Radius for Substrate-Independent Property Measurement of Thin Films, MRS Proc. 522 (1998) 27. doi:10.1557/PROC-522-27.

[74] A. Kleinbichler, M.J. Pfeifenberger, J. Zechner, N.R. Moody, D.F. Bahr, M.J. Cordill, New Insights into Nanoindentation-Based Adhesion Testing, JOM. 69 (2017) 2237–2245. doi:10.1007/s11837-017-2496-2.

[75] D.B. Marshall, A.G. Evans, Measurement of adherence of residually stressed thin films by indentation. I. Mechanics of interface delamination, J. Appl. Phys. 56 (1984) 2632–2638. doi:10.1063/1.333794.

[76] C. Rossington, A.G. Evans, D.B. Marshall, B.T. Khuri-Yakub, Measurements of adherence of residually stressed thin films by indentation. II. Experiments with ZnO/Si, J. Appl. Phys. 56 (1984) 2639–2644. doi:10.1063/1.333795.

[77] A. Roshanghias, G. Khatibi, R. Pelzer, J. Steinbrenner, On the effects of thickness on adhesion of TiW diffusion barrier coatings in silicon integrated circuits, Surf. Coatings Technol. 259 (2014) 386–392. doi:10.1016/j.surfcoat.2014.10.065.

[78] A.A. Volinsky, J.B. Vella, W.W. Gerberich, Fracture toughness, adhesion and mechanical properties of low-K dielectric thin films measured by nanoindentation, Thin Solid Films. 429 (2003) 201–210. doi:10.1016/S0040-6090(03)00406-1.

[79] A. Lee, B.M. Clemens, W.D. Nix, Stress induced delamination methods for the study of adhesion of Pt thin films to Si, Acta Mater. 52 (2004) 2081–2093. doi:10.1016/j.actamat.2004.01.003.

[80] H.H. Yu, J.W. Hutchinson, Delamination of thin film strips, Thin Solid Films. 423 (2003) 54–63. doi:10.1016/S0040-6090(02)00973-2.

[81] S.J. Bull, Failure mode maps in the thin film scratch adhesion test, Tribol. Int. 30 (1997) 491–498. doi:10.1016/S0301-679X(97)00012-1.

[82] S.J. Bull, Failure modes in scratch adhesion testing, Surf. Coatings Technol. 50 (1991) 25–32. doi:10.1016/0257-8972(91)90188-3.

[83] P.A. Steinmann, Y. Tardy, H.E. Hintermann, Adhesion testing by the scratch test method: The influence of intrinsic and extrinsic parameters on the critical load, Thin Solid Films. 154 (1987) 333–349. doi:10.1016/0040-6090(87)90377-4.

[84] S. Venkataraman, D.L. Kohlstedt, W.W. Gerberich, Microscratch analysis of the work of adhesion for Pt thin films on NiO, J. Mater. Res. 7 (1992) 1126–1132. doi:10.1557/JMR.1992.1126.

[85] N.R. Moody, R.Q. Hwang, S. Venka-taraman, J.E. Angelo, D.P. Norwood, W.W. Gerberich, Adhesion and fracture of tantalum nitride films, Acta Mater. 46 (1998) 585–597. doi:10.1016/S1359-6454(97)00243-7.

[86] S.J. Bull, E. G.-Berasetegui E., Chapter 7 An overview of the potential of quantitative coating adhesion measurement by scratch testing, in: Tribol. Interface Eng. Ser., 2006: pp. 99–114. doi:10.1016/S0167-8922(06)80043-X.

[87] A. Kleinbichler, J. Todt, J. Zechner, S. Wöhlert, D.M. Többens, M.J. Cordill, Annealing effects on the film stress and adhesion of tungsten-titanium barrier layers, Surf. Coatings Technol. 332 (2017) 376–381. doi:10.1016/j.surfcoat.2017.07.087.

[88] J.D. Yeager, D.J. Phillips, D.M. Rector, D.F. Bahr, Characterization of flexible ECoG electrode arrays for chronic recording in awake rats, J. Neurosci. Methods. 173 (2008) 279–285. doi:10.1016/j.jneumeth.2008.06.024.

[89] Q. Ma, A four-point bending technique for studying subcritical crack growth in thin

films and at interfaces, J. Mater. Res. 12 (1997) 840–845. doi:10.1557/JMR.1997.0122.

Publication I

Published in *Advanced Engineering Materials*

DOI: 10.1002/adem.201600665

Thin film adhesion of flexible electronics influenced by interlayers

A. Kleinbichler[1], M. Bartosik[2,3], Bernhard Völker[1] and M. J. Cordill[1,2]

[1]Erich Schmid Institute for Material Science, Austrian Academy of Sciences, Jahnstraße 12, Leoben, Austria, 8700

[2]Dept. Material Physics, Montanuniversität Leoben, Jahnstraße 12, Leoben, Austria, 8700

[3] Institute of Materials Science and Technology, TU Wien, Getreidemarkt 9, Vienna, Austria 1060

With the emergence of flexible electronics in the fields of medical sensors and foldable displays, there is a need to understand the interfacial behavior between active conducting elements and compliant polymer substrates, on which the devices are fabricated. Compression induced delamination is one technique that can be utilized to assess interfacial adhesion of flexible substrates that only uses the resulting buckle dimensions to quantitatively evaluate adhesion. It is found that spontaneous buckles formed in the Au film without the interlayer after deposition, while external loading is required to delaminate the Au film with the Ta adhesion layer indicating a higher adhesion energy.

1. Introduction

Flexible devices and sensors are a new field in the electronics sector and are used in a large variety of applications, such as foldable displays [1-2] or as neural electrodes in medicine [3-4]. The primary goal of designing flexible electronics is to achieve large (>10%) strains, without losing electronic functionality. Many designs to achieve this goal, consist of small islands of rigid electronics placed on a flexible polymer substrate and connected using metallic lines. In this design, the adhesion between lines and the underlying substrate is of great importance to device reliability. Failure of flexible electronic materials occurs in two forms, either the metallic conducting components fracture via through thick- ness crack formation or the metallic layers delaminate from the substrate. The cracking failure has been thoroughly addressed with several testing techniques, the most popular being tensile straining [5-9] and bending[10-13]. Both of these methods examine the cracking behavior as well as the electrical behavior. Techniques used to evaluate the adhesion of thin films to rigid substrates have advanced our understanding of adhesion and its mechanisms[14–19]. While, these

methods work well for films on rigid substrates in the case of flexible electronics, the matter becomes more challenging and the methods and models for rigid substrates cannot always be employed. Newly introduced methods, like tensile induced delamination [20,21] or compression induced buckling [22,23], can instead be utilized. These techniques work well for brittle films [24–26], but require an extensive amount of straining for ductile films [27] or an overlayer to induce delamination at lower levels of strain [28,29].

Noble metals, such as Au or Ag, are the materials of choice for the connecting lines between the semiconducting islands. It is advantageous to use these metals, because they are ductile, have a low electric resistance, and can be easily deposited and patterned. Unfortunately, these metals, sometimes, have trouble adhering to the polymer substrates used in flexible electronics. Therefore, interlayers, like Ti, Ta, and Cr, are used to improve the adhesion of the noble metal to the polymer substrate [26,27,30]. In order to measure the effective- ness of interlayers on the adhesion energy, simple and effective methods are used. Since, the conducting metals used are ductile, methods that can induce defined areas of delamination are desired. Buckling based techniques are ideal, because plastic deformation is minimized and buckle delamination is well understood [31–33]. Spontaneous buckling can occur, when the residual stress of the film is large and compressive, typically in the range of 0.5–2 GPa, but normally does not occur on polymer substrates because the substrate can accommodate the film stress by macroscopically bending. However, tensile induced delamination was shown to be effective at creating buckles in a ductile film system of 50nm Cu with a 10nm Cr interlayer [26]. In this work, compression induced delamination will be used to cause a 300nm Au film to buckle upon unloading rather than during loading. Buckles that form during tensile unloading will be compared to spontaneous buckles and used to measure the adhesion energy. With the proper utilization of the different buckling phenomena, the adhesion energy of the interface, and how much the additions of interlayers improves adhesion can be quantified.

2. Experiments

The Au films were deposited onto the substrate without any plasma pre-treatment of the polyimide (PI). The 300nm thick Au films were sputter deposited with and without at 10nm Ta interlayer using a DC Magnetron system onto the 50mm thick Polyimide (Kapton) substrates, following the same process of Yeager et al [3,34]. The Ta film was used as an interlayer to improve the adhesion between Au and PI.

After removal from the deposition chamber, the Au–PI system (without Ta)

delaminated spontaneously at the metal- polymer interface in the form of straight sided and telephone cord buckles due to the high compressive residual stress in the films (approximately 500MPa, measured with the buckle dimensions discussed later). Typical dimensions of spontane- ous buckles range from a few 100 nm to a few micrometers in height and length, respectively. In order to measure the buckle dimensions, two different devices are used, the atomic force microscope (AFM) and the confocal laser scanning micro- scope (CLSM). A Veeco Dimension AFM and a 3D CLSM Olympus LEXT OLS4100, which uses a laser-wavelength of λlaser¼405nm were utilized. Because its maximum lateral image size is 80 x 80 µm and vertical limit of 6 µm, the AFM was used only to image smaller buckles. The CLSM can be used to measure all buckles sizes, since its vertical limit depends on the distance of the objective to the sample. The same buckles on the Au film have been imaged with both methods to ensure comparability of the results. Gwyddion [35] was used to analyze the images and measure the dimensions of the buckles.

The Au–Ta–PI film system did not spontaneously delaminate after deposition. Therefore, straining samples were cut using a scalpel to approximately 5 mm in width and 35 mm in length. The film-substrate system was incrementally strained in tension to different levels of maximum strain (2 to 14%) and unloaded to a force of 2N using an Anton Paar TS 600 straining stage. The incremental load-unload experiments were performed in-situ under an optical light microscope and in-situ with X-ray diffraction (XRD). The latter was used to determine the stresses, which developed in the Au films at the maximum applied strains and when the sample was in an unloaded condition (approximately 2N load) along the applied strain direction. For this, the tensile device was mounted on the Eulerian cradle of a Seifert 3000 PTS X-ray diffractometer, so that the sample surface was in reflection geometry. The diffractometer was equipped with polycapillary optics on the primary side, soller slits, a monochromator and a scintillation detector on the secondary side. The spot size of the monochromatic Cu Kα radiation was about 3 mm. The relatively large beam size enabled the assessment of volume-averaged properties. The in-plane stresses were determined with the $\sin^2 \Psi$ method[36] ($\sin^2 \Psi$ range 0-0.7 (-)). A Pseudo-Voigt fit function was used to determine the peak positions of the (220) Au reflections. The measured strains were converted into stresses using X-ray elastic constants (XECs) (1/2 S_2)[37] for (220) Au reflections. XECs were calculated from single-crystal elastic constants assuming the Hill model with the software ElastiX [38]. Additional optical light microscopy, scanning electron microscopy (SEM), focused ion beam (FIB) cross-sectioning, AFM and CLSM were also used for the post-characterization of the samples.

The buckle dimensions directly relate to the critical buckling stress and the delamination driving, or residual, stress of the film at the interface. The stresses and the interfacial fracture energies can be calculated using the well-known Hutchinson and Suo model [31]. The method is based on the Euler beam theory. The required inputs are the buckle height, *δ*, and the half buckle width, *b*, the film thickness, *h*, as well as the elastic properties of the film (elastic modulus, *E*, and Poisson's ratio, *ν*) (Figure 1). With these values the critical buckling stress, σ_b, and the driving stress, σ_d, can be calculated by using [31]

$$\sigma_b = \frac{\pi E}{12(1-\nu^2)}\left(\frac{h}{b}\right)^2, \tag{1}$$

$$\sigma_d = \sigma_b\left[\frac{3}{4}\left(\frac{\delta}{h}\right)^2 + 1\right]. \tag{2}$$

The critical buckling stress is the stress necessary to cause film delamination and the driving stress propagates the buckles. The interfacial fracture energy, *Γ(Ψ)*, for spontaneous buckles is given as

$$\Gamma(\Psi) = \left[\frac{(1-\nu^2)h}{2E}\right](\sigma_d - \sigma_b)(\sigma_d + 3\sigma_b) \tag{3}$$

and is used to calculate the adhesion energy of the interfaces.

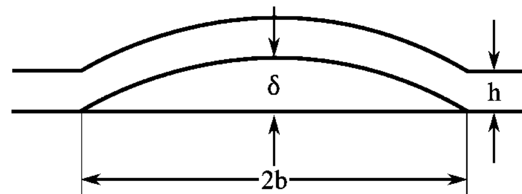

Figure 1: Schematic diagram of a buckle *cross-section showing the measurements of buckle height, δ, buckle width, 2b, and* film thickness, *h*.

3. Results

As previously mentioned, the Au–PI film spontaneously delaminated after deposition, while the Au–Ta–PI did not delaminate. Therefore, a loading-unloading experiment was performed to create buckles to access the adhesion energy. After straining to a maximum strain of 15% and unloading the sample, straight buckles perpendicular to the straining direction (Figure 2) were observed. Normally, buckles form parallel to the straining direction when tensile induced delamination is used, because a compressive stress builds up due to the difference in the Poisson's ratio between film and substrate[20,39]. The appearance and spacing of the buckles perpendicular to the straining direction is similar to cracking of brittle films under

tension. It should be noted that this is not the first observation of compression induced delamination of Au on PI. Renault, et al. [33] first observed this in a 320nmthick Au film and Coupeau et al. [40,41] have extensively studied how buckles form, under compression loading in Ni films on polycarbonate.

Figure 2: Optical micrograph of the *Au-Ta-Pi film strain 15% and unloaded. The straight buckles formed perpendicular to the straining* direction (arrow).

In order to determine the maximum amount of strain required to cause buckling, the incremental load-unload program was utilized to observe the delamination in-situ with an optical light microscope. The loading segments varied between 2 and 14% strain, while the unloading segments always went to 2 N load (approximately zero load). Optical micrographs were taken at the peak strains and at every 1% decreasing strain during unloading. Figure 3 shows a series of optical micrographs froman in-situ experiment. As shown in the figure at 0% strain (Figure 3a), no buckles are observed. At a maximum strain of 8% (Figure 3b) small buckles parallel to the straining direction (arrow in Figure 3a) are visible at a pre- existing scratch. Upon unloading to a strain of 3% (Figure 3c), buckles perpendicular to the straining direction are observed, mostly clustered at a series of scratches. When the sample is loaded in tension up to 10% strain (Figure 3d), the buckles that formed are now flat and only the small parallel buckles are visible. Unloading again produces perpendicular buckles (Figure 3e), with an increasing density away from the initial scratch cluster. Loading to 12% (Figure 3f), flattens the buckles and during unloading (Figure 3g) even more buckles are present, have elongated or have joined other buckles. At the maximum applied strain of 14% (Figure 3h), the film surface is again mostly flat. The last three images (Figure 3i–k) illustrate, how the buckles form and that the density increases during the removal of the tensile load. What can be observed in Figure 3, is that with each increasing load step, existing interface cracks grow or more are nucleated which, in turn, produces more buckles upon unloading. Finally, Figure 3l shows the measured buckle spacing as a function of the unloading strain starting from 14% strain. The buckle spacing during unloading follows the same trend as crack spacing during

tensile loading, where the spacing decreases until saturation or plateau is reached. The saturation buckle spacing is attained approximately at7% unloading strain with a value of about 35mm. Note that in Figure 3l, the X-axis is reversed, starting fromthe maximum applied strain at the left and decreasing to zero strain. From this and subsequent in-situ optical experiments, it was found that approximately 6–8% maximum strain is required to cause delamination upon unloading.

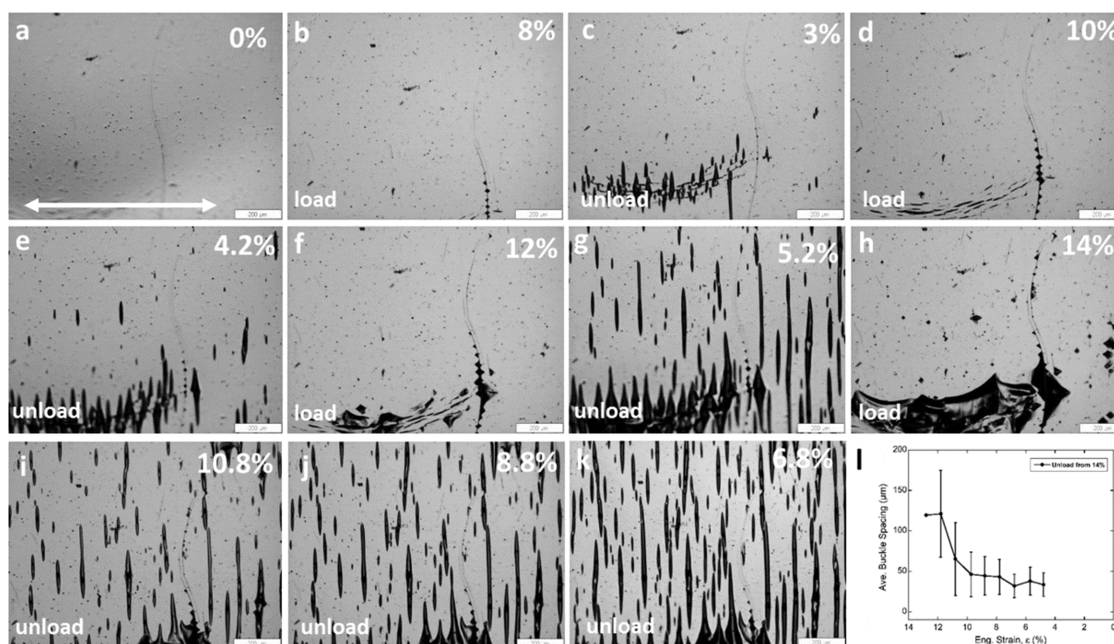

Figure 3: In-situ optical incremental *load-unload experiment. The arrow in (a) indicates the straining direction. In (a), (b), (d), (f) and (h) the film is under tension and (c), (e), and (g), the film is in an unloaded state, and (i)-(k) is a series during unloading. The buckle spacing decreases with decreasing strain (buckle density increases) and reaches a saturation spacing at approximately 7% unloading strain (l). Note* that x-axis in (l) is reversed.

It is known that buckles will form in a thin film, when a large enough compressive stress is present. In order to confirm the presence of a compressive stress, in-situ XRD using the sin2c method was employed to determine the stress in the Au film at the maximum applied strains and at a load of 2 N. The same incremental load-unload program, as the in-situ optical experiments, was used to capture the stress in the film at buckling, but only to 10% maximum strain. Tensile stresses on the order of 450–500 MPa were measured at the maximum strains, while at the minimum load a compressive stress was measured at each unloading step (Figure 4). The constant maximum tensile stresses are expected and are similar to the stresses measured for a continuous tensile loading experiment (without unloads). A 300 nm sputtered Au film on PI reaches a peak stress of about 450 MPa when strained and measured in-situ with XRD [29]. In the unloaded state, the measured stresses are initially 90 MPa compressive

and steadily increase to a constant value of about 350 MPa compressive after a maximum applied strain of 6%. Comparing the in-situ XRD to the optical experiments, finds that there is a good agreement between the two tests. Buckling was observed after maximum applied strains of 6–8% during the in-situ optical experiments and at the same range of strain, the compressive stresses reach a plateau. The value of the plateau is also similar to other in-situ XRD results, where buckling is known to occur. For example a Cr–Cu–Ti [28] film system on PI or a 50nmCu film with a 10 nm Cr interlayer on PI [26] show stress plateaus at the similar levels of strain, where buckles form during tensile induced delamination. The stress plateau during unloading occurs because the critical buckling stress was reached.

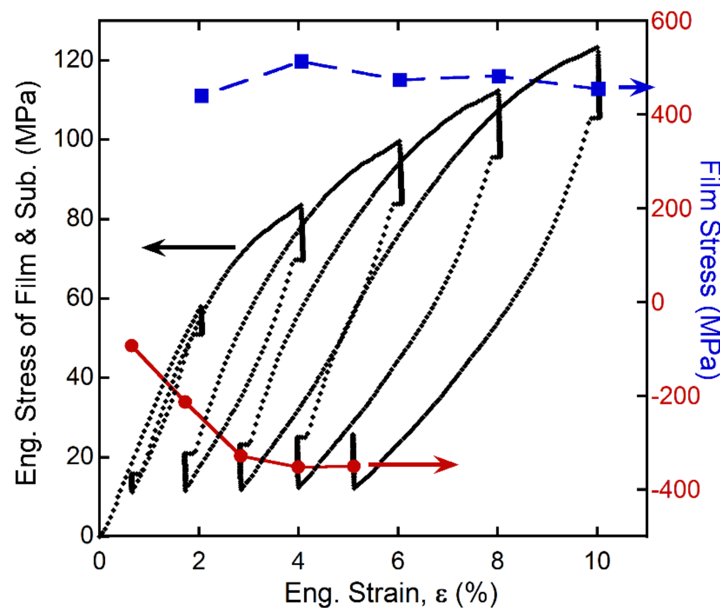

*Figure 4: In-situ XRD experiment results of the incrementally loaded-unloaded Au-Ta-PI film. At the peak and unloaded strains, the stress in the film was determined using the $sin^2\psi$ method. Tensile stresses were found at the peak strains (blue squares) and compressive stresses at unload (red circles). The load drops and load rises are due to the viscoelastic properties of the poly*imide.

To calculate the adhesion energy of the Au–PI film, the spontaneous buckle dimensions were measured with the AFM (Figure 5a) and with the CLSM (Figure 5b). The AFM image shows a 50 x 50 mm area with single buckle of about 1mmin height. The CLSM image shows a 250 x 250 mm area of the gold film with seven single buckles and connected telephone cord buckles. Figure 5b also illustrates that the delamination starts as single straight-sided buckles, but then continues to propagate as telephone cord buckles. This is a common delamination process in biaxially stressed films with spontaneous buckles because of the large amount of shear stresses [42,43]. The buckles, in the white box, in Figure 5b are the same as in Figure

5a. To compare the findings, the same seven single buckles were measured with both imaging methods. These were the only buckles that could be measured with the AFM due to height restrictions. It is obvious that CLSM images a larger area and it is possible to measure more buckles from a single image. The height of the buckles vary and the telephone cord buckles are much taller than the single buckles, more than 5mm in height. Therefore, the AFM is not able to measure most of the telephone cord buckles due to the maximum deflection limit of the cantilevers. The sample height for the CLSM is only limited to the distance of the objective to the sample, which is a few millimeters. In Figure 5c, the cross-sections of the same buckle measured with the two different methods is shown. The marked profiles in the Figure 5a and b indicate where the cross-sections have been taken. Figure 5c shows that the buckle profiles are in good agreement and provide a similar height, δ, and the buckle width, $2b$, for the same buckle.

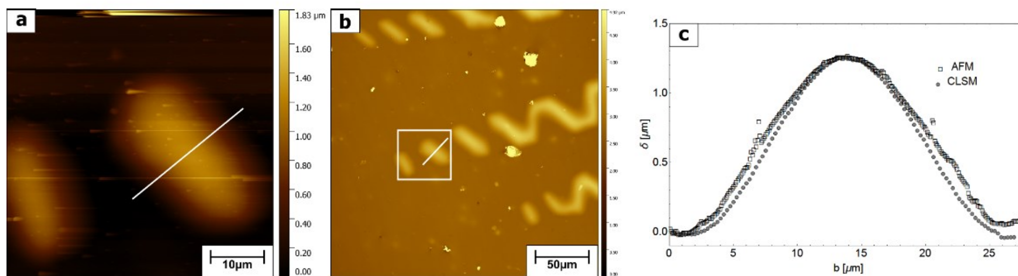

Figure 5: (a) AFM height image of the gold film with two spontaneous buckles. (b) CLSM image of an area with the same buckles as in the AFM image. (c) Cross-section of the same buckle taken at approximately the same position.

Using the elastic properties of $E_{Au=}$77 GPa, and the Poisson's ratio ν_{Au}=0.44 of gold, the stresses calculated from the data of both imaging techniques with the Hutchinson and Suo model [31] are in good agreement. For example, when AFM measurements are used to calculate the critical buckling stress, the value is σ_b=76±24 MPa, compared to the CLSM where σ_b=74±23 MPa is determined. These results were then used to determine the interfacial fracture energies, G(C), using the spontaneous buckles. The G(C) calculated from the values measured, with the AFM are $\Gamma(\Psi)$=0.7±0.3 Jm^{-2} and for the CLSM $\Gamma(\Psi)$=0.8±0.3 Jm^{-2}. The interfacial adhesion values are similar to that for the same interface measured with four point bending (0.8 Jm^{-2}) [3].

From the buckles, which formed on the incremental load-unload samples, the adhesion was also calculated using the Hutchinson and Suo model. The model was chosen because the buckles form spontaneously due to the build-up of compressive stress in the film. Due to the

fact that the compression induced buckles were quite large, only CLSM was used to measure the buckle dimensions (height and width). The buckle heights are almost three times larger than the spontaneous buckles, which formed on the Au–PI (Figure 6). FIB cross-sectioning was used to determine that the Ta–PI interface fails (Figure 7).The critical buckling stress of approximately 350MPadetermined by using Equation 1, nicely correlates with the onset of the leveling off of the compressive stresses observed by XRD (Figure 4). The adhesion energy is also higher for the Au–Ta–PI system. Using Equations 1 through 3 and the elastic properties of Au, the adhesion energy of the Au–Ta–PI film system was determined to be $\Gamma(\Psi)=11.7\pm2.2\ Jm^{-2}$, which is much higher than the Au–PI without the Ta interlayer and illustrates that interlayers can quantitatively improve adhesion of metal-polymer interfaces. A comparison of the measured adhesion energy with four point bending [3] finds that the adhesion energy calculated with the compression induced buckles is larger. The higher measured adhesion energy could be due to the large amount of plastic deformation that the film undergoes that the model does not take fully into account. Possible corrections to the model are currently being investigated.

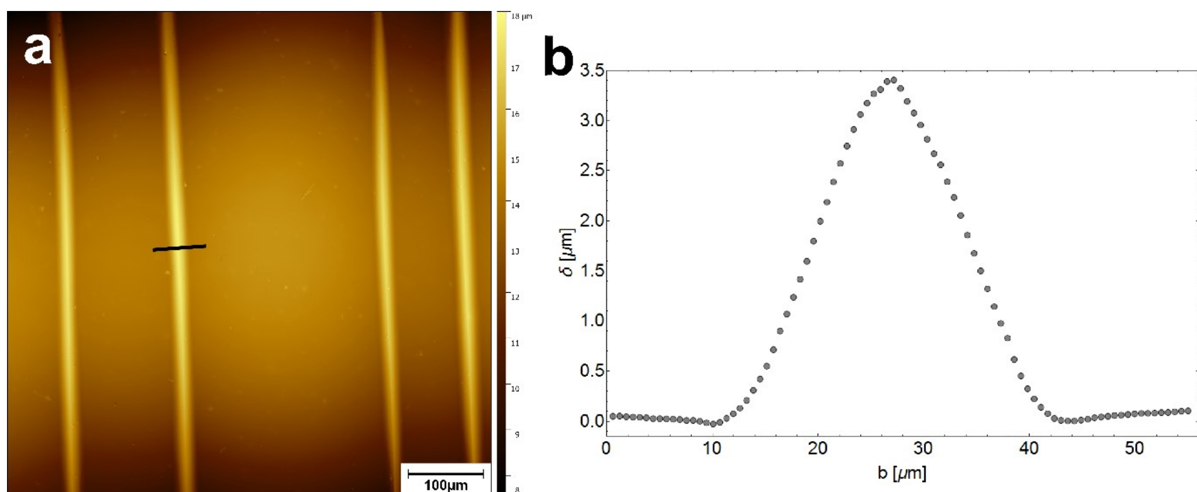

Figure 6: (a) CLSM image of an area with the same buckles as in the AFM image. (b) Cross-section of the buckle taken indicated by the black line in (a).

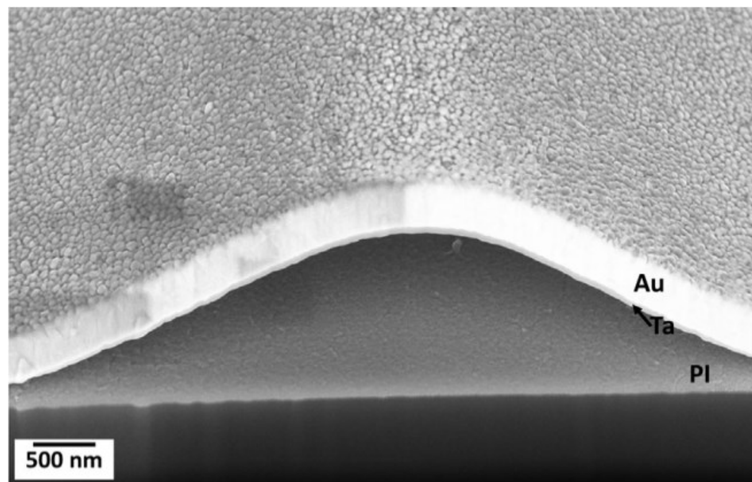

Figure 7: FIB cross-section of a buckle indicating that the Ta-PI interface failed as well as demonstrating that localized necking concentrated at the top of the buckle does not occur.

4. Discussion

Using spontaneous buckles as well as compression induced buckles, the Hutchinson and Suo model [31] could be applied to quantitatively measure adhesion of a metal-polymer interface. It has been shown that a Ta interlayer can greatly improve the adhesion of Au to PI. This was demonstrated by the adhesion calculation as well as by the fact that tensile straining was required to fracture the interface. The formation of long straight buckles perpendicular to the straining direction after unloading from a large applied tensile strain is of interest. From the in-situ XRD experiments, compressive stresses were measured after unloading of the same magnitude found during tensile induced buckling when the buckles form parallel to the straining direction. The compressive stresses measured after unloading increase with increasing applied maximum strain until a plateau was reached. This result indicates that the stresses need to build-up, reaching or exceeding the critical buckling stress before buckling can occur. The stress accumulation is driven by the tensile straining. With each loading step the Au film plastically deforms in the form of localized thinning or necking. Evidence of the necking is shown with an AFM deflection image (Figure 8a, arrows). The small undulations are necking areas and are uniformly distributed over the whole film surface and are not concentrated with the buckle. Uniform plastic deformation in the form of necking has been observed for ductile Cu films on polymer substrates when strained in-situ with AFM [44-46]. In these cases only necking was detected with no buckle delamination because the critical buckling stress was not met. Through the necking mechanism the film's total length is slightly

increased and the increase in length helps the formation of buckles at interface defects during straining as previously shown in Figure 3.

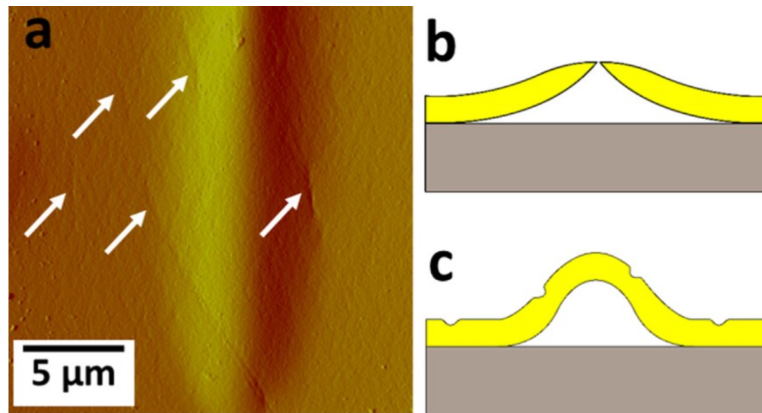

Figure 8: (a) AFM deflection image of a tensile induced buckle illustrating the uniform plastic deformation over the whole film surface and buckle through necking. Schematic diagram of the original free-standing film failure mechanism (b) where the film only deforms at the buckled regions (after ref. 47) and (c) the observed mechanism of uniform deformation of the film with delamination.

Another aspect of the tensile induced delamination that is noteworthy is the fact that after the film delaminates, plastic deformation does not concentrate at the free-standing film areas (buckles) as originally believed [47]. This early theory postulated that if a film is well bonded to a flexible substrate, the substrate will suppress strain localization in the film and results in much larger fracture strains than observed for free-standing films. The original theory also states that when a film becomes free-standing it is more likely to neck and fracture only in the free-standing portions of the film at strains only slightly beyond the elastic limit [47]. Therefore, good adhesion is necessary to suppress the deformation of the film, because if the film delaminates the free-standing portion would have no substrate to suppress the continued plastic deformation (necking) and fail. Figure 8b is a schematic diagram of the original theory. However, the incremental straining experiments demonstrate that even after buckles form free-standing areas, the film continues to uniformly plastically deform. An idealized schematic diagram of the uniform necking is shown in Figure 8c to demonstrate the observed deformation and delamination model. The pre-existing necks are the favored deformation sites and not the free-standing buckles as originally believed in ref. [47]. The FIB cross-section (Figure 7) clearly illustrates that the top of the buckle is not more prone to necking than an adhered portion of the film because the buckle has a uniform thickness. The experimental evidence shown here can be used to update the theoretical models to advance

flexible electronics by enhancing their reliability. The relationship between film deformation under tensile strain and interfacial adhesion is key to further flexible electronic reliability.

5. Conclusions

Flexible electronics are fabricated on compliant polymer substrates and this affects how the adhesion between the metal or ceramic films and the compliant polymer substrate can be measured. The adhesion of a compressively stressed metal-polymer interface can be calculated with the Hutchinson and Suo model using the dimensions of spontaneous buckles. In this study the delamination behavior of the Au-PI film system with and without a Ta interlayer was examined using spontaneously produced buckles (Au-PI) and compression induced buckling (Au-Ta-PI). Incremental tensile straining was used to induce buckles of the Au-Ta-PI system. After 6-8% applied strain, buckles perpendicular to the straining direction formed during unloading. In-situ optical microscopy and XRD straining experiments revealed that after 6-8% applied strain, a compressive stress large enough to induce buckling develops due to the elongation of the Au film during straining. The film elongates because the Au film plastically deforms via uniform necking across the whole film. Necking occurs on account of the good adhesion between the film and substrate which helps to suppress catastrophic failure. This uniform deformation is in contradiction to the original theory that when a film delaminates from the substrate and becomes free-standing, plastic deformation will localize only at free-standing buckled areas. The improved adhesion that the Ta interlayer provides the Au-PI interface and the formation of the buckles perpendicular to the straining direction were crucial factors necessary to determine how film deformation and delamination are connected. With this new understanding the lifetime and reliability of flexible electronics can be extended.

References

[1] A.C. Siegel, S.T. Phillips, M.D. Dickey, N. Lu, Z. Suo, G.M. Whitesides, Adv. Funct. Mater. 2010, 20, 28.

[2] J.A. Rogers, Z. Bao, K. Baldwin, A. Dodabalapur, B. Crone, V.R. Raju, V. Kuck, H. Katz, K. Amundson, J. Ewing, P. Drzaic, Proc. Natl. Acad. Sci. U. S. A. 2001, 98, 4835.

[3] J.D. Yeager, D.J. Phillips, D.M. Rector, D.F. Bahr, J. Neurosci. Methods 2008, 173, 279.

[4] B.A. Hollenberg, C.D. Richards, R. Richards, D.F. Bahr, D.M. Rector, J. Neurosci. Methods 2006, 153, 147.

[5] D.C. Agrawal, R. Raj, Acta Metall. 1989, 37, 1265.

[6] G. Rochat, Y. Leterrier, P. Fayet, J. Manson, Thin Solid Films 2003, 437, 204.

[7] S. Olliges, P.A. Gruber, V. Auzelyte, Y. Ekinci, H.H. Solak, R. Spolenak, Acta Mater. 2007, 55, 5201.

[8] P.A. Gruber, E. Arzt, R. Spolenak, J. Mater. Res. 2009, 24, 1906.

[9] O. Glushko, M.J. Cordill, Exp. Tech. 2014, 40, 303.

[10] W.P. Vellinga, J.T.M. De Hosson, P.C.P. Bouten, J. Appl. Phys. 2011, 110, 7.

[11] Q. Guan, J. Laven, P.C.P. Bouten, G. de With, Thin Solid Films 2016, 611, 107.

[12] O. Glushko, M.J. Cordill, A. Klug, E.J.W. List-Kratochvil, Microelectron. Reliab. 2016, 56, 109.

[13] G.D. Sim, Y. Hwangbo, H.H. Kim, S.B. Lee, J.J. Vlassak, Scr. Mater. 2012, 66, 915.

[14] K.L. Mittal, Electrocompon. Sci. Technol. 1976, 3, 21.

[15] A.A. Volinsky, N.R. Moody, W.W. Gerberich, Acta Mater. 2002, 50, 441.

[16] M. Lane, R.H. Dauskardt, A. Vainchtein, H. Gao, I. Introduction, J. Mater. Res. 2000, 15, 2758.

[17] D.B. Marshall, A.G. Evans, J. Appl. Phys. 1984, 56, 2632.

[18] A. Bagchi, A.G. Evans, Thin Solid Films 1996, 286, 203.

[19] M.J. Cordill, D.F. Bahr, N.R. Moody, W.W. Gerberich, IEEE Trans. Device Mater. Reliab. 2004, 4, 163.

[20] M.J. Cordill, F.D. Fischer, F.G. Rammerstorfer, G. Dehm, Acta Mater. 2010, 58, 5520.

[21] J. Andersons, S. Tarasovs, Y. Leterrier, Thin Solid Films 2009, 517, 2007.

[22] G. Parry, C. Coupeau, J. Colin, a. Cimetière, J. Grilhé, Acta Mater. 2004, 52, 3959.

[23] G. Parry, J. Colin, C. Coupeau, F. Foucher, A. Cimetiere, J. Grilhe, Acta Mater. 2005, 53, 441.

[24] M.J. Cordill, A.A. Taylor, Thin Solid Films 2015, 589, 209.

[25] A.A. Taylor, M.J. Cordill, L. Bowles, J. Schalko, G. Dehm, Thin Solid Films 2013, 531, 354.

[26] V.M. Marx, C. Kirchlechner, I. Zizak, M.J. Cordill, G. Dehm, Philos. Mag. 2015, 95, 1982.

[27] B. Putz, R.L. Schoeppner, O. Glushko, D.F. Bahr, M.J. Cordill, Scr. Mater. 2015, 102, 23.

[28] M.J. Cordill, V.M. Marx, C. Kirchlechner, Thin Solid Films 2014, 571, 302.
[29] M.J. Cordill, O. Glushko, B. Putz, Front. Mater. 2016, 3, 1.
[30] S. Frank, U.A. Handge, S. Olliges, R. Spolenak, Acta Mater. 2009, 57, 1442.
[31] J.W. Hutchinson, Z. Suo, Adv. Appl. Mech. 1992, 29, 63.
[32] F. Cleymand, C. Coupeau, J. Colin, J. Grilhé, Eur. Phys. J. Appl. Phys. 2000, 10, 3.
[33] P.O. Renault, P. Villain, C. Coupeau, P. Goudeau, K.F. Badawi, Thin Solid Films 2003, 424, 267.
[34] J.D. Yeager, D.F. Bahr, Thin Solid Films 2010, 518, 5896.
[35] D. Nečas, P. Klapetek, Open Phys. 2012, 10, 181.
[36] L. Spieß, G. Teichert, R. Schwarzer, H. Behnken, C. Genzel, in Mod. Röntgenbeugung SE - 13, Vieweg+Teubner2009, 453.
[37] I.C. Noyan, J.B. Cohen, Residual Stress: Measurement by Diffraction and Interpretation, Springer-Verlag, New York 2013.
[38] H. Wern, N. Koch, T. Maas, in Mater. Sci. Forum, 2002, 127.
[39] F. Toth, F.G. Rammerstorfer, M.J. Cordill, F.D. Fischer, Acta Mater. 2013, 61, 2425.
[40] C. Coupeau, J.F. Naud, F. Cleymand, P. Goudeau, J. Grilhé, Thin Solid Films 1999, 353, 194.
[41] M. George, C. Coupeau, J. Colin, J. Grilhe, Thin Solid Films 2003, 429, 267.
[42] M.J. Cordill, D.F. Bahr, N.R. Moody, W.W. Gerberich, Mater. Sci. Eng. A 2007, 443, 150.
[43] J.-Y. Faou, G. Parry, S. Grachev, E. Barthel, Phys. Rev. Lett. 2012, 108, 1.
[44] V.M. Marx, F. Toth, A. Wiesinger, J. Berger, C. Kirchlechner, M.J. Cordill, F.D. Fischer, F.G. Rammerstorfer, G. Dehm, Acta Mater. 2015, 89, 278.
[45] J. Berger, O. Glushko, V.M. Marx, C. Kirchlechner, M.J. Cordill, JOM 2016, 68, 1640.
[46] M.J. Cordill, O. Glushko, J. Kreith, V.M. Marx, C. Kirchlechner, Microelectron. Eng. 2014, 137, 96.
[47] Y. Xiang, T. Li, Z. Suo, J.J. Vlassak, Appl. Phys. Lett. 2005, 87, 1.

ime and reliability of flexible electronics can be extended.

Publication II

Published in *Microelectronic Engineering*

DOI: 10.1016/j.mee.2016.10.02

Buckle Induced Delamination Techniques to Measure the Adhesion of Metal Dielectric Interfaces

A. Kleinbichler[1,2], J. Zechner[1], M. J. Cordill[2]

[1]KAI – Kompetenzzentrum Automobil- und Industrieelektronik GmbH, Technologiepark Villach, Europastraße 8, Villach, Austria 9524

[2]Erich Schmid Institute for Material Science, Austrian Academy of Sciences and Dept. Material Physics, Montanuniversität Leoben, Jahnstraße 12, Leoben, Austria, 8700

Abstract

Adhesion of thin metal films on dielectric substrates is one of the most important properties in microelectronic devices due to the fact that interface adhesion determines the device lifetime and reliability. In order to improve the lifetime of these devices, substrate treatments and adhesion layers are often utilized, making a quantitative assessment of adhesion of the utmost importance. A key example of a metal film common in many microelectronic devices is Tungsten-Titanium (WTi), which is used as a diffusion barrier and an adhesion layer. Several testing methods and mechanics-based models have been developed over the last decades to quantitatively evaluate interface adhesion of thin metal films on rigid substrates. For thin films on rigid substrates (i.e. dielectrics or silicon) the most viable methods are mechanical techniques such as nanoindentation and scratch induced delamination because of the simplicity of the test setup and sample preparation. During indentation or scratching stresses are induced into the film system which can cause interface separation in the form of buckles. By measuring the dimensions of the buckle and employing the appropriate model, the interfacial adhesion energy can be quantitatively determined. These techniques were utilized to induce interface delamination of a WTi film on different borophosphosilicate glass (BPSG) substrates. The comparison of the results from the different techniques will provide more insight into the techniques applicability and help to better characterize the adhesion of similar film systems.

Keywords: adhesion, thin films, nanoindentation, scratch, buckle.

1. Introduction

In microelectronic devices a large number of interfaces between different metals and dielectrics are present. The lifetime and reliability of such devices greatly depend on the mechanical stability of these interfaces. For a better understanding of these interfaces a quantitative adhesion test method is required. Many experimental methods and theoretical models have been devised to investigate the adhesion of dissimilar materials [1–3]. Of special interest in the microelectronics industry are the interfaces between metallic conductors and dielectric glasses, because of their wide use but usually weak adhesion [2–4]. The combination of tungsten based metals as barrier materials and borophosphosilicate glass as the dielectric are frequently used in microelectronic devices. Several chemical and mechanical studies have been conducted to investigate the interface and assess the adhesion of this kind of metal to dielectric layers which has been proven to be a weak interface [5–7].

Some of the common adhesion measurement methods are not only rather lengthy and come with extensive sample preparation but also lack the according experimental yield for quantitative adhesion assessment, such as four-point bending (4PB) [5,6,8,9] or double cantilever beam testing [7]. From a scientific and industrial point of view it is important to identify which method is suited best for the materials and the size regime in question. Of interest to this study are spontaneous buckling and stressed overlayers [2,10–12], scratch based [3,13–18] and nanoindentation [2,19–21] methods are used to quantitatively measure adhesion energies. These methods work well with hard metal films on rigid substrates to induce delamination in the form of buckles or blisters. For example, spontaneous buckles can form as a result of compressive stress in the film and either form as straight-sided or telephone cords [2,10]. Since spontaneous buckles form without any additionally applied mechanical force, they are one of the most reliable and easiest ways to measure the adhesion energy of an interface. In the case where there is not enough residual stress to cause spontaneous buckling additional mechanical force is necessary to cause delamination of the film. This can be done by scratching [13–17] or indenting the surface with a nanoindenter [2,3,11,19–21]. When scratch testing is used to evaluate adhesion a sharp indenter tip is drawn across a surface until at a critical load film failure occurs. The nature of the failure strongly depends on the properties of the film and substrate and occurs in form of through thickness cracking or buckling of the film but also plastic pile-up around the scratch trace. Nanoindentation, a method originally used for mechanical property measurements, has proven to be a good technique for inducing well-defined areas of delamination to measure the

adhesion of thin films. When a high enough load is applied by the indenter tip, a crack is induced at the interface which propagates to produce a delamination. The delamination can be a circular blister or a spontaneous buckle.

In the case of hard metal films and rigid glass substrates the buckling response is mostly elastic and the induced buckles or blisters can be analyzed by the model developed by Hutchinson and Suo [1]. Plastic effects due to film buckling are not considered in this model, although they become relevant in the case of softer substrates and very high film stresses [22]. The stresses and the interfacial fracture energies can be calculated using the geometry of the buckles produced. The necessary measurements are the buckle height, δ, buckle width, $2b$, as well as the thickness of the film, h as well as the elastic modulus, E, and the Poisson's ratio, ν of the film. In the case of spontaneous buckles the critical buckling stress, σ_b, and the driving (or residual) stress, σ_d, can be calculated by using eqns. (1) and (2) [1],

$$\sigma_b = \frac{\mu^2 E}{12(1-\nu^2)}(h/b)^2, \tag{1}$$

$$\sigma_d = \sigma_b[c_1(\delta/h)^2 + 1], \tag{2}$$

with $\mu^2 = \pi^2$ and $c_1 = 3/4$. The mixed mode interfacial fracture energy, $\Gamma(\psi)$, in the following termed the adhesion energy, for spontaneous buckles is given in eqn. (3).

$$\Gamma(\psi) = \left[\frac{(1-\nu^2)h}{2E}\right](\sigma_d - \sigma_b)(\sigma_d + 3\sigma_b). \tag{3}$$

In the case of indentation induced blisters the Hutchinson and Suo model for circular blisters can be used [1], under the condition that the blisters are circular, should be large compared to the indentation imprint and no radial or base cracking is caused due to the indentation [2]. Two different blister geometries can form which depend on the length of the interface crack. If the crack exceeds a certain length the film double buckles and the blister is pinned at the center, if not it single buckles and is modeled as an unpinned blister [1,2,19–21]. The formulas for the critical buckling stress and the driving stress are the same as for spontaneous buckles except for the factor μ^2, which is 14.68for unpinned and 42.67 for pinned blisters, and $c_1 = 0.2473(1+\nu) + 0.2231(1-\nu^2)$. Using the stress calculated with eqns. (1) and (2), the mixed mode adhesion energy for the indentation blisters can be calculated from eqn. (4),

$$\Gamma(\psi) = c_2[1 - (\sigma_b/\sigma_d)^2]\frac{(1-\nu)h\sigma_d^2}{E}, \tag{4}$$

with $c_2 = [1 + 0.9021(1 - \nu)]^{-1}$. The mixed mode adhesion energies calculated from eqns. (3) and (4) are a measure for the practical work of adhesion since it depends on the phase angle of loading, ψ, which gives the relation between normal and shear forces present at the interface given by eqns. (5) and (6) [1-3]. The phase angle of loading can be approximated for straight sided blisters by

$$\psi = tan^{-1}\left[\frac{4\,cos(\omega) + \sqrt{3}\,\delta/h\,sin(\omega)}{-4\,sin(\omega) + \sqrt{3}\,\delta/h cos(\omega)}\right], \quad (5)$$

and for circular blisters by

$$\psi = tan^{-1}\left[\frac{cos(\omega) + 0.2486(1+\nu_1)\delta/h sin(\omega)}{-sin(\omega) + 0.2486(1+\nu_1)\delta/h cos(\omega)}\right], \quad (6)$$

with $\omega = 52.1°$ and assumes no elastic mismatch in the case of a rigid substrate [1]. The knowledge of the phase angle allows for the normal mode (mode I) adhesion energy, Γ_I, to be calculated with eqn. (7),

$$\Gamma_I = \Gamma(\psi)/[1 + tan^2\{(1 - \lambda)\psi\}], \quad (7)$$

with $\lambda = 0.3$ which is a parameter defining the shear mode contribution to the interfacial fracture toughness and assumes a brittle interface [1]. The mode I adhesion energy only considers the normal forces used for interface separation where the phase angle is $0°$. This can be considered as the practical work of adhesion consisting of the true work of adhesion and the energies dissipated in the film and substrate [3]. Over the last decades the model of Hutchinson and Suo has been advanced to include elasticity corrections [22] and utilized to study how the buckle shape influences adhesion [10,23–25]. Parry et al. [22] use Dundurs Parameters to correct for any elastic contributions experienced by the substrate. The buckle shape can also have an influence on the calculated adhesion energies. For example, Faou et al. [23] have shown that the ψ angle varies as a function of the telephone cord which would affect the Mode I values. The highest ψ angles were found at the curve of the telephone cord and the lower ψ angles near the point of inflection of the buckle. Cordill et al. [25] demonstrated that when telephone cords are measured across the point of inflection and modelled as straight sided buckles with the Hutchinson and Suo model [1] the values were the same as straight buckles. Another model by Faou et al. [24] that could be employed to evaluate interface adhesion is to use the telephone cord wavelengt. This model uses the telephone cord wavelength, λ, instead of the buckle width, b and height, δ, as well as

parameters determined from a cohesive zone model FEM simulation to assess the Mode I adhesion energy. In the following the adhesion energies of a tungsten alloy film with two differently treated dielectric substrates are investigated through the use of three different mechanical adhesion testing techniques. The experimental and calculation results are compared and their viability for the film-substrate systems at hand are discussed.

2. Materials and Methods

Two sets of films were provided by Infineon Technologies Austria AG. They consisted of two 725 µm thick silicon wafers with a dielectric layer and a metal barrier film. In the first deposition step, 800 nm of borophosphosilicate glass (BPSG) was deposited on both wafers using plasma enhanced chemical vapor deposition. One of the two BPSG films was annealed at 600°C for 160 seconds. The Young's modulus of BPSG lies between 60 and 70 GPa. After that a 300 nm thick Tungsten-Titanium (WTi) film was sputter deposited onto both wafers where the tungsten film had 20 at% of Ti. The films were deposited under conditions that induced a compressive residual stress of about 1 GPa (measured by wafer bow). Scratch- and nanoindentation experiments were conducted with a Keysight G200 nanoindenter. For the scratch test a Berkovich tip was used with the sharp side of the tip being the scratch front. The scratch distance of all experiments was 500 µm and the distance between the scratches was set to 500 µm to avoid interaction with other scratches. The utilized load range was between 100-500 mN with a scratch velocity of 30 µm/s. For indentation induced delamination two conical diamond tips were used, 1 µm and 5 µm in diameter, with a load range between 100-500 mN. The indents were set about 500 µm apart from each other to avoid any interaction with other indents. Scratches and indents were examined with a light microscope to quickly identify if delaminations occurred and these examinations were repeated over a period of weeks to account for further buckle development over time. A Zeiss LEO 1540 XP focused ion beam (FIB) microscope was used to investigate the failing interfaces and extent of the deformations as well as any deformation due to the mechanical loading. To measure the geometric dimensions of the buckles a Veeco Dimension DI3000 atomic force microscope (AFM) was used. The buckle measurements were made from the AFM images using Gwyddion [26], to calculate film stresses and adhesion energy through the use of the according model. The Young's modulus of WTi was determined from nanoindentation experiments using the continuous stiffness method and a well-calibrated Berkovich tip. The modulus was measured to be $E_{WTi} = 171.8\, GPa$. The Poission's ratio of WTi was

determined using a simple rule of mixture with $\nu_W = 0.28$ and $\nu_{Ti} = 0.32$, which calculated to $\nu_{WTi} = 0.288$.

3. Results and Discussion

The three different methods were employed to produce delamination at the BPSG-WTi-interface, and further used to evaluate the adhesion energy of the samples with the unannealed and the annealed BPSG. The first delaminations observed were spontaneous buckles on the unannealed sample at the edges of the wafer where no additional forces were applied (Figure 1a). These spontaneous buckles had the well-known telephone cord shape and formed due to the compressive residual stress in the film. The buckles grew to relieve the stress in the film until the residual stress had been relieved to a point where it is lower than the critical buckling stress [2,19,23,25]. The telephone cord buckles were modeled as straight sided blisters and measured from straight wall to straight wall as indicated by the white line in Figure 1a and the corresponding profile in Figure 1c, if measured at any other point additional geometric correction factors have to be taken into account [10,25]. More than 30 buckle measurements were taken from the spontaneous buckles to assure good statistics for the calculation of the adhesion energy.

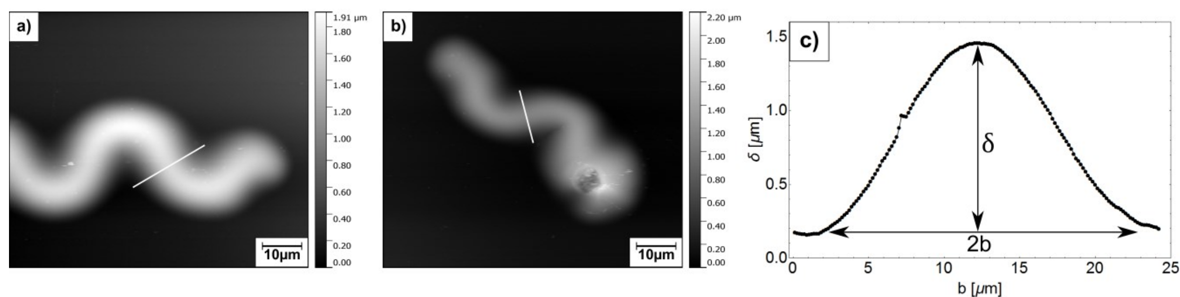

Figure 1: AFM height images of different spontaneous buckles. (a) A spontaneous telephone cord buckle which developed after deposition of the WTi film. (b) A spontaneous buckle induced by indentation. The white lines indicate how the buckles were measured. (c) A representative buckle profile from (a) and where the buckle height and width measurements are made.

Using the nanoindenter, scratch tests were conducted on both samples with a Berkovich tip. It was found that the scratch traces acted as points of origin for spontaneous straight sided buckles (Figure 2a) on both samples. The inspection of the scratch traces found that buckles were produced at all loads, although with different frequency. In the range of 300-500 mN

almost all of the scratches on the unannealed sample had buckles originating from their traces, on the annealed sample only every third scratch resulted in delamination. These buckles included a sharp angle with the scratch trace and some of these buckles took the form of telephone cords after growing further along the side of the trace (Figure 2b). It was observed that the traces made with the maximum load of 500 mN had the most buckles. Almost all of these buckles were symmetric and uncracked, although at the higher loads spallation of the WTi film from the BPSG can occur. Fifteen scratches were made for each maximum load and approximately 20 buckle profiles were measured per sample and modeled as spontaneous buckles. Due to the amount of plastic deformation and the complicated stress field of the moving indenter involved in scratching, the error in the adhesion calculation can be slightly higher even after selecting the buckles with symmetric profiles away from the scratch trace. By measuring the buckle profile sufficiently far away from the scratch trace the plastic deformation could be avoided. Scratch testing is a very good method to investigate hard coatings on hard substrates because the considerable plastic deformation is less of a problem for these materials [4,5]. However, at higher scratch loads, the risk of cracking at the buckle base or spallation of the buckles should not to be underestimated.

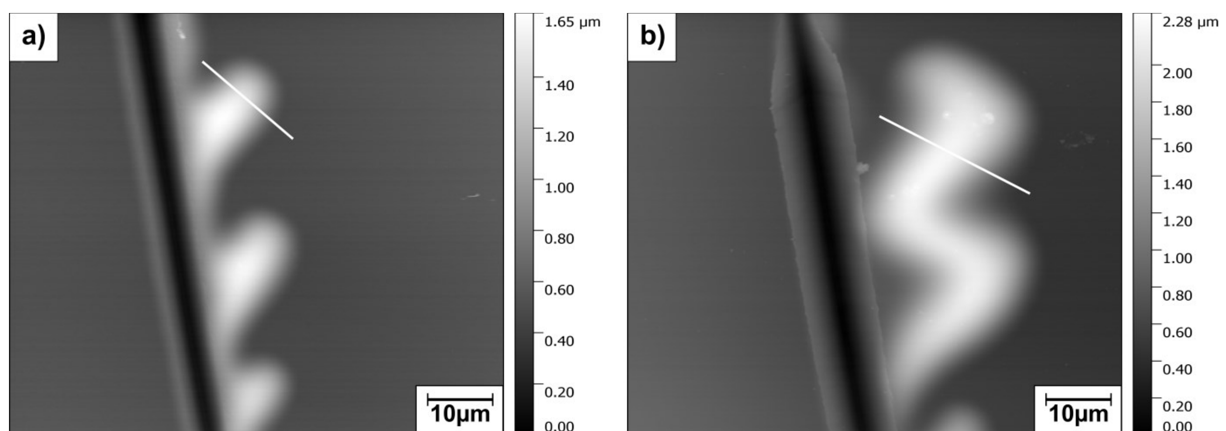

Figure 2: AFM height images of buckles originating from scratch traces, made with a maximum load of 500 mN. (a) Straight sided buckles growing outwards from the trace. (b) A spontaneous telephone cord buckle growing along the scratch trace. The positions where the buckle profiles are measured are indicated by the white line and are similar in shape to Figure 1c.

The annealed and unannealed samples were indented with the conical tips and circular indentation blisters as well as spontaneous buckles were produced. An example of spontaneous buckle formation from an indent is shown in Figure 1b where the indents acted as a point of origin for spontaneous telephone cord delamination (Figure 1b) and grew over

the course of a week. Both forms of blisters, pinned (Figure 3a) and unpinned (Figure 3b), were observed at maximum loads around 300 mN [1,2]. Pinned indentation blisters (Figure 3c) exhibit a torus-like form because the center of the delamination is held at the center of the indent imprint, while the unpinned blisters (Figure 3d) resemble a more cone like-shape and the centers are not "pinned" at the indent imprint. The unpinned blisters were observed only on the unannealed sample at a similar load. Unpinned blisters often had extensive radial cracking and were not considered in the adhesion calculation. This is due to the fact that cracks represent another form of energy dissipation which can change the calculated adhesion energy [1,27]. It should be noted that some of these delaminations were not completely symmetric, but were included in the adhesion calculation. For the measurement of the indentation blisters only blisters much larger than the imprint of the indent with no or as little cracking as possible were considered. At least 20 indents were made per load and the number of useable blisters for the adhesion calculation that the experiment produced was about 8% for the unannealed BPSG and 15% for the annealed BPSG in the load range of 300-400 mN. Not included here are the indents that produced spontaneous buckles which, although being the result of indentation, are modeled as spontaneous delaminations.

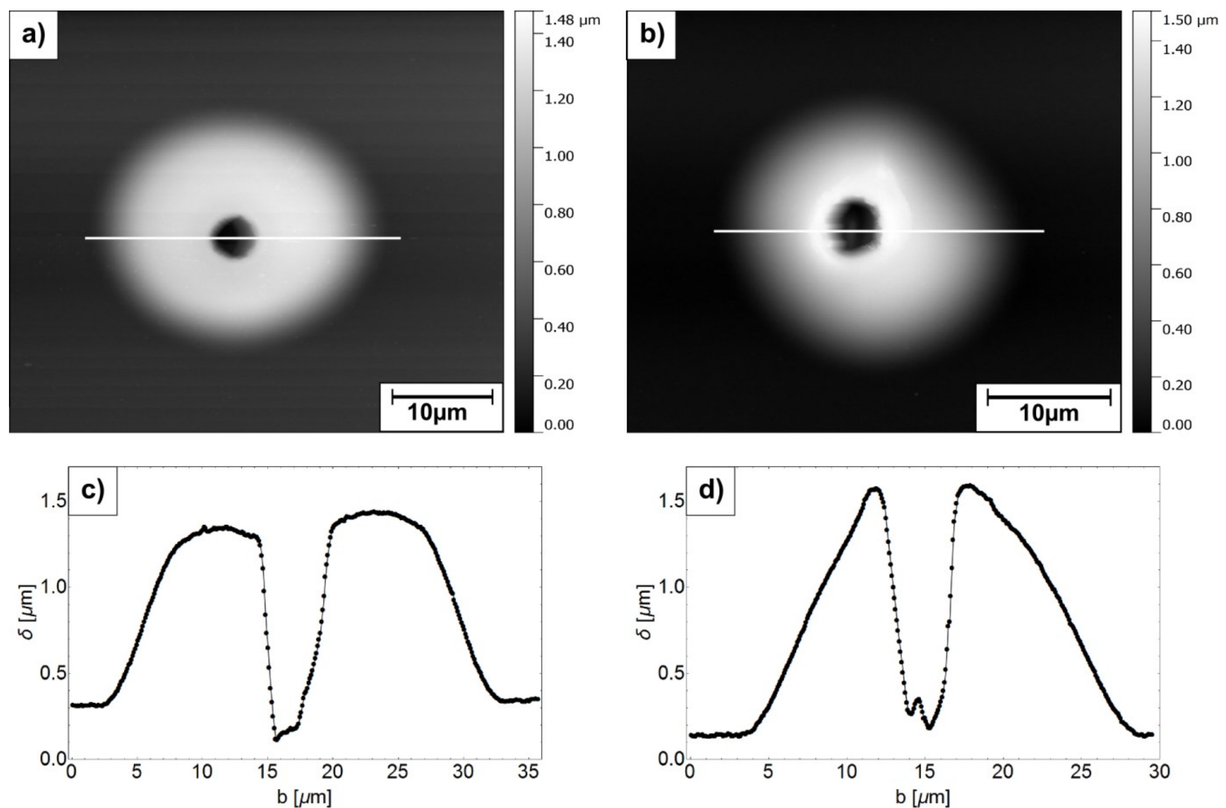

Figure 3: AFM height images and profiles of indentation blisters. (a) A pinned indentation blister produced by a maximum load of 300 mN with a 5 µm conical tip. (b) An unpinned

blister produced at a maximum load of 300 mN using a 1 μm conical tip. The difference in the geometry is observed in the in the profiles of the (c) pinned and (d) unpinned blister indicated by the white lines in (a) and (b).

To investigate the delaminating interface of the buckles FIB-cross-sectional cuts were performed. The delamination occurred at the WTi-BPSG interface, separating the metal from the dielectric, in the case of the spontaneous and scratch buckles (Figure 4a and 4b). It is also seen that the plastic deformation due to the scratch is locally confined to the scratch trace. The indentation blisters on the other hand, showed considerable spallation of the BPSG substrate for all buckles (Figure 4c) and the interface crack kinks from the BPSG-Si interface to the WTi-BPSG interface. This type of multiple interface fracture under a nanoindenter has been previously observed [11,28]. Indentation loads of 400 mN or higher often resulted in a fracture at the base of the buckles and led to the buckle spalling off the substrate. Fracture of the BPSG substrate could cause problems at high loads, hindering the formation of blisters or leading to cracking of other interfaces as illustrated in Figure 4c. When other interfaces are failing, the measured adhesion energy will also be altered.

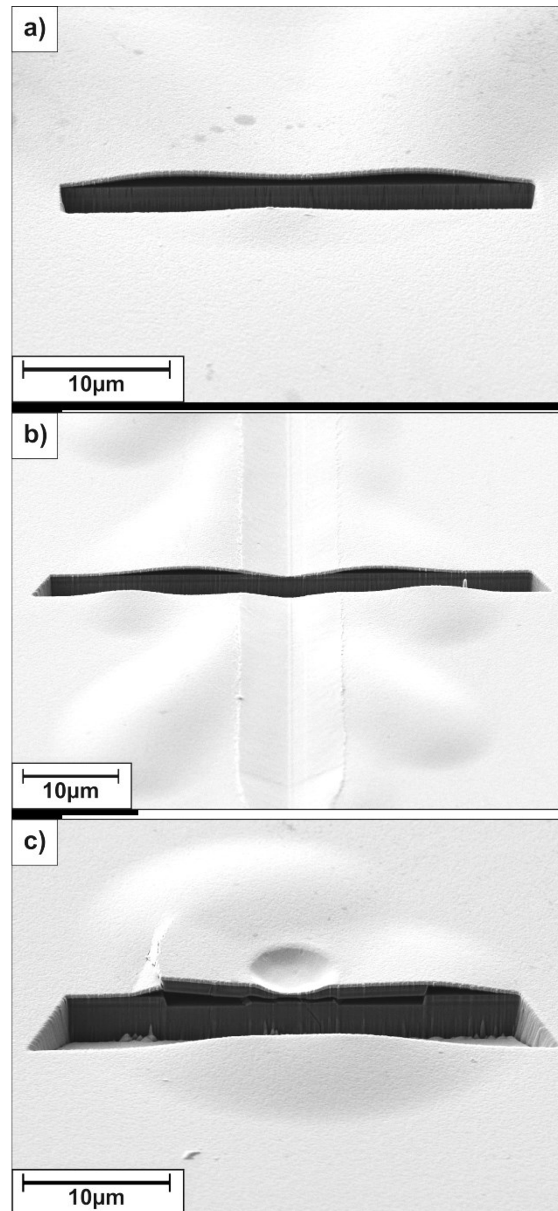

Figure 4: FIB cross-sections of all three types of buckles. Cross-section of a (a) spontaneous telephone cord buckle and (b) normal to the scratch trace and the buckles showing the delamination occurred at the metal dielectric interface. (c) Indentation blister showing delamination of the BPSG from the Si wafer and subsequent fracture of the BPSG and WTi film.

The mixed mode as well as the mode I adhesion energies were calculated for the different forms of buckles and are listed in Table 1. Although the buckles produced with the scratch test are of spontaneous nature they are treated separately to distinguish between the delamination methods. Almost no differences in the quantitative adhesion energies are observed either between the samples or the methods. The exception is for the indentation blisters which gave a slightly lower value for the adhesion energy due to the fracture along the

BPSG-Si interface. The energies calculated from the spontaneous and scratch buckles match well within the margin of error. It was observed that more delaminations were produced on the unannealed BPSG substrate which could be a qualitative indication of a lower adhesion value. The calculations have also been conducted using the correction factors proposed by Parry et al [22] using the Dundurs parameters and it was determined that the difference in the calculated stress and adhesion energies was marginal compared to the uncorrected values.

Table 1: Summary of the calculated adhesion energies for the WTi film on unannealed and annealed BPSG using three different buckle geometries.

Sample	**Unannealed BPSG**		**Annealed BPSG**	
	$\Gamma(\psi)$ [J/m²]	Γ_I [J/m²]	$\Gamma(\psi)$ [J/m²]	Γ_I [J/m²]
Spontaneous buckles	*2.48±0.36*	*0.51±0.08*	*2.59±0.62*	*0.54±0.13*
Scratches	*2.72 ±0.74*	*0.66±0.19*	*3.14±0.85*	*0.65±0.17*
Indents	*1.91 ±0.43*	*0.77±0.27*	*2.1±0.5*	*0.87±0.24*

Comparing the results of the mixed mode adhesion energy (Table 1) to Völker et al [5,6], who also measured WTi of the same composition on similar BPSG substrates with 4PB and calculated the adhesion energy of the system as 4.9 J/m². A reason for the discrepancy in adhesion energy is most likely due to an additional annealing step of 400°C after the WTi film deposition and before the 4PB experiments. This annealing step caused the Ti of the oversaturated WTi film to segregate to the interface, creating a Ti layer at the interface, which greatly improved the adhesion of the film to its substrate [5,6,15,29,30]. Since this annealing step was omitted for the samples discussed here, the calculated adhesion energies compare more to those of pure tungsten (W) on glass-like substrates. Völker et al [6] calculated the mixed mode adhesion energy of W on BPSG with 4PB to be 3 J/m² which was also annealed to relax the film stress. In order to compare these results to those found in literature, the phase angle of loading ψ for 4PB is about 42°, in the case of the buckles ψ is calculated from eqn. (5) and (6) and lies between -87° and -90° for all methods, showing a large amount of shear forces present which is expected from buckling [1]. Cordill et al [2] calculated mixed mode energies from spontaneous buckles of a 300nm W film on a silicate glass substrate with a residual compressive stress of 2.2 GPa to 1.7 J/m², for the same sample with no residual stress to 2 J/m² from spontaneous buckles and 2.6 J/m² from indentation. These results compare well to the values calculated from the spontaneous and scratch buckles in Table 1. It can be concluded that the energies calculated from the investigated samples can be seen as a lower bound for unannealed WTi on BPSG.

4. Conclusion

Comparing the results of the three methods to induce delamination showed that the calculation from the spontaneous and scratch buckles matched each other well and that the difference is within the margin of error on each sample. The FIB cross-sections showed that separation occurred at the WTi-BPSG interface. The difference in adhesion energy between the unannealed and the annealed BPSG is marginal but was observed in all three measurements. Calculation of the adhesion energy from the blisters caused by nanoindentation also led to the delamination of the BPSG-Si and to adhesion values different from those, determined using the other techniques. The method best suited to induce delamination for the WTi-BPSG interface is scratch testing since in this investigation nanoindentation was followed by substrate fracture and spontaneous buckles did not always form. The scratch technique gave good statistics to quantify the adhesion energy and is the most efficient considering test time in relation to buckle-yield. The adhesion values calculated in the course of this study can be seen as a lower bound for the interface strength of WTi on BPSG where no anneal was applied to the metal film.

Acknowledgements

The authors want to thank S. Wöhlert and T. Pelisset of Infineon Technologies Austria AG and V. Maier-Kiener of Erich Schmid Institute Austria. This work was jointly funded by the Austrian Research Promotion Agency (FFG: Project No. 846579) and the Carinthian Economic Promotion Fund (KWF, contract KWF-1521/26876/38867) further financial support by the Austrian Federal Government (837900) within the framework of the COMET Funding Program is appreciated.

References

[1] J.W. Hutchinson, Z. Suo, Mixed Mode Cracking in Layered Materials, Adv. Appl. Mech. 29 (1991) 63–191. doi:10.1016/S0065-2156(08)70164-9.

[2] M.J. Cordill, D.F. Bahr, N.R. Moody, W.W. Gerberich, Recent Developments in Thin Film Adhesion Measurement, IEEE Trans. Device Mater. Reliab. 4 (2004) 163–168. doi:10.1016/j.msea.2006.08.027.

[3] A.A. Volinsky, N.R. Moody, W.W. Gerberich, Interfacial Toughness Measurements for Thin Films on Substrates, Acta Mater. 50 (2002) 441–466. doi:10.1016/S1359-6454(01)00354-8.

[4] S.A. Varchenya, A. Simanovskis, S. V. Stolyarova, Adhesion of thin metallic films to non-metallic substrates, Thin Solid Films. 164 (1988) 147–152. doi:10.1016/0040-6090(88)90125-3.

[5] B. Völker, W. Heinz, K. Matoy, R. Roth, J.M. Batke, T. Schöberl, et al., Interface fracture and chemistry of a tungsten-based metallization on borophosphosilicate glass, Philos. Mag. 6435 (2014) 1–15. doi:10.1080/14786435.2014.913108.

[6] B. Völker, W. Heinz, K. Matoy, R. Roth, J.M. Batke, T. Schöberl, et al., Mechanical and chemical investigation of the interface between tungsten-based metallizations and annealed borophosphosilicate glass, Thin Solid Films. 583 (2015) 170–176. doi:10.1016/j.tsf.2015.03.047.

[7] K. Matoy, T. Detzel, M. Müller, C. Motz, G. Dehm, Interface fracture properties of thin films studied by using the micro-cantilever deflection technique, Surf. Coatings Technol. 204 (2009) 878–881. doi:10.1016/j.surfcoat.2009.09.013.

[8] R.H. Dauskardt, M. Lane, Q. Ma, N. Krishna, Adhesion and debonding of multi-layer thin film structures, Eng. Fract. Mech. 61 (1998) 141–162. doi:10.1016/S0013-7944(98)00052-6.

[9] P.G. Charalambides, H.C. Cao, J. Lund, A.G. Evans, Development of a test method for measuring the mixed mode fracture resistance of bimaterial interfaces, Mech. Mater. 8 (1990) 269–283. doi:10.1016/0167-6636(90)90047-J.

[10] M.W. Moon, H.M. Jensen, J.W. Hutchinson, K.H. Oh, A.G. Evans, The characterization of telephone cord buckling of compressed thin films on substrates, J. Mech. Phys. Solids. 50 (2002) 2355–2377. doi:10.1016/S0022-5096(02)00034-0.

[11] A.A. Volinsky, J.B. Vella, W.W. Gerberich, Fracture toughness, adhesion and mechanical properties of low-K dielectric thin films measured by nanoindentation, Thin Solid Films. 429 (2003) 201–210. doi:10.1016/S0040-6090(03)00406-1.

[12] G. Parry, J. Faou, S. Grachev, E. Barthel, Towards interface toughness measurement in nanometric films, 13th Int. Conf. Fract. (2013) 1–4.

[13] S.J. Bull, E. G.-Berasetegui E., Chapter 7 An overview of the potential of quantitative coating adhesion measurement by scratch testing, in: Tribol. Interface Eng. Ser., 2006: pp. 99–114. doi:10.1016/S0167-8922(06)80043-X.

[14] S.J. Bull, Failure mode maps in the thin film scratch adhesion test, Tribol. Int. 30 (1997) 491–498. doi:10.1016/S0301-679X(97)00012-1.

[15] A. Kinbara, S. Baba, A. Kikuchi, T. Kajiwara, K. Watanabe, Adhesion measurement of thin films on glass substrates, Thin Solid Films. 171 (1989) 93–98. doi:10.1016/0040-6090(89)90036-9.

[16] M.P. de Boer, M. Kriese, W.W. Gerberich, Investigation of a new fracture mechanics specimen for thin film adhesion measurement, J. Mater. Res. 12 (1997) 2673–2685. doi:10.1557/JMR.1997.0357.

[17] S.J. Bull, Failure modes in scratch adhesion testing, Surf. Coatings Technol. 50 (1991) 25–32. doi:10.1016/0257-8972(91)90188-3.

[18] P.A. Steinmann, Y. Tardy, H.E. Hintermann, Adhesion testing by the scratch test method: The influence of intrinsic and extrinsic parameters on the critical load, Thin Solid Films. 154 (1987) 333–349. doi:10.1016/0040-6090(87)90377-4.

[19] D.B. Marshall, A.G. Evans, Measurement of adherence of residually stressed thin films by indentation. I. Mechanics of interface delamination, J. Appl. Phys. 56 (1984) 2632–2638. doi:10.1063/1.333794.

[20] M.D. Kriese, W.W. Gerberich, N.R. Moody, Quantitative adhesion measures of multilayer films: Part I. Indentation mechanics, J. Mater. Res. 14 (1999) 3007–3018. doi:10.1557/JMR.1999.0404.

[21] M.D. Kriese, W.W. Gerberich, N.R. Moody, Quantitative adhesion measures of multilayer films: Part II. Indentation of W/Cu, W/W, Cr/W, J. Mater. Res. 14 (1999) 3019–3026. doi:10.1557/JMR.1999.0405.

[22] G. Parry, J. Colin, C. Coupeau, F. Foucher, A. Cimetière, J. Grilhé, Effect of substrate compliance on the global unilateral post-buckling of coatings: AFM observations and finite element calculations, Acta Mater. 53 (2005) 441–447. doi:10.1016/j.actamat.2004.09.039.

[23] J.-Y. Faou, G. Parry, S. Grachev, E. Barthel, How Does Adhesion Induce the Formation of Telephone Cord Buckles?, Phys. Rev. Lett. 108 (2012) 116102. doi:10.1103/PhysRevLett.108.116102.

[24] J.Y. Faou, G. Parry, S. Grachev, E. Barthel, Telephone cord buckles - A relation between wavelength and adhesion, J. Mech. Phys. Solids. 75 (2015) 93–103. doi:10.1016/j.jmps.2014.11.008.

[25] M.J. Cordill, D.F. Bahr, N.R. Moody, W.W. Gerberich, Adhesion measurements using telephone cord buckles, Mater. Sci. Eng. A. 443 (2007) 150–155. doi:10.1016/j.msea.2006.08.027.

[26] D. Nečas, P. Klapetek, Gwyddion: an open-source software for SPM data analysis, Open Phys. 10 (2012) 181–188. doi:10.2478/s11534-011-0096-2.

[27] S. Faulhaber, C. Mercer, M.W. Moon, J.W. Hutchinson, A.G. Evans, Buckling delamination in compressed multilayers on curved substrates with accompanying ridge cracks, J. Mech. Phys. Solids. 54 (2006) 1004–1028. doi:10.1016/j.jmps.2005.11.005.

[28] A. Lee, B.M. Clemens, W.D. Nix, Stress induced delamination methods for the study of adhesion of Pt thin films to Si, Acta Mater. 52 (2004) 2081–2093. doi:10.1016/j.actamat.2004.01.003.

[29] S.W. Russell, S.A. Rafalski, R.L. Spreitzer, J. Li, M. Moinpour, F. Moghadam, et al., Enhanced adhesion of copper to dielectrics via titanium and chromium additions and sacrificial reactions, Thin Solid Films. 262 (1995) 154–167. doi:10.1016/0040-6090(94)05812-1.

[30] G. Dehm, M. Rühle, H.D. Conway, R. Raj, A microindentation method for estimating interfacial shear strength and its use in studying the influence of titanium transition layers on the interface strength of epitaxial copper films on sapphire, Acta Mater. 45

(1997) 489–499. doi:10.1016/S1359-6454(96)00213-3.

Publication III

Published in *The Journal of The Minerals, Metals & Materials Society*

DOI: 10.1007/s11837-017-2496-2

New insights into nanoindentation based adhesion testing

A. Kleinbichler[1,2], M. J. Pfeifenberger[2], J. Zechner[1], N.R. Moody[3], D.F. Bahr[4], M. J. Cordill[2*]

[1]KAI – Kompetenzzentrum Automobil- und Industrieelektronik GmbH, Technologiepark Villach, Europastraße 8, Villach, Austria 9524

[2]Erich Schmid Institute for Material Science, Austrian Academy of Sciences and Dept. Material Physics, Montanuniversität Leoben, Jahnstraße 12, Leoben, Austria, 8700

[3]Sandia National Laboratories (Retired), Livermore, CA 94550 USA

[4]School of Materials Engineering, Purdue University, West Lafayette IN 47907 USA

*Corresponding Author: megan.cordill@oeaw.ac.at

Abstract

Nanoindentation, or instrumented indentation, is a versatile technique that is most often used to measure the elastic modulus and hardness of thin film systems. It can also be employed to measure thin film interfacial adhesion energies by producing well-defined areas of delamination. When combined with the proper mechanics-based model and characterization of the failing interfaces, nanoindentation induced delamination is a powerful tool to quantify interfacial fracture properties. New improvements to the technique, first introduced by Marshall and Evans in the 1980s, are demonstrated using a Tungsten-Titanium/Silicon Nitride (WTi/Si_3N_4) film system on a rigid silicon wafer where the WTi acts as a stressed overlayer. Focused ion beam cross-sectioning and confocal laser scanning microscopy are used to characterize failing interfaces, additional fracture events observed in the load-displacement curves, and determine the adhesion energy using not only symmetric, ideally shaped buckles, but also irregular shaped and half-delaminated buckles.

Keywords: adhesion, thin films, nanoindentation, buckling

1. Introduction

Thin film adhesion has been investigated since the early days of fabrication in the fields of microelectronics and protective coatings. Early pioneers such as Mittal, Weaver, and Chapman [1–3] helped define the field of thin film adhesion and brought testing methods to the forefront during the late 1970s and 1980s. These early adhesion tests were mostly qualitative or semi-quantitative measurements and included peel tests, tape tests, scratch and the lap shear test. In the late 1980s and 1990s a new generation of materials scientists and mechanics researchers introduced indentation based techniques, stressed overlayers, four point bending, and bulge testing with their appropriate models to quantify the adhesion energy of an interface [4–11]. These methods and combinations of methods have now become commonplace for those researchers working in the thin film adhesion area [12–16].

Having well-adhering films for micro and nanoelectronics, hard coatings, and flexible electronics is still a challenge as well as a fruitful area of research and development. Films are becoming both thinner and thicker, more chemically complex, and substrates are becoming more diverse (metals, ceramics, polymers, etc.). There is continued growth in technique development to quantify interface adhesion and to tackle the new interfaces and film systems. Some use indentation [17,18], while others use complex micro-mechanical bending geometries and perform the experiments *in situ* with pico-indenters in the scanning electron microscope (SEM) or transmission electron microscope (TEM) [19,20]. In the flexible electronics area (films on compliant polymer substrates), tensile induced delamination is prominent [21,22]. Nanoindentation, focused ion beam (FIB) milling and confocal laser scanning microscopy (CLSM) are bringing more insight to adhesion testing as well as increasing the imaging areas compared to other available methods (atomic force microscopy (AFM) or profilometry). Nanoindenters are now a basic measurement tool at most research institutes and their practicality for these tests increases when scratching and imaging are used in conjunction with the more common indenting procedures. FIB allows for site-specific cross-sectioning at the microscale to quickly identify a failing interface and additional fracture events that may have occurred with an indent or scratch. FIB is also useful to create transmission electron microscopy samples using the lift-out method for the examination of film microstructure and interface structure. CLSM is a 3D surface imaging technique that is ten times faster than AFM and has a higher resolution compared to a profilometer. With this technique larger delaminations, both in height and width, can be analyzed and used to measure adhesion [23].

An early indentation induced interfacial fracture test was developed by Marshall and Evans [5,6]. Improvements and updates to the original models of Marshall and Evans [5] and Hutchinson and Suo [10] were added by Kriese, et al. [9] and Cordill et al. [12]. Briefly, the Marshall and Evans model required that the indent volume remain within the film (Fig. 1a). This implies that the substrate does not deform under the indent, nor the formation of pile-ups around the indent to occur. It is important that the volume of the indent remains within the film thickness because the stress induced by the indent is utilized in the model and was shown to work well for thick films on hard and stiff substrates. When the film thickness is reduced, causing a delamination where the indent remains in the film is difficult. By adding a stressed overlayer, as performed by Kriese, et al. [9] (Fig. 1b) the depth of the indent could be increased and the possibility of blister formation increased due to a compressive stress in the overlayer. Kriese, et al. also introduced an extended model for the buckling of a bi-layer system. Further advancements [12] helped determine when an indentation delamination was a pinned or unpinned circular blister (Fig. 1c,d) and when the indent volume can be ignored due to substrate deformation. More work is still being performed on how the load-displacement curves can be better utilized to determine delamination and buckle formation, for example with acoustic emission analysis [24]. However, cross-sectioning with the FIB is an efficient method to use for the interpretation of the load-displacement curve, and allows for the observation of the failing interface as well as any interface or substrate fracture events which can result in pop-ins in the load-displacement curves. Film and substrate deformation of the indent as well as the pinned/unpinned buckle geometry can also be assessed better with FIB cross-sectioning. Most of these fracture events cannot be observed using *in situ* indentation in the SEM because they occur under the indent. Evaluation of adhesion energies is enhanced with knowledge of how the film and substrate are deforming and/or fracturing.

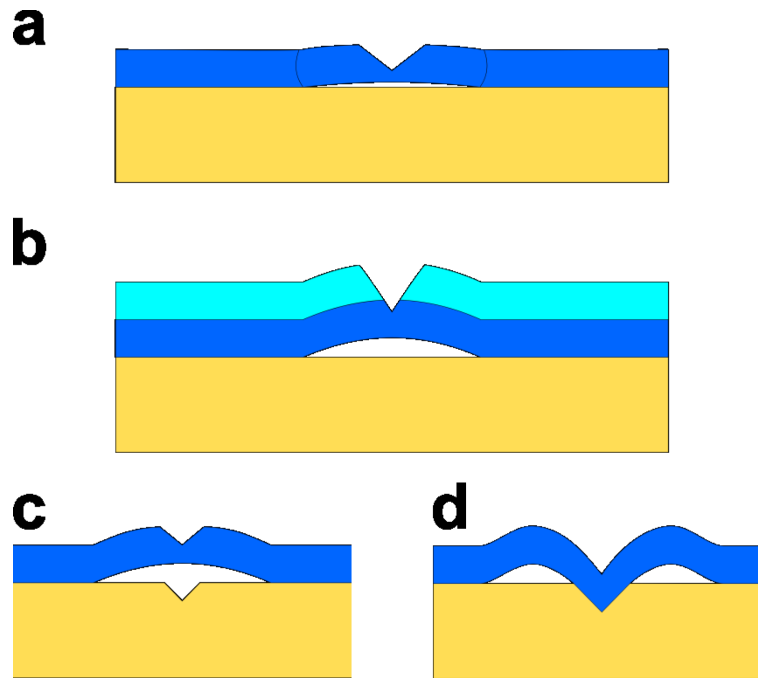

Figure 2: Nanoindentation induced delamination models by a) Marshall and Evans, b) Kriese et al. with a stressed overlayer and Cordill et al. with c) unpinned and d) pinned buckle geometries.

This study will demonstrate the use of nanoindentation-based techniques to measure the adhesion of barrier layers. Barrier layers provide chemical stability to conduction metallizations for microelectronic devices. A prime example is silicon nitride, Si_3N_4, which is used as an ion-barrier material, oxidation barrier, insulator or as an etch mask. Using a Tungsten-Titanium (WTi) stressed overlayer combined with nanoindentation, well-defined areas of delamination can be produced. The produced delaminations were measured with AFM and CLSM, while FIB cross-sectioning was used to identify the failing interface and additional fracture and deformation events present in the load-displacement curves. The combination of the two characterization techniques will be shown to improve the understanding of the evolution of the buckles under indentation loading.

2. Materials and Experiment

The samples investigated consisted of silicon wafers (725 µm thick) with 800 nm of borophosphosilicate glass (BPSG) deposited using plasma enhanced chemical vapor deposition (PECVD), followed by 400 nm of PECVD silicon nitride (Si_3N_4). To act as an adhesion and diffusion barrier layer, a 300 nm thick Tungsten-Titanium (WTi) film was sputter deposited on the Si_3N_4 where the tungsten film contained 20 at% of Ti. The WTi film

was deposited under conditions that induced a compressive residual stress of about 1.5 GPa (measured with X-ray diffraction).

Nanoindentation was conducted with a Keysight G200 nanoindenter. A 90° conical diamond tip with a 1 µm tip-diameter and a load range between 100-500 mN was used to generate indentation induced delamination. Fifteen indents were made per maximum load in this range which was increased in intervals of 50 mN. The indents were set in a grid being 250 µm apart from each other to avoid any interaction of the formed blisters, indent plastic zones or fracture events. After indentation, all resulting delaminations were imaged with an AFM (Veeco Dimension DI3000) or CLSM (Olympus LEXT OLS 4100). The buckle measurements were made from the AFM and CLSM images using Gwyddion [25] and the model of Hutchinson and Suo [10] modified for a bi-layer film using the theory of Kriese, et al. [9] was used to calculate film stresses and adhesion energies. The elastic modulus of WTi was determined from nanoindentation experiments using the continuous stiffness method and a well-calibrated Berkovich tip to be E = 171.8 GPa and the Poisson's ratio of WTi was estimated using a simple rule of mixture with $\nu = 0.288$. The modulus and Poisson's ratio of Si_3N_4 was taken from Vlassak et al. [26] where these properties E = 222 GPa and $\nu = 0.27$ were measured by bulge testing.

Cross-sections were made using a femtosecond laser and FIB. A femtosecond pulsed laser, which provides an ablation rate 4-6 orders of magnitude higher than a Ga^+ ion beam [27], was used to reduce the time needed for the rough cut of the buckle cross-section. The use of a femtosecond pulsed laser allows structuring of materials with ideally no heat affected zone due to the ultrashort pulse duration, but the shock wave of the ablation process can lead to the injection of dislocations. The amorphization of Si, or periodic surface structures in the range of a few hundred nanometers in depth are generated when using a laser in the ultrashort pulse regime [28]. For the investigation of the failing interfaces these modifications needed to be removed, thus requiring a polishing step with the FIB. In this study, a recently developed prototype, which combines the high material removal rate of a femtosecond pulsed laser with the high precision of a FIB, was used [29].

The cross-section processing route employing the femtosecond laser is sketched in Fig. 2. For each cross-section a line first cut with the femtosecond laser serves as a pre-preparation step (indicated as green dashed lines in Fig. 2). Afterwards the final cross-section is polished via FIB milling (indicated as orange rectangles in Fig. 2). The laser pre-preparation step used a laser wavelength of 515 nm, a laser pulse repetition rate of 1 kHz, a pulse duration of 318 fs and a fluence of 0.52 J/cm^2. For this step, a 150 µm long line was

scanned with 1 mm/s in 60 passes and took only about 10 s. The focal spot diameter of approximately 25 µm accounts for the width of the laser cut as can be seen in the top view in Fig. 2a and 2c. For the subsequent FIB milling, a current of 2 nA and an accelerating voltage of 30 kV were used. Exemplary for an 8 x 80 μm^2 large rectangle milled in 1 pass, the processing time was 1000 s. Fig. 2b and 2d show the FIB polished cross-sections in a tilted view.

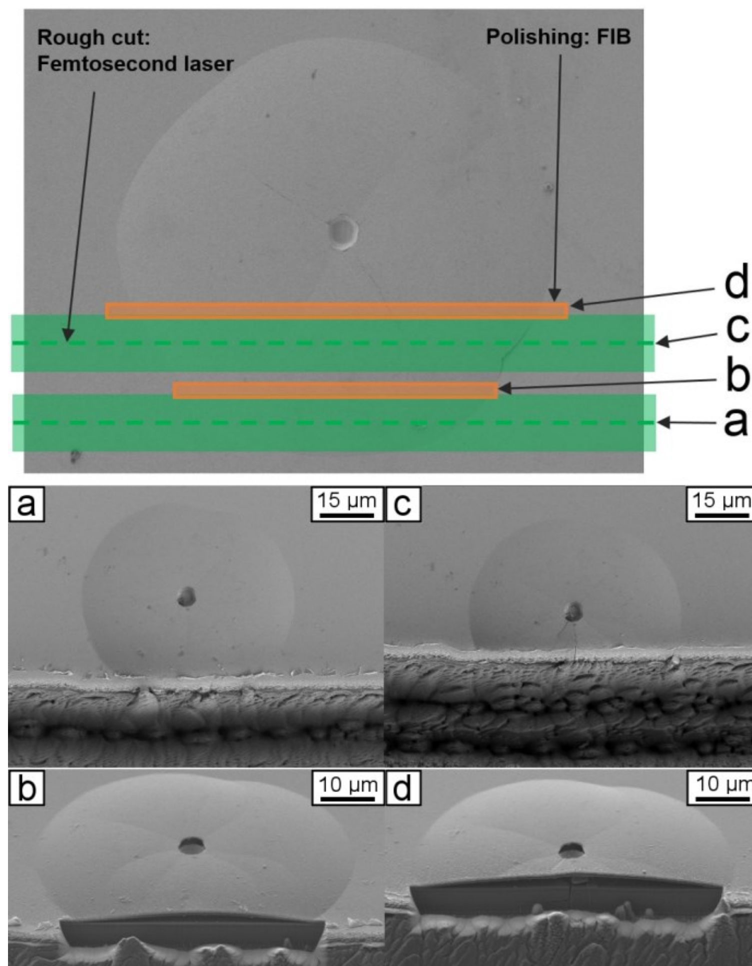

Figure 3: Route for the processing of large buckle cross-sections using a femtosecond laser and a FIB. a) and c) show the sample after the femtosecond laser rough cuts. b) and d) display the FIB polished cross-sections in a tilted view.

3. Indentation Induced Delaminations

Indentations with loads between 300-500 mN in the WTi-Si_3N_4 film system produced delaminations. At higher loads (400-500 mN), the buckles partially or completely spalled from the substrate. Buckles usable for adhesion measurements were produced in the load range of 300-350 mN (Fig. 3). For this study 13 buckles without spallation having a symmetric circular shape were analyzed. The buckles often exhibited significant radial cracking at loads higher than 300 mN

and indents made with lower loads showed almost no radial cracking. Indents with loads lower than 250 mN did not produce buckles. By investigating the spallation areas of the indents in the CLSM images it can be determined that the failing interface is the Si_3N_4-BPSG. However, information about any substrate fracture events observed in the load-displacement curves (Fig. 4) cannot be investigated.

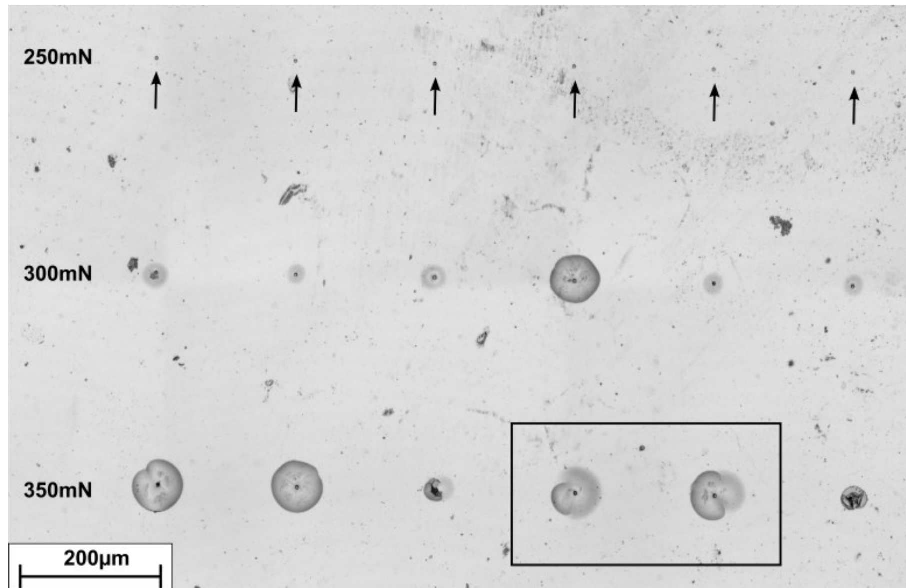

Figure 4: Indentation buckle overview in a load range of 250-350 mN. Indents made with 250 mN did not produce buckles (indicated by arrows). At 300 mN two sizes of buckles were produced, small (about 30 µm width) and large (about 60 µm width). Loads of 350 mN resulted in two types of delamination, either large circular buckles or film spallation. The box indicates the half-buckles that are discussed in Table I.

The FIB cross-sections revealed that during indenting multiple forms of cracking occurred in the film stack. For the indents at 250 mN interface delamination was not produced and the cross-section shows no observable interface fracture (Fig. 4a). However, cracks in the Si_3N_4 film can be observed directly under the indent which can be linked to the pop-in event in the load-displacement curve. Of interest is that the indent deforms the lower BPSG layer and WTi and Si_3N_4 thicknesses remain relatively constant under the indent. At 300 mN multiple interfaces have separated as shown in Fig. 4b,c. Interface cracks develop between the Si_3N_4 and BPSG as well as between the BPSG and Si. The interface crack between BPSG and Si originates directly under the indenter tip, extends for a few micrometers and eventually kinks up to the Si_3N_4 interface (Fig. 4b). This type of fracture under the indenter has been observed in other film systems [30]. Once the interface crack has kinked it propagates along the Si_3N_4-BPSG interface until it either extends for another 30 µm to become a small buckle (Fig. 4b) or it grows a further 70 µm into a large buckle (Fig. 4c). It can be seen from the

cross-section in Fig. 4b that the small buckle is a result of two interfaces separating (Si_3N_4-BPSG and BPSG-Si) and the kinking of the crack rather than a single interface separation. This tortuous crack path influences the calculation of the adhesion energy using the buckle in Fig. 4b.

Fig. 4c shows that the interface crack between the Si_3N_4 and BPSG extends much longer (70 µm in width) and that the buckle height is increased (2-3 µm), the interface crack then propagates until it kinks through the Si_3N_4 film as shown in the inset of Fig. 4c. Hence, the whole buckle is the result of this interface separation and is indicated in the load-displacement curve in Fig. 4c, where a large pop-in occurred during the hold time at a load of 300 mN. The cross-section also shows the fracture under the indenter tip extended through the BPSG and into the Si substrate as a single vertical crack. When the load was increased to 350 mN film failure occurred in two ways. The interface crack propagates similar to the case of 300 mN load, forming a large buckle with a diameter of about 70 µm, or the interface crack kinks towards the surface during interface crack propagation and spallation occurs, as shown in Fig. 4d. Both of these events are indicated in the load-displacement curve by a large pop-in event between 300 and 350 mN, as shown in Fig. 4d for a spalled buckle. From the pop-in events alone it is not possible to differ between buckle formation and spallation (compare load-displacement curves of Fig. 4c and 4d). Some of the buckles produced were irregularly shaped and with localized spallation and chipping created half-buckles (box in Fig. 3). Additionally, while the small buckles show no sign of radial cracking around the indent, the large buckles do and the extent increases with increasing load (Fig. 4c), which aids the spallation of the buckle (Fig. 4d). In this particular system, the WTi film acts as a stressed overlayer with its large residual compressive stress, helping to control the delamination of the Si_3N_4 barrier layer as well as supporting this brittle film to prevent it from spalling from the BPSG. As seen in Fig. 4d, the Si_3N_4 film cracks at the base of the buckles causing spallation before adhesion could be measured. The FIB cross-sections also confirm that the indentation buckles have an unpinned geometry because the indents were not connected to the substrate at the center of the indent.

A range of loads and number of indents is necessary to understand how delamination and fracture events transpire. As demonstrated in Fig. 4, pop-ins do not always indicate interface fracture and can relate to fracture events of the underlying films or substrate. The FIB cross-sections also identified that the WTi, Si_3N_4, and BPSG films co-deformed, most likely due to the low modulus of the BPSG (E = 70 GPa). With this hard-on-soft system, Marshall and Evans should not be applied as the volume of the indent would be challenging to

determine. Large pop-ins correlated to interface fracture and occurred at approximately the same load in this system (around 300 mN). However, not all film-substrate systems will behave in such a repeatable manner and should carefully characterized.

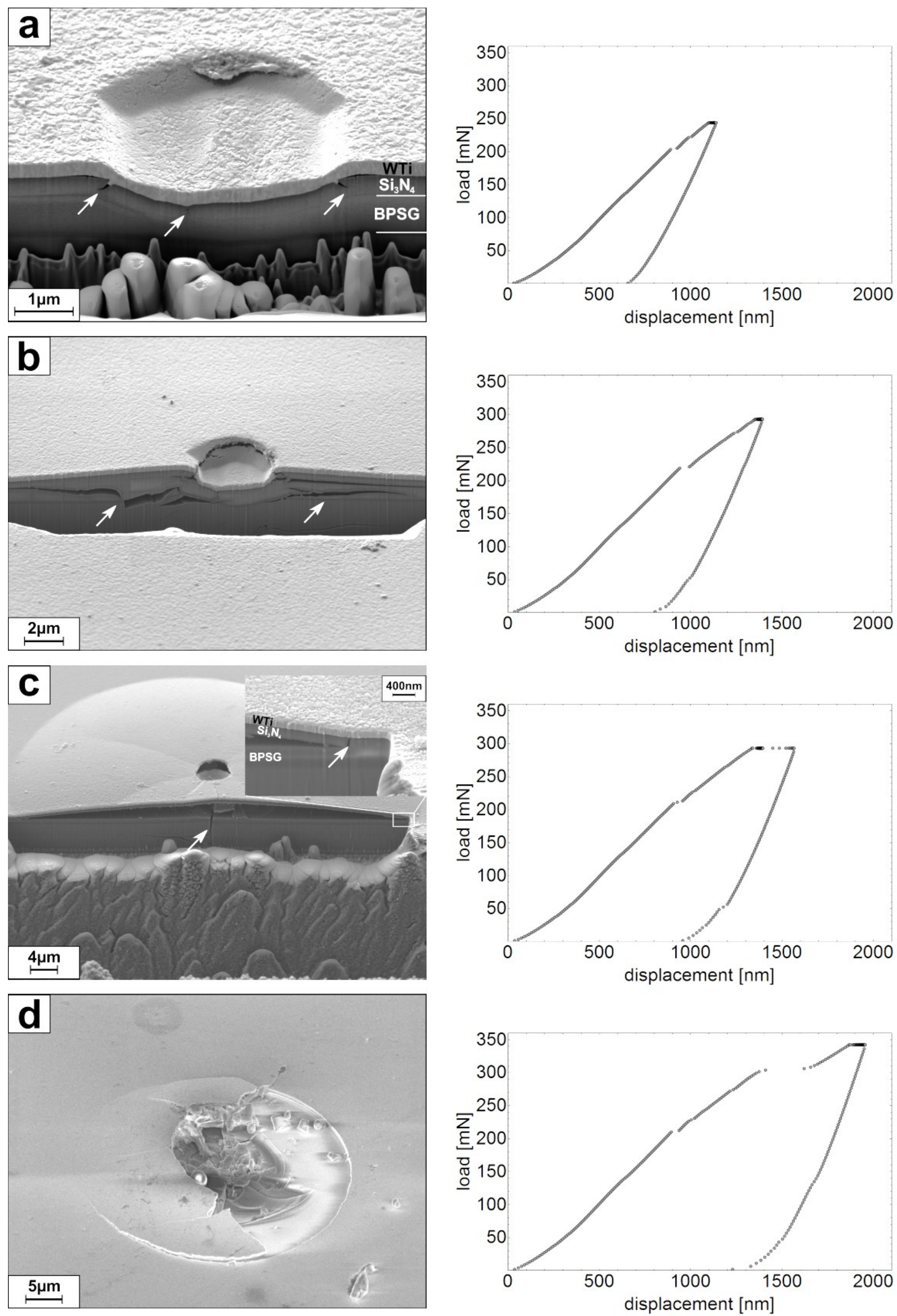

Figure 5: FIB cross-sections of indents made with loads of a) 250 mN, b) and c) 300 mN and d) 350 mN. The load-displacement curves are shown next to the corresponding indent. The cross-sections show the development of the interface crack and the fracture underneath the indenter with increasing load. The load-displacement curves reveal the pop-in events associated with the fracture and delamination events. Arrows indicate cracks of interest discussed in the text.

4. Quantifying the Adhesion Energy

A large and a small buckle, similar to those in Fig. 4b and 4c, used for adhesion calculation are shown in Fig. 5. The model is only valid for buckles with a symmetric circular shape. While the small buckles were imaged by AFM (Fig. 5a,b), the large buckles were imaged with CLSM (Fig. 5c,d) [31] because the buckle dimensions were too large for AFM. The buckle heights and widths from each buckle were used to calculate the adhesion energy from the profiles indicated in Fig. 5.

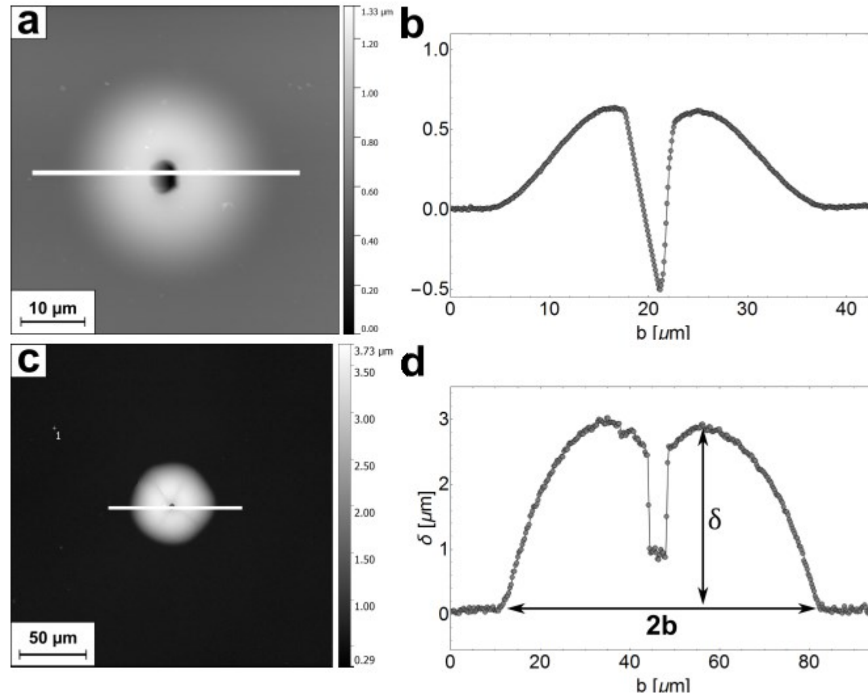

Figure 6: AFM and CLSM images of indentation buckles, both produced by a load of 300 mN, with the white line indicating where the buckle is measured. a) AFM image of a small buckle and (b) the according profile displaying an unpinned geometry. c) Large buckle imaged with CLSM with the corresponding profile (d).

The profiles of the AFM and CLSM images and FIB cross-sectioning suggest that the indentation buckles can be modeled as unpinned circular buckles according to Hutchinson and Suo [10]. Marshall and Evans is not used in this case because the indent does not remain within the film thickness and deforms the substrate. Only buckles that are much larger than the indentation imprint with a continuous circular base and very little radial cracking should be used for adhesion calculation [12]. The adhesion of the Si_3N_4-BPSG interface has been calculated using the Hutchinson and Suo model [10] where the stresses and the interfacial fracture energies can be calculated using the geometry of the produced buckles. The necessary measurements are the buckle height, δ, buckle width, $2b$, as well as the thicknesses of the

buckling films, h_i, where the index $i=1,2$ denoting the sequence of the films starting from the surface, as well as the elastic moduli, E_i, and the Poisson's ratios, ν_i of the contributing films. In the case of a multi-layered film the model of Kriese et al. was used, where a combined second moment of inertia, I_T, is calculated for the buckling WTi- Si_3N_4 film system [9], using Eqn. (1),

$$I_T = \sum_{i=1}^{2} \frac{1}{12} n_i k h_i^3 + n_i k h_i \left(\overline{Y} - y_i\right)^2. \quad (1)$$

For definitions of all of the variables, the reader is referred the Supplemental Material. This moment of inertia is then used to calculate the critical buckling stress, σ_b, in Eqn. (2),

$$\sigma_b = \frac{\mu^2}{khb^2}\left[\frac{E_1}{1-\nu_1{}^2}\right](I_T), \quad (2)$$

with $\mu^2=14.68$ for an unpinned buckle [10,12], h is the total thickness of the buckling films, E_1 and ν_1 are the elastic modulus and Poisson's ratio of the WTi top layer, respectively. The driving (or residual) stress, σ_d, can be calculated by using Eqn. (3) [10],

$$\sigma_d = \sigma_b[c_1(\delta/h)^2 + 1], \quad (3)$$

with $c_1=0.2473(1+\nu)+0.2231(1-\nu^2)$ for circular indentation buckles. Using the stresses calculated with Eqns. (2) and (3), the mixed mode adhesion energy for the indentation buckles is,

$$\Gamma(\Psi) = c_2[1 - (\sigma_b/\sigma_d)^2]\frac{(1-\nu_w)h\sigma_d{}^2}{E_w}, \quad (4)$$

with $c_2=[1+0.9021(1-\nu_w)]^{-1}$, E_w and ν_w are the elastic modulus and Poisson's ratio of the whole buckling system, respectively [9]. The mixed mode adhesion energy calculated from Eqn. (4) is a measure for the practical work of adhesion since it depends on the phase angle of loading, Ψ, which gives the relation between normal and shear forces present at the interface. A more detailed discussion on mode mixity can be found the Supplemental Material.

The mixed mode adhesion energies calculated from the different indentation buckles produced are summarized in Table I in order to demonstrate how the buckle shape, size and fracture behavior influences the calculation of the adhesion energies and the associated buckling stresses. When comparing the large and small blisters a rather large difference in buckling stresses is found even though the mixed mode adhesion energies of the buckles are only slightly different. As observed in Fig. 4b the small buckle is a combination of multiple

interface separations and film cracking, and as a result the buckle dimensions cannot contribute to the failure of the specific Si_3N_4-BPSG interface. Neither the Hutchinson and Suo model, nor the Marshall and Evans model, account for additional fracture events. The additional fracture events most likely inhibited the growth of the buckle half-width (interface crack) into a large buckle and led to the higher buckling stress. Therefore, the calculated values for the small buckles in Table I do not represent the true practical work of adhesion of the film system. The large buckles are mainly the result of the interface separation of the Si_3N_4 and the BPSG (Fig. 4c) and the values of $\Gamma(\Psi)$ in Table I are the true practical adhesion energies of this interface. Additionally, irregularly shaped buckles, where a portion of the buckle was spalled off the surface or did not develop due to the radial cracking (Fig. 3) have been investigated. The half-buckles were measured in a way that included only the unspalled or fully developed part of the buckle (Fig. 4d). The results show that the calculated values are in good agreement with the full buckles and demonstrated that they can be utilized to measure adhesion. Finally, the widths of the completely spalled buckles were measured in order to calculate the buckling stress compared to the large and half-buckles and the buckling stress was only slightly lower compared to the unspalled buckles. What Table I demonstrates is that with proper characterization of the failing interface, not only the “ideal” buckles can be used to evaluate the adhesion energy with nanoindentation, but also irregular buckles without too much additional substrate fracture are valuable (compare Large and Half-Buckles). The $\Gamma(\Psi)$ are reasonable for ceramic-ceramic interfaces and agreed well with Ma et al. [32] where adhesion energy of a Si_xN_y/SiO_2 interface and was reported to be 1.2-1.8 J/m². The values are also in the same range of some metal-glass systems, for instance Pt/Ti on SiO_2 which was determined to be 1.8 J/m² [12].

Table I: Summary of average half buckle widths (b), buckling stresses (σ_b), and mixed mode adhesion energies ($\Gamma(\Psi)$) from the buckles produced by nanoindentation shown in Figs. 3 and 4. The standard deviations are based on the number of measurements of each buckle type (about 15-20 measurements on 4-10 buckles).

Buckle Type	*Ave. b[µm]*	*Ave.* σ_b*[MPa]*	*Ave.* $\Gamma(\Psi)$ $[J/m^2]$
Small (Figure 4b)	15.8±1.7	525.7±115	1.13±0.31
Large (Figure 4c)	31.7±2.8	128.9±23	1.35±0.28
Half (Figure 3)	30.9±4.2	138.1±32	1.36±0.16
Spalled (Figure 4d)	33.4±3.1	116.2±22	-

It should be noted that nanoindentation induced delamination has a few limitations. For example, the technique should only be applied to film systems on rigid substrates. Nanoindentation induced delamination will not work for films on compliant/polymer substrates or with compliant layers. Some plastic deformation is necessary to induce the delamination and compliant substrates, at the loads typically used, only elastically deform. Also, typically large indentation loads are needed, therefore, one would need a nanoindenter capable of at least 100mN and higher loads. Post-analysis of the delaminating interface is necessary, but FIB does not have to be used. A simple peel test or careful removal of a buckle can be used to determine the failing interface [33]. However, this does not help for the separation of fracture events from interface fracture when multiple layers or pop-ins are present in the load-displacement curves. Finally, it is best to make several indents at various loads in order to fully understand the film deformation, film fracture and interface fracture processes.

5. Summary

The adhesion energy of a Si_3N_4-BPSG interface has been determined through the use of nanoindentation induced delaminations and a stressed overlayer. Due to the support of the compressive WTi stressed overlayer, nanoindentation can be employed to delaminate and subsequently buckle this interface. The elastic deformation of the metal film induces the necessary stress into the system to cause interface separation and forces the rigid Si_3N_4 film to buckle as a circular buckle. The development of interface separation and buckling falls into a narrow load range between 300-350 mN for this geometry tip. Loads of 300 mN and greater led to the development of Si_3N_4-BPSG interface separation, indicated by a large pop-in. The adhesion energy of the interface calculated from the large and half indentation buckles are in good agreement and show that the adhesive strength of this interface is rather low and comparable to other ceramic-ceramic interfaces. A brittle film can buckle under the right experimental conditions when supported by an elastic compressively stressed overlayer, making this mechanical test method viable for adhesion testing for film systems in microelectronics. Since every multi-layered thin film system may behave differently, complete characterization of the failing interface and load-displacement curves should be carried out to properly calculate adhesion energies. However, nanoindentation induced delamination is a versatile technique that can be easily implemented for a variety of interfaces, especially when augmented by FIB, CLSM and AFM characterization techniques.

Acknowledgements

This work was jointly funded by the Austrian Research Promotion Agency (FFG: Project No. 846579) and the Carinthian Economic Promotion Fund (KWF, contract KWF-1521/26876/38867) further financial support by the Austrian Federal Government (837900) within the framework of the COMET Funding Program is appreciated.

References

1. K. L. Mittal, Electrocompon. Sci. Technol. 3, 21 (1976).

2. C. Weaver, J. Vac. Sci. Technol. A Vacuum, Surfaces, Film. 12, 18 (1975).

3. B. N. Chapman, J. Vac. Sci. Technol. A Vacuum, Surfaces, Film. 11, 106 (1974).

4. A. Bagchi and A. G. Evans, Interface Sci. 3, 163 (1996).

5. D. B. Marshall and A. G. Evans, J. Appl. Phys. 56, 2632 (1984).

6. C. Rossington, A. G. Evans, D. B. Marshall, and B. T. Khuri-Yakub, J. Appl. Phys. 56, 2639 (1984).

7. M. D. Thouless, E. Olsson, and A. Gupta, Acta Metall. Mater. 40, 1287 (1992).

8. M. D. Thouless, Eng. Fract. Mech. 61, 75 (1998).

9. M. D. Kriese, W. W. Gerberich, and N. R. Moody, J. Mater. Res. 14, 3007 (1999).

10. J. W. Hutchinson and Z. Suo, Adv. Appl. Mech. 29, 63 (1992).

11. M. Ortiz and G. Gioia, J. Mech. Phys. Solids 42, 531 (1994).

12. M. J. Cordill, D. F. Bahr, N. R. Moody, and W. W. Gerberich, IEEE Trans. Device Mater. Reliab. 4, 163 (2004).

13. W. W. Gerberich and M. J. Cordill, Reports Prog. Phys. 69, 2157 (2006).

14. A. A. Volinsky, N. R. Moody, and W. W. Gerberich, Acta Mater. 50, 441 (2002).

15. R. P. Birringer, P. J. Chidester, and R. H. Dauskardt, Eng. Fract. Mech. 78, (2011).

16. J. Faou, G. Parry, S. Grachev, and E. Barthel, J. Mech. Phys. Solids 75, 93 (2015).

17. A. Roshanghias, G. Khatibi, R. Pelzer, and J. Steinbrenner, Surf. Coatings Technol. 259, 386 (2014).

18. M. Omiya, K. Koiwa, N. Shishido, S. Kamiya, C. Chen, H. Sato, M. Nishida, T. Suzuki, T. Nakamura, T. Suzuki, and T. Nokuo, Microelectron. Reliab. 53, 612 (2013).

19. R. Konetschnik, R. Daniel, R. Brunner, and D. Kiener, AIP Adv. 7, (2017).

20. K. Matoy, T. Detzel, M. Müller, C. Motz, and G. Dehm, Surf. Coatings Technol. 204, 878 (2009).

21. M. J. Cordill, F. D. Fischer, F. G. Rammerstorfer, and G. Dehm, Acta Mater. 58, 5520 (2010).

22. V. M. Marx, C. Kirchlechner, I. Zizak, M. J. Cordill, and G. Dehm, Philos. Mag. 95, 1982 (2015).

23. M. J. Cordill, O. Glushko, and B. Putz, Front. Mater. 3, 1 (2016).

24. D. F. Bahr, J. W. Hoehn, N. R. Moody, and W. W. Gerberich, Acta Mater. 45, 5163 (1997).

25. D. Nečas and P. Klapetek, Open Phys. 10, 181 (2012).

26. J. J. Vlassak and W. D. Nix, J. Mater. Res. 7, 3242 (1992).

27. M. P. Echlin, M. Straw, S. Randolph, J. Filevich, and T. M. Pollock, Mater. Charact. 100, 1 (2015).

28. M. P. Echlin, M. S. Titus, M. Straw, P. Gumbsch, and T. M. Pollock, Acta Mater. 124, 37 (2017).

29. M. J. Pfeifenberger, M. Mangang, S. Wurster, J. Reiser, A. Hohenwarter, W. Pfleging, D. Kiener, and R. Pippan, Mater. Des. 121, 109 (2017).

30. A. Kleinbichler, J. Zechner, and M. J. Cordill, Microelectron. Eng. 167, 63 (2017).

31. A. Kleinbichler, M. Bartosik, B. Völker, and M. J. Cordill, Adv. Eng. Mater. 19, 1600665 (2017).

32. Q. Ma, J. Mater. Res. 12, 840 (1997).

33. M. J. Cordill, N. R. Moody, and D. F. Bahr, J. Mater. Res. 19, 1818 (2004).

Supplemental Material

Multi-layer evaluation

The combined second moment of inertia, I_T, is calculated by applying the parallel axis theorem to a transformed cross-section where the neutral axis (n.a.) is weighted by the relation of the elastic moduli, E_i, and thicknesses, h_i, of the buckling films, demonstrated by Kriese et al [9], shown in Fig. A1.

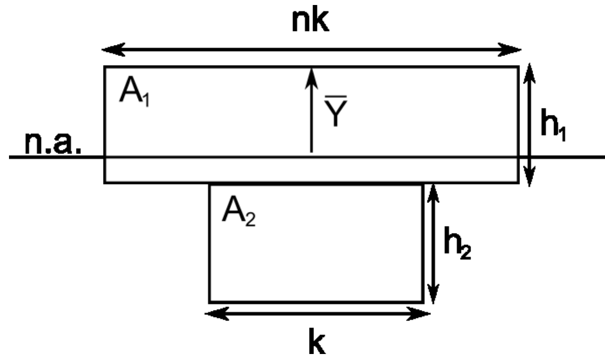

Figure A1: Schematic of the transformed cross-section.

Each film section is transformed into an effective area, A_i, of the same material, given by Eqns. (A1a) and (A1b),

$$A_1 = n_1 k h_1, \quad \text{(A1a)}$$

$$A_2 = n_2 k h_2, \quad \text{(A1b)}$$

with h_i being the thickness of the respective film, k is the unit width, n_1=1 and n_2 is the relation of the material properties of the films, $E_2/(1\text{-}\nu^2)=n_2E_1/(1\text{-}\nu^2)$. The centroids of the of the respective sections are given by Eqns. (A2a) and (A2b),

$$\bar{y}_1 = h_1/2, \quad \text{(A2a)}$$

$$\bar{y}_2 = h_1 + h_2/2.$$
(A2b)

The centroid of the composite is then given by Eqn. (A3),

$$\bar{Y} = \frac{\bar{y}_1 A_1 + \bar{y}_2 A_2}{A_1 + A_2}. \quad \text{(A3)}$$

These values are then inserted into Eqn. (1).

Mode Mixity

The mixed mode adhesion energy calculated from Eqn. (4) is a measure for the practical work of adhesion since it depends on the phase angle of loading, ψ, which gives the relation between normal and shear forces present at the interface given by Eqns. (5) and (6) [10, 12, 14]. The phase angle of loading can be approximated for circular blisters by

$$\psi = tan^{-1}\left[\frac{cos(\omega)+0.2486(1+\nu_1)\delta/h sin(\omega)}{-sin(\omega)+0.2486(1+\nu_1)\delta/h cos(\omega)}\right], \quad (5)$$

With ω=52.1° and assumes no elastic mismatch in the case of a rigid substrate [10]. The knowledge of the phase angle allows for the normal mode (mode I) adhesion energy, Γ_I, to be calculated with Eqn. (6),

$$\Gamma_I = \Gamma(\psi)/[1 + tan^2\{(1-\lambda)\psi\}], \quad (6)$$

with $\lambda = 0.3$ which is a parameter defining the shear mode contribution to the interfacial fracture toughness and assumes a brittle interface [10].

Publication IV

Published in *Surface and Coatings Technology*

DOI: 10.1007/s11837-017-2496-2

Annealing effects on the adhesion of Tungsten-Titanium barrier layers

A. Kleinbichler[1,2], J. Todt[2], J. Zechner[1], S. Wöhlert[3], D. M. Többens[4], M. J. Cordill[2]

[1]KAI – Kompetenzzentrum Automobil- und Industrieelektronik GmbH, Technologiepark Villach, Europastraße 8, Villach, Austria 9524

[2]Erich Schmid Institute for Material Science, Austrian Academy of Sciences and Dept. Material Physics, Montanuniversität Leoben, Jahnstraße 12, Leoben, Austria, 8700

[3]Infineon Technologies AG, Siemensstraße 2, 9500 Villach, Austria

[4]Helmholtz-Zentrum Berlin für Materialien und Energie, Albert-Einstein-Str. 15, 12489 Berlin, Germany

Abstract

Tungsten-titanium (WTi) alloys are important barrier materials in microelectronic devices. Thus the adhesion of WTi to silicate glass substrates influences the reliability of these devices. One factor that affects the adhesion of barrier layers is thermal treatments during and after fabrication. To address the impact of annealing, WTi films deposited on silicate glass substrates were subjected to different annealing treatments. The stress development in the WTi film has been monitored with wafer curvature and X-ray diffraction. Quantitative measurements of the adhesion energies were performed using scratch testing to induce interface delamination. Imaging with atomic force microscopy provided the dimensions of the buckles to quantify adhesion energies. Focused ion beam cross-sections were used to verify the failing interfaces and to inspect any deformation in the film and the substrate caused by scratch testing. It was found that as the annealing time increased, the residual stresses became more compressive and the adhesion energy increased.

Keywords: adhesion, thin films, scratch test, heat treatment, film stress

1. Introduction

Barrier layers are an important part of every integrated circuit. In metal-silicon oxide interfaces barrier layers provide the device with chemical as well as mechanical stability [1]. The chemical stability of the thin film system is meant as the prevention of diffusion of Si from the substrate into the conductive metal creating silicides, which significantly increases the electrical resistance. It is important that the chosen barrier material has a low reactivity with the conductive metallization and the underlying substrate, with thermal stability at high temperatures. A variety of studies have been conducted on this topic over the years following the advances of the microelectronic industry. Transition metals like Cr, Ti, Mo, Nb, Ta and W, are very suitable materials for conductive diffusion barrier layers and several of these films have been investigated in the relevant temperature ranges that these films experience during production an d service [2]. It was found that all of these materials were chemically stable up to 400°C for 1 hour.

A frequently used diffusion barrier for copper and aluminum metallizations is tungsten titanium (WTi) which exhibits good temperature stability and adhesion [3,4]. WTi is a solid solution of W and Ti with W usually being the major component and varying minor amounts of Ti. Several studies on the thermal stability of WTi have been conducted to determine the failure temperature of the film, where copper-silicide (Cu_3Si) start to form. Barrier failure was discovered at temperatures between 700-800°C for different annealing times. Fugger et al [5] investigated the stability of the WTi barrier layer depending on the annealing times with respect to the copper layer on top. It was reported that the WTi barrier layer remained stable up to 600°C for four hours with no copper-silicide (Cu_3Si) formation occurring, although a segregation of Ti into the copper film was observed. The failure temperature was found at 650°C after 4 hours of annealing with the formation of Cu_3Si. No Ti segregation towards the copper film was found when annealing at 400°C for 8 hours. Völker et al [6] found that the segregation of Ti formed a few atom layers of Ti between the doped silicate glass substrate and the WTi layer which promoted the adhesion of the respective layer when annealing the sample to 400°C for 1 hour. This suggests that the adhesion of the WTi film to the substrate could be influenced by the annealing temperature and time.

Mechanical stability is mainly governed by the adhesion of the barrier layer to the conductive metallization and the substrate [1]. Several adhesion testing methods have been successful in quantitatively measuring the adhesion of thin films [7,8]. Common techniques include four point bending (4PB) [6,9–12], microcantilever tests [13,14], nanoindentation

[15–18] and scratch tests [19–22]. Four point bending and microcantilever tests require very elaborate sample preparation and testing procedures which also may change the properties of the interface in question. Nanoindentation and scratch testing, on the other hand, allow the samples to be tested in the desired as-produced condition.

The adhesion of WTi to commonly used substrates like silicon or silicon oxides and its dependence on several parameters such as composition or film thickness, have also been investigated using several different methods [6,9,23,24]. In order to quantitatively measure the adhesion of the WTi film the scratch test has been utilized. This mechanical testing technique which induces compressive stress into the film causing delamination in different forms [19–21,25]. Scratch testing has been successful in inducing buckles in compressively stressed film in a thickness range of a few hundred nanometers [22,26].

The buckles produced with the scratch test can be evaluated by the model proposed by Hutchinson and Suo [27]. In the case of a hard metal film, like WTi, and a rigid glass substrate, very little plasticity is involved in the buckling process which allows for an elastic approximation. The stresses induced in the film and the associated adhesion energy can be calculated from the buckle height, δ, and the half buckle width, b, the film thickness, h, and the elastic properties of the film (elastic modulus, E, and Poisson's ratio, ν). The critical buckling stress, σ_b of the interface and the driving stress, σ_d in the film are calculated using equations (1) and (2),

$$\sigma_b = \frac{\pi^2 E}{12(1-\nu^2)}(h/b)^2, \quad (1)$$

$$\sigma_d = \sigma_b\left[\frac{3}{4}(\delta/h)^2 + 1\right]. \quad (2)$$

The mixed mode adhesion energy, $\Gamma(\Psi)$, which represents the practical work of adhesion, is given by equation (3)

$$\Gamma(\Psi) = \left[\frac{(1-\nu^2)h}{2E}\right](\sigma_d - \sigma_b)(\sigma_d + 3\sigma_b). \quad (3)$$

In this study the adhesion of the WTi barrier layer to a silicate glass substrate is measured as a function of the annealing time. The annealing temperature was set at 400°C because the barrier layer experiences this annealing temperature for different time periods during production. The information about how the adhesion is influenced by the annealing time will

allow for the optimization of the annealing time in order to achieve the best interfacial strength for the WTi-BPSG interface.

2. Experiment

The studied samples were provided by Infineon Technologies Austria AG. They consisted of 725 μm thick silicon wafers with a diameter of 200 mm, coated with a dielectric layer and a metal barrier film. In the first deposition step, 800 nm of Borophosphosilicate glass (BPSG) was deposited on the wafers using plasma enhanced chemical vapor deposition followed by annealing at 900°C. The 300 nm thick Tungsten-Titanium (WTi) barrier layer film was sputter deposited onto the BPSG where the W film contained 20 at% of Ti. The WTi films were deposited under conditions that induced a compressive residual stress of about 1.5 GPa measured by wafer bow.

Equally sized pieces (1x1.5cm) of the wafers were annealed to 400°C using a heating rate of 10°C/min and the temperature was held for 30 min, 45 min, 1 and 2 hours. The annealing treatment was conducted in a vacuum chamber using a k-Space Associates Multi-Beam Optical Sensor (MOS) wafer curvature system in order to monitor the stress evolution in-situ during annealing. The chamber operated at a pressure of about 10^{-4} mbar. Additionally, the stress in the WTi film has been measured for one sample heated in-situ to 400°C with a hold time of 1 hour with synchrotron X-ray diffraction (XRD). This experiment was carried out on the KMC-2 [28] beamline at BESSY II, Helmholtz-Zentrum Berlin für Materialien und Energie (HZB) using monochromatic radiation with a wavelength of 1.5504Å (equivalent to Cu-Kα_1, 8048 eV), a spot size of 0.3 mm diameter and a Bruker VÅNTEC 2000 area detector operated with an exposure time of 7 seconds. The film stresses were determined utilizing the $sin^2\psi$ method [29] by measuring the shift in the WTi (110) peak which has been observed before [5,30,31]. The in-situ heating was conducted with an Anton Paar DHS 1100 heating device with a graphite dome under a residual air pressure of 10 mbar. The sample was heated with an effective rate of 12.5°C/min from room temperature up to 400°C. The temperature was increased in steps of 25°C, with a hold time of 2 minutes to record the peak position. During the subsequent hold time of 1 hour at 400°C the peak position were recorded in 10 minutes intervals. Afterwards, the sample was cooled down to 50°C in the same manner as the heating, again monitoring the peak position at each 25°C step. However, the times to reach these temperatures steps increased below 100°C due to the residual heat in the device, resulting in omitting the last temperature step from 50°C to 25°C.

In order to measure the film stress, it was necessary to experimentally determine the X-ray elastic constant $1/2s_2$ of the WTi solid solution, which connects the lattice strain to the stress in the film. For this purpose, a procedure proposed by Eiper et al [32] was used and a new wafer was produced without the BPSG layer between the WTi and the Si substrate. This method determines the lattice strain d_ψ^{hkl} for different orientations of the film via the peak shift relative to the unstressed peak position. The macroscopic stress σ_{11} in the film is calculated from the curvature R of the silicon substrate, which is determined using the silicon (400) peak that lies perpendicular to the sample surface, and the Stoney formula [33],

$$\sigma_{11} = \frac{E_S}{6(1-\nu_S)} \frac{h_S{}^2}{h_f} \frac{1}{R}, \quad (4)$$

where h_s is the thickness of the substrate, h_f is the thickness of the film, E_S is the elastic modulus and ν_S is the Poisson's ration of the Si substrate. Following this, the $sin^2\psi$ equation [29],

$$\frac{\partial d_\psi{}^{hkl}}{\partial sin^2\psi} = \frac{1}{2} s_2{}^{hkl} d_0{}^{hkl} \sigma_{11}, \quad (5)$$

with d_0^{hkl} being the unstressed lattice spacing for the peak lattice plane family hkl and ψ the angle between the sample's surface normal and the crystal planes, is solved for the X-ray elastic constant $1/2s_2^{hkl}$. It should be noted, that this constant depends on the peak hkl used for stress analysis due to the possibility of crystallographic elastic anisotropy. Additionally the film stresses were measured using the $sin^2\psi$ method in a laboratory XRD after each annealing treatment in the wafer curvature vacuum chamber. The laboratory instrument was a Rigaku SmartLab 5-Axis X-ray diffractometer equipped with Cu-Kα radiation, parabolic multilayer mirror incident optics, a graphite diffracted beam monochromator and a scintillation counter.

The scratch test experiments were performed on a Keysight G200 nanoindenter using a Berkovich tip. Both the sharp edge and the broad face of the pyramidal tip were utilized as the scratch front in order to induce different stress fields during scratching [19–21]. The scratch distance of all experiments was 500 µm and the distance between the scratches was set to 500 µm to avoid interaction with other scratches or the induced delaminations. The maximum load range was between 100-500 mN with a scratch velocity of 30 µm/s and at least five scratches were made for each maximum load and tip orientation. The scratches were performed so that the load was steadily increased until it reached the maximum prescribed load. Scratches were first examined with an optical light microscope to identify if delaminations occurred and were

repeated over a period of days and weeks to account for further buckle development. A Zeiss LEO 1540 XP focused ion beam (FIB) microscope was used to examine the failed interfaces and any deformation due to the mechanical loading. To measure the buckle dimensions a Veeco Dimension DI3000 atomic force microscope (AFM) was used. The buckle measurements were taken from the AFM height images using Gwyddion software [34] and the film stresses and adhesion energy were calculated using the Hutchinson and Suo model [27] using Eqs. (1-3). The elastic modulus of the as-deposited and the annealed WTi films was determined from nanoindentation experiments using the continuous stiffness method and a well-calibrated, sharp Berkovich tip (not the same tip used for the scratching experiments). The modulus was measured to be E_{WTi} = 171.8 GPa for the as-deposited film, at an indentation depth of about 30 nm which corresponds to 10% of the total film thickness. For the annealed WTi films no change in the elastic modulus was observed within the margin of error (Table I). These values are necessary for the calculation of the adhesion energies. The Poisson's ratio of WTi was determined using the rule of mixtures with ν_W = 0.28 and ν_{Ti} = 0.32, which yields ν_{WTi}=0.288.

In order to investigate possible changes of the interface chemistry the WTi film was removed from the BPSG substrate using Polyurethane Protective Tape with an acryl based adhesive. The substrate was then analyzed with Auger electron spectroscopy (AES) using a PHI 4700 Thin Film Analyzer with a scanned area of $20 \, x \, 20$ µm.

Table I: Measured elastic moduli (in GPa) of the WTi films after different annealing treatments.

As-deposited	400°C/30 min	400°C/45 min	400°C/1 hr	400°C/2 hr
171.8 ± 11	173.2 ± 27	179.8 ± 26	169.5 ± 16	180.1 ± 14

3. Results and Discussion

Wafer curvature and with in-situ XRD measurements revealed an increasing change in residual stress in the samples to more compression due to the annealing times. Results from wafer curvature measurements are presented in Figure 1a. The longer the hold time at 400°C the more compressively stressed the films became. After 30 minutes of annealing the WTi film stress increased by about 4%, after one hour by 11% and by 22% after two hours compared to the original film stress. The increased stress remained after the cooling to room

temperature. The same behavior was also observed in the in-situ XRD heating measurement for a hold time of 1 hour shown in Figure 1b. The absolute values of the film stress differed from those measured with wafer curvature since the curvature of the whole sample system including the BPSG and Si was measured, resulting in lower overall stress values [35]. For the in-situ XRD heating experiments the film behavior was qualitatively similar to the wafer curvature measurements. The compressive stress in the WTi film also increased during the hold time and remained about 10% higher compared to before annealing, which illustrates that the stress develops mainly in the WTi film. The magnitude of the error bars in Figure 1b may be a result of thermal fluctuations during the measurement and the slight texture in the WTi film. The increase of compressive stress during the hold time may help to induce delaminations during scratching. However, it is also possible that the increase in stress may lead to an increase of adhesion due to the segregation of the Ti to the interface [6].

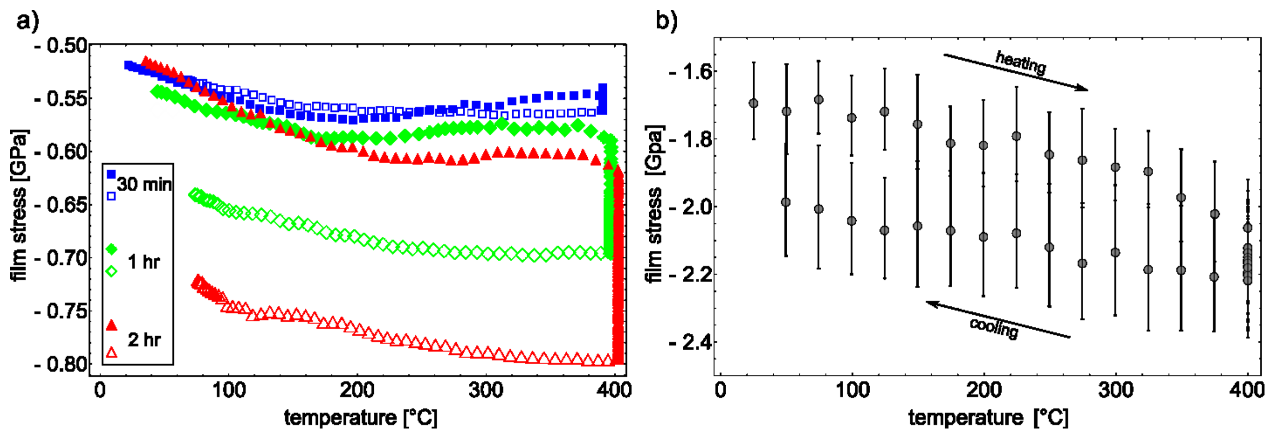

Figure 7: The development of stress in the sample system and the film, measured by (a) wafer curvature for the samples annealed for 30 min, 1 hour and 2 hours and (b) by in-situ XRD for a sample annealed for 1 hour. The solid symbols in (a) represent the heating and the open symbols represent the cooling cycle. The temperature axis of the 30 min and the 2 hour annealed sample was shifted by –5°C and +5°C, respectively, to avoid the overlap of the curves. Both measurement methods reveal that the compressive stress in the film increased as a function of the hold time at 400°C.

The scratch tests resulted in buckling of the WTi film at the sides of the scratch traces. The moving indenter tip acted as an activator for buckling and the delamination grows away from the trace due to the residual stress in the film [22]. Using the optical light microscope it was observed that buckling occurred on the as-deposited and the annealed samples after the scratch tests were performed. The buckles included a sharp angle with the trace in the scratch

direction and grew away from the trace as shown in Figure 2. A similar buckle growth behavior was observed before [22].

The scratches on the as-deposited sample with maximum loads of 300 – 500 mN exhibited buckles using both indenter tip orientations (sharp and broad). For maximum loads of 300 mN each scratch produced an average of 3 buckles, at 400 mN 5 buckles per scratch were observed and at 500 mN more than 10 buckles were produced utilizing the sharp side of the tip. An example is shown in Figure 2a. Scratches made with a maximum load of 200 mN occasionally induced buckles but not on a regular basis. When using the broad side of the tip similar amounts of buckles were produced at the same loads, however, some of the buckles were spalled off the surface and through thickness cracking of the film increasingly occurred at loads of 400 mN and higher [19–21]. It was also observed that the higher the maximum load, the earlier along the scratch trace buckling occurred for the as-deposited film and was not observed for the annealed samples.

For the sample annealed at 400°C for 30 minutes the scratches performed with the sharp side of the tip did not produce any buckles at any of the maximum loads. Only scratches using the broad side of the tip were able cause interface separation. At maximum loads of 400 and 500 mN, scratches produced an average of about 2 to 3 buckles growing outward from the trace. The buckles on the sample annealed for 30 min have the same morphology as those on the as-deposited samples (Figure 2b). Similar to the sample with 30 min of annealing time, the scratches on the sample annealed for 45 min resulted in buckles with both tip orientations, at maximum loads of 400 and 500 mN. At loads of 400 mN fewer buckles were produced than at 500 mN, where 2 to 3 buckles formed per scratch. After annealing the sample for 1 hour, the scratches made with the sharp and broad side of the tip produced buckles at maximum loads of 400 and 500 mN (Figure 2c). The amount of buckles was evenly distributed between the maximum loads. The buckles appeared to develop at random sites along the trace with no clear connection to maximum load or scratch distance. The annealing treatment of 2 hours resulted in a similar number and distribution of buckles as the 1 hour annealing.

The role of the tip orientation changed with each annealing duration, however, on average the broad side of the tip seemed to be more efficient at inducing buckling, even though this orientation can be accompanied by more spallation. Blunting of the tip is also a factor, since the tip was exposed to a significant amount of wear during scratch testing and can also influence the buckle development [19–21].

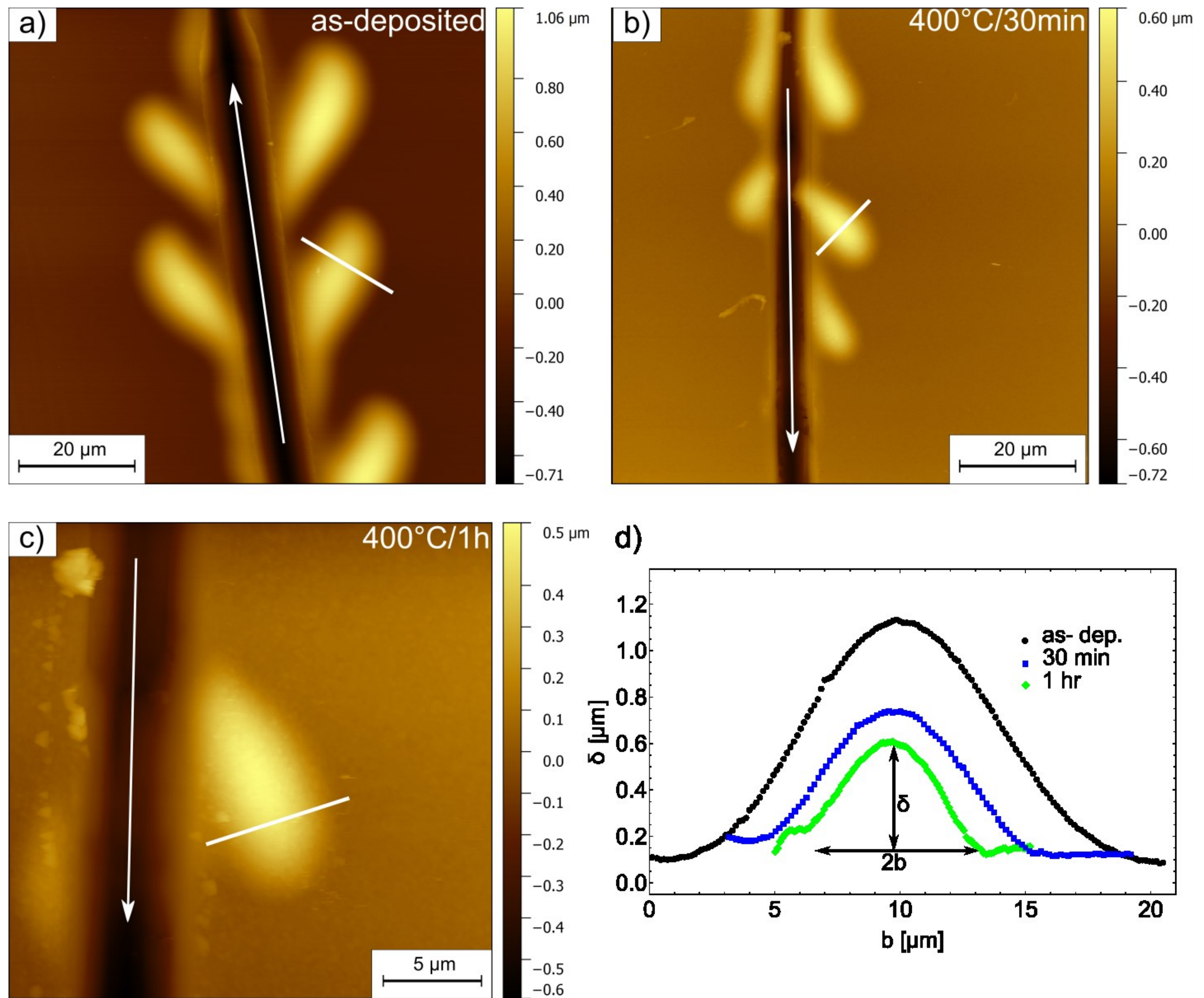

Figure 2: AFM height images of the scratch-induced buckles produced on the (a) as-deposited and films annealed at 400°C for (b) 30 min and (c) one hour with the arrows indicating the scratch direction. All buckles shown here were produced from scratches with a maximum load of 400 mN (scratch direction indicated by white arrows). The height profiles of these buckles indicated by the white lines in (a-c) are shown in (d) with the required measurements for the adhesion calculation depicted. A clear decrease in buckle height and width can be observed with increasing annealing time.

Generally, the amount of buckles significantly decreased as a result of the increasing annealing times and qualitatively suggests an increase in the adhesion energy. In order to quantitatively evaluate the adhesion of the film to the substrate the buckles were imaged with the AFM and the heights and widths measured. Each buckle was measured in three different places to ensure good statistics. When comparing the buckle dimensions for the different annealing treatments it can clearly be seen that the buckle sizes decreased with increased

annealing times shown in Figure 2d, where the AFM profiles illustrate the decrease in buckle width and height. This behavior is another qualitative indicator of increase of the adhesion energy due to the annealing treatments.

Even though the film stresses increased due to the annealing, the buckle dimensions decreased. However, according to Eq. 1 and 2 the buckles should became larger, given that the adhesion energy is constant. The stresses of the WTi film measured with XRD and calculated from the buckle dimensions using Eq. 2 are shown in Figure 3 and illustrate that the compressive stresses increase with longer annealing times. The values of film stress compare well up to 45 min of annealing time. For longer hold times the calculated values start to deviate from the measured values, when the buckles become much smaller. The deviation is most likely due to the fact that the calculation is very sensitive to the measured buckle dimension and slight errors can change the result. The fact that the buckles actually become smaller despite the increasing film stress can be attributed to increased adhesion energy. However, as shown in Figure 3, the error of the measured and the calculated film stresses for 1 and 2 hours of annealing overlap at the higher end, indicating that the difference may not be very significant.

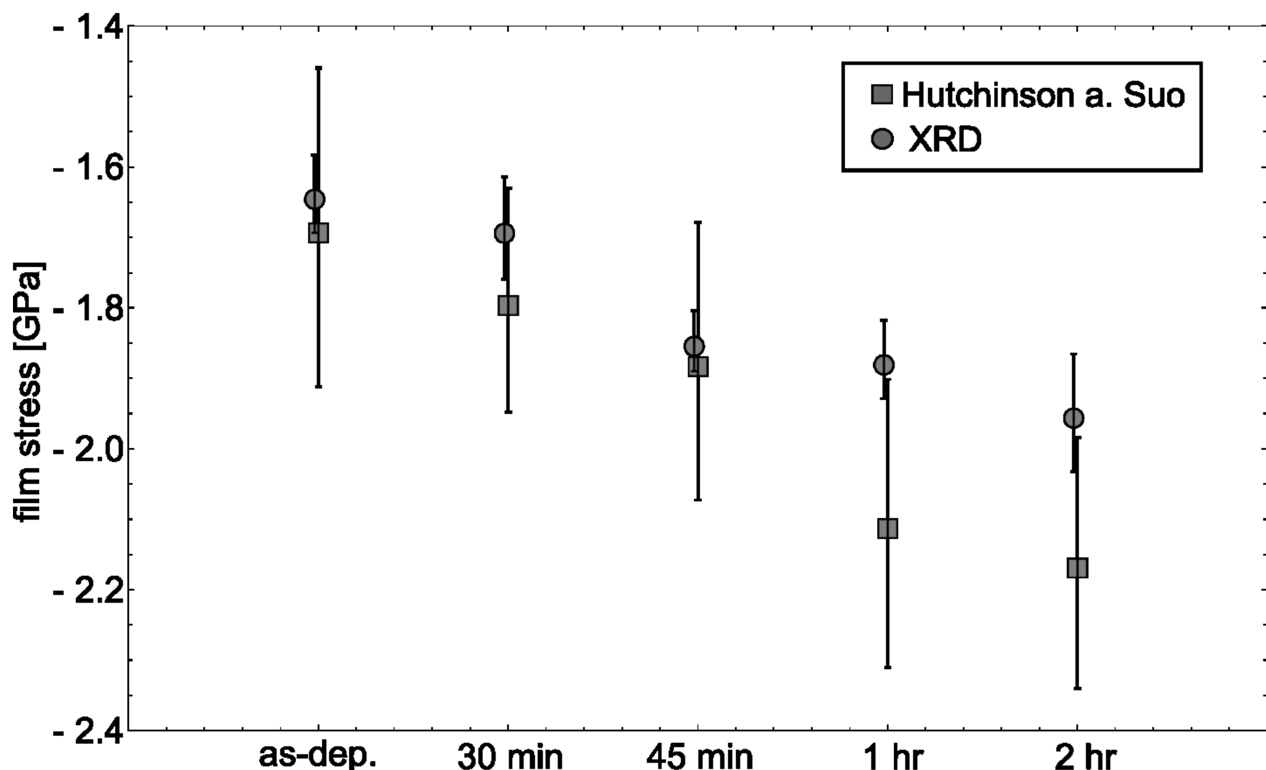

Figure 3: Film stress of the as-deposited and the annealed samples measured by XRD and calculated from Eq 2. An increase of compressive stress due to annealing time can be seen for the measured and the calculated film stress values.

The FIB cross-sections in Figure 4 demonstrate the interface separation for a buckle growing outward from the scratch trace. It is important to measure the profile of the buckles at a place far enough away from the trace, as illustrated in Figure 2 (white lines). This is the equilibrium region of the buckle where the height and width are constant with respect to the delamination growth direction and are more representative of the interface behavior. If the buckle is measured too close to the scratch trace the interfacial crack path might still be connected to the trace due to plastic deformation of the film and substrate. The measurements of the height and width of the buckles were taken sufficiently far away from the trace in order to avoid the areas where the buckle size could have been affected by plastic deformation from the scratch trace.

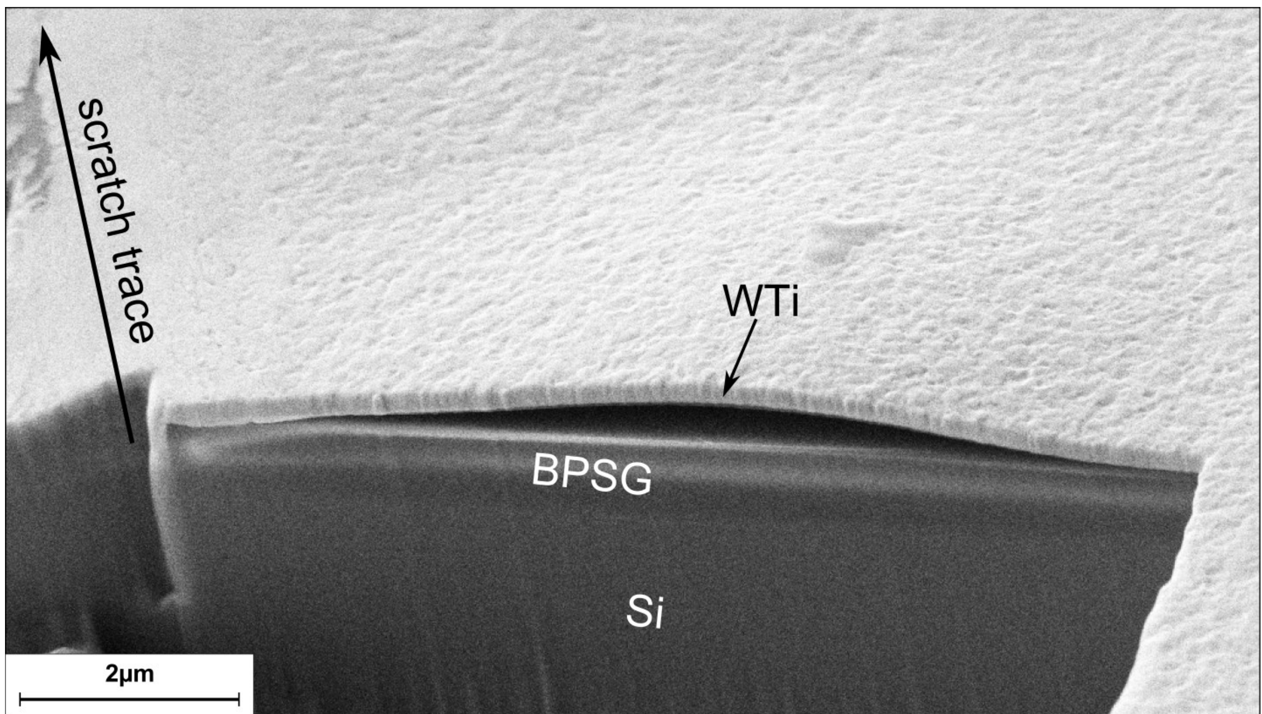

Figure 4: FIB cross-section of a buckle initiated from a scratch trace, made with a maximum load of 400 mN on a sample annealed for 30 minutes. A clear interface separation between the BPSG and the WTi film can be seen.

The film stress and mixed mode adhesion energy $\Gamma(\Psi)$ were calculated from the measured buckle dimensions, the film thickness and elastic properties using the model by Hutchinson and Suo (Eqs. 1-3) [27]. The buckles were modeled as spontaneous straight sided buckles. The results for the adhesion energies are shown in Figure 5. A significant increase in the adhesion energy after annealing was determined from the respective buckles. The adhesion energy of the as-deposited film was 2.7 J/m² and increased continuously to 4.7 J/m²

after two hours of annealing at 400°C. The adhesion energy for the as-deposited WTi film is similar to that of pure tungsten on glasslike substrates, which is know from literature to be in the range of 2.5-3 J/m² [9,13,15,22]. This indicates that the Ti content in the alloy does not significantly contribute to the adhesion of the system in the as-deposited state. The annealing treatment increased the adhesion of the system most likely due to the segregation of Ti from the WTi solid solution towards the interface, creating a titanium film that is only a few atom layers thick and promotes adhesion [6,9]. This process takes more than 30 minutes since a significant increase in adhesion was not detected within the margin of error. However, the adhesion of the WTi film increased continuously with increasing annealing time up to 2 hours. Longer annealing times have not yet been investigated, however, from Figure 5 it appears as though the adhesion energy reached a plateau around 4.7 J/m² since the difference between the 1 and 2 hour annealing times is only ~0.2 J/m², which is basically the resolution of the measurement. It should be noted that, longer annealing times would also increase the production time and costs of devices and can also have a negative impact on barrier stability.

The mixed mode adhesion energy calculated for the 1 and 2 hour annealing times compare well to the values measured from other methods for similar samples. For instance, 4PB performed by Völker et al [6,9] calculated an adhesion energy of 4.9-6 J/m² and microcantilever experiments by Matoy et al [13] which resulted in adhesion energies of 4.3 J/m². Fugger et al [5] detected a further increase of Ti segregation towards the copper above the WTi layer up to 16 hours of annealing at 600°C. Völker et al [9] investigated the effect of different contents of Ti (15at%-25at%) in the WTi alloy on adhesion and found no significant change in adhesion energy between the different films chemistries. This would further suggest that a saturation of Ti segregation at the BPSG interface is reached after more than two hours of annealing at 400°C when the adhesion of the WTi film is equal to pure Ti of about 6 J/m² [9].

The AES analysis of the BPSG surface revealed that Ti was present on all samples and W was not detected on the BPSG surface after the removal of the WTi film with the tape. A quantification of the Ti amount was not possible due to the overlap of Ti, TiOx and $TiSi_2$ Auger peaks.

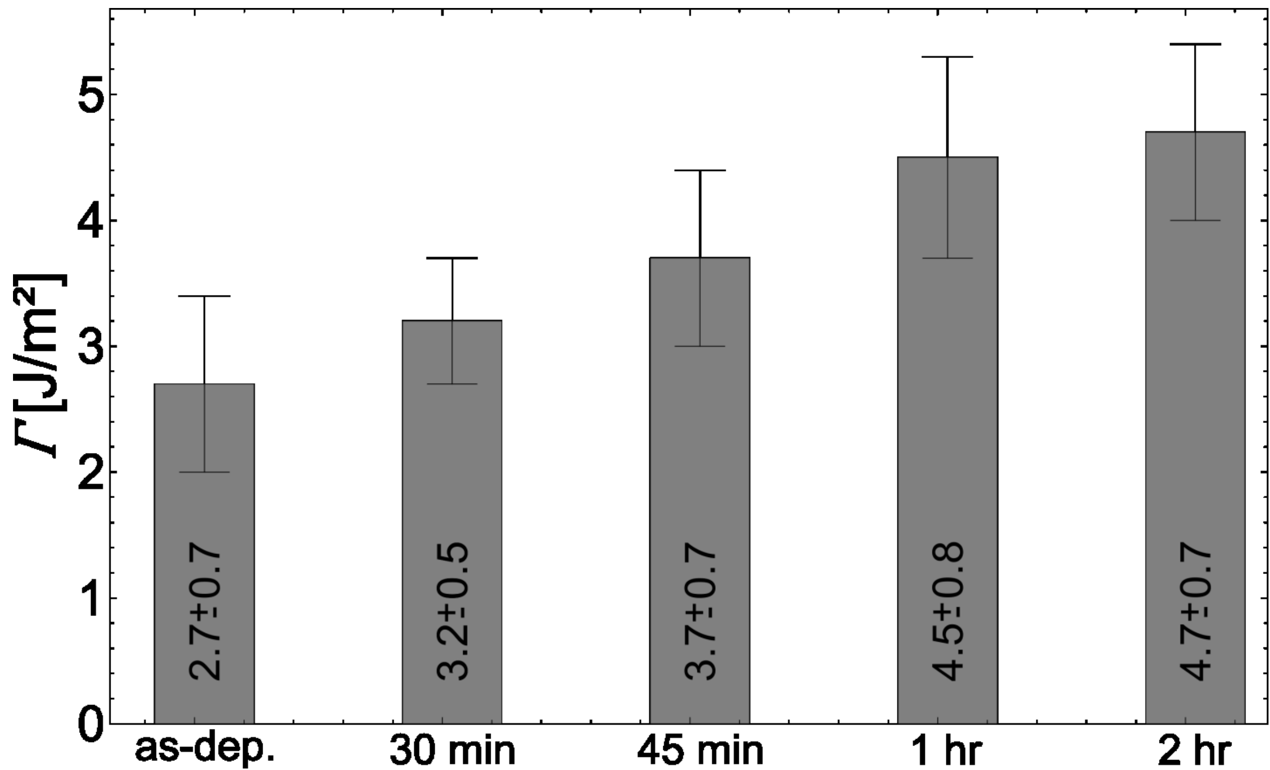

Figure 5: The mixed mode adhesion energies, Γ(Ψ), for the as-deposited and the annealed WTi films. The adhesion energy increases continuously with the annealing time up to approximately 1-2 hours.

4. Conclusion

The current study illustrated how the duration of annealing treatments affect the film stress and the adhesion of a WTi barrier layer alloy to BPSG. The stress in the WTi film became increasingly more compressive the longer it was annealed at 400°C, demonstrated by in-situ wafer curvature and synchrotron XRD experiments. Through the use of scratch induced delaminations the adhesion energies of the WTi barrier layer and BPSG substrate could be quantitatively measured. The buckle size and amount decreased significantly as the annealing times were increased and the calculated film stresses were in good agreement with the stresses measured with laboratory XRD. From the buckle dimensions the adhesion energy of the WTi film to the BPSG substrate was calculated and showed the increase of interface strength with annealing time, revealing a plateau between 1 and 2 hours annealing time. The increase of film stress and adhesion is believed to be due to the segregation of Ti from the film, which changes the interface chemistry.

Acknowledgements

The authors want to thank C. Trost, B. Putz and A. Leitner of the Erich Schmid Institute and T. Pelisset, V. Haberl and S. Zoth of Infineon Technologies Austria AG for experimental assistance. The authors would like to acknowledge HZB for the allocation of synchrotron radiation beamtime and thankfully acknowledges the financial support by HZB (project 16224035-ST). This work was jointly funded by the Austrian Research Promotion Agency (FFG: Project No. 846579) and the Carinthian Economic Promotion Fund (KWF, contract KWF-1521/26876/38867) further financial support by the Austrian Federal Government (837900) within the framework of the COMET Funding Program is appreciated.

References

[1] S.P. Murarka, Multilevel interconnections for ULSI and GSI era, Mater. Sci. Eng. R Reports. 19 (1997) 87–151. doi:10.1016/S0927-796X(97)00002-8.

[2] H. Ono, T. Nakano, T. Ohta, Diffusion barrier effects of transition metals for Cu/M/Si multilayers (M=Cr, Ti, Nb, Mo, Ta, W), Appl. Phys. Lett. 64 (1994) 1511–1513. doi:10.1063/1.111875.

[3] S.Q. Wang, S. Suthar, C. Hoeflich, B.J. Burrow, Diffusion barrier properties of TiW between Si and Cu, J. Appl. Phys. 73 (1993) 2301–2320. doi:10.1063/1.353135.

[4] J.-C. Chiou, K.-C. Juang, M.-C. Chen, TiW(N) as diffusion barriers between Cu and Si, J. Electrochem. Soc. 142 (1995) 2326–2331. doi:http://dx.doi.org/10.1149/1.2044295.

[5] M. Fugger, M. Plappert, C. Schäffer, O. Humbel, H. Hutter, H. Danninger, et al., Comparison of WTi and WTi(N) as diffusion barriers for Al and Cu metallization on Si with respect to thermal stability and diffusion behavior of Ti, Microelectron. Reliab. 54 (2014) 2487–2493. doi:10.1016/j.microrel.2014.04.016.

[6] B. Völker, W. Heinz, K. Matoy, R. Roth, J.M. Batke, T. Schöberl, et al., Interface fracture and chemistry of a tungsten-based metallization on borophosphosilicate glass, Philos. Mag. 6435 (2014) 1–15. doi:10.1080/14786435.2014.913108.

[7] A.A. Volinsky, N.R. Moody, W.W. Gerberich, Interfacial Toughness Measurements

for Thin Films on Substrates, Acta Mater. 50 (2002) 441–466. doi:10.1016/S1359-6454(01)00354-8.

[8] K.L. Mittal, The role of the interface in adhesion phenomena, Polym. Eng. Sci. 17 (1977) 467–473. doi:10.1002/pen.760170709.

[9] B. Völker, W. Heinz, K. Matoy, R. Roth, J.M. Batke, T. Schöberl, et al., Mechanical and chemical investigation of the interface between tungsten-based metallizations and annealed borophosphosilicate glass, Thin Solid Films. 583 (2015) 170–176. doi:10.1016/j.tsf.2015.03.047.

[10] R.H. Dauskardt, M. Lane, Q. Ma, N. Krishna, Adhesion and debonding of multi-layer thin film structures, Eng. Fract. Mech. 61 (1998) 141–162. doi:10.1016/S0013-7944(98)00052-6.

[11] A.M. Brown, M.F. Ashby, Correlations for Diffusion Constants., Acta Metall. 28 (1980) 1085–1101. doi:10.1016/0001-6160(80)90092-9.

[12] P.G. Charalambides, H.C. Cao, J. Lund, A.G. Evans, Development of a test method for measuring the mixed mode fracture resistance of bimaterial interfaces, Mech. Mater. 8 (1990) 269–283. doi:10.1016/0167-6636(90)90047-J.

[13] K. Matoy, T. Detzel, M. Müller, C. Motz, G. Dehm, Interface fracture properties of thin films studied by using the micro-cantilever deflection technique, Surf. Coatings Technol. 204 (2009) 878–881. doi:10.1016/j.surfcoat.2009.09.013.

[14] T.P. Weihs, S. Hong, J.C. Bravman, W.D. Nix, Mechanical deflection of cantilever microbeams: A new technique for testing the mechanical properties of thin films, J. Mater. Res. 3 (1988) 931–942. doi:10.1557/JMR.1988.0931.

[15] M.J. Cordill, D.F. Bahr, N.R. Moody, W.W. Gerberich, Recent Developments in Thin Film Adhesion Measurement, IEEE Trans. Device Mater. Reliab. 4 (2004) 163–168. doi:10.1016/j.msea.2006.08.027.

[16] M.D. Kriese, W.W. Gerberich, N.R. Moody, Quantitative adhesion measures of multilayer films: Part I. Indentation mechanics, J. Mater. Res. 14 (1999) 3007–3018. doi:10.1557/JMR.1999.0404.

[17] M.D. Kriese, W.W. Gerberich, N.R. Moody, Quantitative adhesion measures of

multilayer films: Part II. Indentation of W/Cu, W/W, Cr/W, J. Mater. Res. 14 (1999) 3019–3026. doi:10.1557/JMR.1999.0405.

[18] D.B. Marshall, A.G. Evans, Measurement of adherence of residually stressed thin films by indentation. I. Mechanics of interface delamination, J. Appl. Phys. 56 (1984) 2632–2638. doi:10.1063/1.333794.

[19] S.J. Bull, Failure mode maps in the thin film scratch adhesion test, Tribol. Int. 30 (1997) 491–498. doi:10.1016/S0301-679X(97)00012-1.

[20] S.J. Bull, E. G.-Berasetegui E., Chapter 7 An overview of the potential of quantitative coating adhesion measurement by scratch testing, in: Tribol. Interface Eng. Ser., 2006: pp. 99–114. doi:10.1016/S0167-8922(06)80043-X.

[21] S.J. Bull, Failure modes in scratch adhesion testing, Surf. Coatings Technol. 50 (1991) 25–32. doi:10.1016/0257-8972(91)90188-3.

[22] A. Kleinbichler, J. Zechner, M.J. Cordill, Buckle Induced Delamination Techniques to Measure the Adhesion of Metal Dielectric Interfaces, Microelectron. Eng. (2016). doi:10.1016/j.surfcoat.2016.08.074.

[23] A. Roshanghias, G. Khatibi, R. Pelzer, J. Steinbrenner, On the effects of thickness on adhesion of TiW diffusion barrier coatings in silicon integrated circuits, Surf. Coatings Technol. 259 (2014) 386–392. doi:10.1016/j.surfcoat.2014.10.065.

[24] A. Roshanghias, R. Pelzer, G. Khatibi, J. Steinbrenner, Thickness dependency of adhesion properties of TiW thin films, in: Proc. 16th Electron. Packag. Technol. Conf. EPTC 2014, 2014: pp. 192–195. doi:10.1109/EPTC.2014.7028417.

[25] P.A. Steinmann, Y. Tardy, H.E. Hintermann, Adhesion testing by the scratch test method: The influence of intrinsic and extrinsic parameters on the critical load, Thin Solid Films. 154 (1987) 333–349. doi:10.1016/0040-6090(87)90377-4.

[26] D.F. Bahr, J.W. Hoehn, N.R. Moody, W.W. Gerberich, Adhesion and acoustic emission analysis of failures in nitride films with a metal interlayer, Acta Mater. 45 (1997) 5163–5175. doi:10.1016/S1359-6454(97)00180-8.

[27] J.W. Hutchinson, Z. Suo, Mixed Mode Cracking in Layered Materials, Adv. Appl. Mech. 29 (1991) 63–191. doi:10.1016/S0065-2156(08)70164-9.

[28] D.M. Többens, S. Zander, KMC-2: an X-ray beamline with dedicated diffraction and XAS endstations at BESSY II, J. Large-Scale Res. Facil. JLSRF. 2 (2016) 1–6. doi:10.17815/jlsrf-2-65.

[29] I.C. Noyan, J.B. Cohen, Residual stress: measurement by diffraction and interpretation, Springer-Verlag, Berlin, 1987.

[30] A.G. Dirks, R.A.M. Wolters, A.J.M. Nellissen, On the microstructure-property relationship of WTi(N) diffusion barriers, Thin Solid Films. 193–194 (1990) 201–210. doi:10.1016/S0040-6090(05)80028-8.

[31] I.J. Raaijmakers, T. Setalvad, A.S. Bhansali, B.J. Burrow, L. Gutai, K.B. Kim, Microstructure and barrier properties of reactively sputtered Ti-W nitride, J. Electron. Mater. 19 (1990) 1221–1230. doi:10.1007/BF02673336.

[32] E. Eiper, K.J. Martinschitz, I. Zizak, N. Darowski, J. Keckes, X-ray elastic constants determined by the combination of sin2 ψ and substrate-curvature methods, Zeitschrift Für Met. 96 (2005) 1069–1073.

[33] G.G. Stoney, The Tension of Metallic Films Deposited by Electrolysis, Proc. R. Soc. A Math. Phys. Eng. Sci. 82 (1909) 172–175. doi:10.1098/rspa.1909.0021.

[34] D. Nečas, P. Klapetek, Gwyddion: an open-source software for SPM data analysis, Open Phys. 10 (2012) 181–188. doi:10.2478/s11534-011-0096-2.

[35] P.A. Flinn, Principles and applications of wafer curvature techniques for stress measurements in thin films, Mat Res Soc Symp Proc. 130 (1989) 41–51. doi:10.1557/PROC-130-41.

Publication V

Manuscript submitted for publication

Scratch induced thin film buckling for quantitative adhesion measurements

A. Kleinbichler[1,2], M. J. Pfeifenberger[2], J. Zechner[1], S. Wöhlert[3], M. J. Cordill[2]

[1]KAI – Kompetenzzentrum Automobil- und Industrieelektronik GmbH,
Technologiepark Villach, Europastraße 8, Villach, Austria 9524

[2]Erich Schmid Institute for Material Science, Austrian Academy of Sciences and Dept.
Material Physics, Montanuniversität Leoben, Jahnstraße 12, Leoben, Austria, 8700

[3]Infineon Technologies AG, Siemensstraße 2, 9500 Villach, Austria

Abstract

The adhesion of thin films is one of the most important factors for the reliability of microelectronic devices and the semiconductor industry requiring quantitative testing methods to effectively compare these interfaces. Several techniques have been developed over the last decades with scratch induced delamination being a rarely studied method. For compressively stressed films on rigid substrates scratching can cause buckling failure ideal to determine the adhesion quantitatively by modeling the delaminations according to the Hutchinson and Suo model. Two different sample systems, a tungsten-titanium film on a silicate glass (single metal film) and a silicon nitride film on a silicate glass with a tungsten-titanium overlayer (dielectric with stressed overlayer), have been tested using a ramp load method in the range of 100-500 mN. This study demonstrates that the scratching resulted in buckles parallel to the scratch trace and triggered further spontaneous buckling. Using the dimensions of the scratch induced buckles the adhesion energies of the interfaces were quantified for the two film systems. It was shown that the adhesion energy of the tungsten-titanium/silicate glass interface was measured to be 2.7 J/m² and for the silicon nitride/silicate glass interface was determined to be 1.4 J/m². The results illustrate that the scratch test can be utilized for quantitative adhesion testing of thin films in cases where other methods do not work and suggest that scratch induced delamination is a valuable addition to established adhesion measurement techniques.

Keywords: adhesion, thin films, scratch test, buckling

1. Introduction

The adhesion of thin films is of the utmost importance for the reliability of microelectronic devices and protective coatings. Over the last decades many different experimental methods have been developed to quantitatively assess the adhesion of thin films [1–3]. Successful techniques are four point bending (4PB) [4–6], bulge testing [2], microcantilever tests [7], spontaneous buckling [8–10] and nanoindentation [2,11,12]. One method that has almost been forgotten is scratch testing [13] due to the difficulty to obtain quantitative adhesion energies.

Scratch testing has been a well-known method to assess the wear resistance and the fracture of thin films and coatings. However, the results are mainly qualitative by revealing the critical load a film detaches from its substrate. It has been shown that for a better understanding of the scratch test a careful evaluation of the failure mode of the coating as a response to the scratch is necessary [14–16]. These failure modes depend on a large range of parameters such as the hardness and elastic modulus of the film in relation to the substrate, the scratch load, tip form and size as well as film thickness and residual stress. The two failure modes generally associated with the adhesion of the film to the substrate are spallation, where a segment of the coating is detached and lifted away from the substrate ahead of the scratch tip, and buckling, where the film deflects away from the substrate as a result of the stress induced around the moving scratch tip [14]. Both of these failure modes can be used to quantitatively assess the adhesion energy of an interface. The spallation failure can be quantified under certain conditions as demonstrated by Venkataraman et al. [17] by using the geometry of the spalled area, the width of the scratch trace and the critical load of spallation to calculate the adhesion energy. While Moody et al. [18] showed that a scratch can trigger a uniform width buckle at the side of the scratch trace which could be used to assess the adhesion of a thin film.

A buckle can be used to calculate the adhesion energy of an interface by measuring its dimensions and using the model developed by Hutchinson and Suo [19]. Using the half-buckle width, b, and height, δ, the critical stress for interface separation, σ_b, and the driving stress which is the residual stress in the film, σ_d, can calculated from equations (1) and (2),

$$\sigma_b = \frac{\mu^2 E}{12(1-\nu^2)}(h/b)^2, \qquad (1)$$

$$\sigma_d = \sigma_b[c_1(\delta/h)^2 + 1], \qquad (2)$$

with the film thickness, h, the elastic modulus, E, and Poisson's ratio, ν, of the film. The geometry factors μ^2 is π^2 and c_1 = 3/4 in the case of a straight buckle [11,19]. The mixed mode adhesion energy, $\Gamma(\Psi)$, which represents the practical work of adhesion, can then be calculated from equation (3),

$$\Gamma(\Psi) = \left[\frac{(1-\nu^2)h}{2E}\right](\sigma_d - \sigma_b)(\sigma_d + 3\sigma_b) \quad (3)$$

In the case that the buckle is pinned at the center of the imprint the geometry factors μ^2 changes to 42.67 and $c_1 = 0.2473(1+\nu)+0.2231(1-\nu^2)$ and the mixed mode adhesion energy is then calculated from equation (4),

$$\Gamma(\Psi) = c_2[1 - (\sigma_b/\sigma_d)^2]\frac{(1-\nu)h\sigma_d{}^2}{E}, \quad (4)$$

with $c_2 = [1+0.9021(1-\nu)]^{-1}$. Kriese et al. [20] described that, in the case of a multilayer or a stressed overlayer when two or more films are buckling, the equation for the buckling stress has to be adjusted with a combined second moment of inertia, I_T. Details can be found in Ref. [20].

This study will demonstrate that the scratch test can be used to induce buckling in two different film systems, a single metal film on a silicate glass and a dielectric film with stressed overlayer on a silicate glass. The scratch buckles can propagate in two different ways, parallel to the trace and away from the trace as telephone cords, depending on the deformation induced by the tip and the stress in the film system. Using the buckle dimensions the adhesion energies of the two interfaces will be calculated and compared to results of other techniques.

2. Experiment

Two sample wafers were provided by Infineon Technologies Austria AG. Each sample consisted of a 725 µm thick silicon wafer with a diameter of 200 mm, coated with a dielectric layer, a ceramic and a metal barrier film. In the first deposition step the wafers were coated with 800 nm of Borophosphosilicate glass (BPSG) using plasma enhanced chemical vapor deposition (PECVD) followed by annealing at 900°C. Afterwards, 400 nm of PECVD silicon nitride (Si_3N_4) was deposited on one of the wafers. Finally, a 300 nm thick tungsten titanium (WTi) barrier layer film was sputter deposited on both wafers, where the W film contained 20 at% of Ti. The WTi films were deposited under conditions that induced a compressive residual stress of about 1.5 GPa measured by X-ray diffraction. The Si_3N_4 film was effectively without residual stress due to annealing. The configurations of the produced

samples were as follows, one Si wafer with BPSG/WTi and one Si wafer with BPSG/Si_3N_4/WTi.

The scratch experiments were performed on a Keysight G200 nanoindenter using a Berkovich tip. Both the sharp edge and the broad face of the pyramidal tip were utilized as the scratch front in order to induce different stress fields during scratching [13–15]. The scratch distance of all experiments was 500 µm and the distance between the scratches was set to 500 µm to avoid interaction with other scratches or the induced delaminations. The maximum load range was between 100-500 mN with a scratch velocity of 30 µm/s and at least five scratches were made for each maximum load and tip orientation. Scratches were first examined with an optical light microscope to identify if delaminations occurred and were repeated over a period of days and weeks to account for further buckle development. A Zeiss LEO 1540 XP focused ion beam (FIB) microscope and a Zeiss Auriga femtosecond laser system and FIB [21] was used to examine the failed interfaces and any deformation due to the mechanical loading. The procedure using the femtosecond laser is described in [12]. To measure the buckle dimensions a Veeco Dimension DI3000 atomic force microscope (AFM) and an Olympus LEXT OLS 4100 confocal laser scanning microscope (CLSM) were used. The buckle measurements were taken from the AFM and CLSM height images using the free software Gwyddion [22] and the adhesion energies were calculated using the Hutchinson and Suo model [19] (eqns. 1-4). More than 20 different buckles were measured for each sample system to provide sufficient statistics for the adhesion energies. The elastic modulus and the hardness of the WTi films and BPSG films were determined from nanoindentation experiments using the continuous stiffness method and a well-calibrated, sharp Berkovich tip (not the same tip used for the scratching experiments). The modulus and hardness of WTi was measured to be E_{WTi} = 171.8 GPa and H_{WTi}=14 GPa, respectively. The modulus and hardness of the BPSG film was E_{BPSG} = 55.4 GPa and H_{BPSG} = 5 GPa. These values were measured at an indentation depth of about 30 nm which corresponds to 10% of the total film thickness. The Poisson's ratio of WTi was determined using the rule of mixtures with v_W = 0.28 and v_{Ti} = 0.32, which yields v_{WTi} = 0.288. The modulus, Poisson's ratio and hardness of Si_3N_4 were taken from Vlassak et al. [23] where these properties E_{Si3N4} = 222 GPa and v_{Si3N4} = 0.27 were measured by bulge testing and H_{Si3N4} = 21 GPa determined from nanoindentation.

3. Results

3.1. WTi/BPSG System

The results of the scratch tests, made with the sharp side of the Berkovic tip being the scratch front, on the WTi/BPSG samples are shown in Figure 1. The buckles developed mainly on scratches with maximum loads of 300 mN and continued to develop up to maximum loads of 500 mN, as was previously observed [24]. Figure 1 shows that the buckles on the WTi/BPSG system formed parallel to the scratch trace and as spontaneous telephone cord buckles originating from the scratch trace. Post scratch observations with an optical microscope revealed that the buckles parallel to the trace formed first as a direct result of the scratch. These buckles developed either on one side or on both sides of the trace, as seen in Figure 1a and b, respectively. This was most likely due to non-uniformities of the scratch tip which have a large influence on the scratch test [13,16]. Parallel buckles mostly formed right after scratching but also could emerge several hours after testing. Spontaneous buckles developed from the parallel buckles and propagate as telephone cords according to the film stress distribution after several hours or even a few days after testing [25]. Spontaneous buckles emerged randomly along the parallel buckles, probably where an interface defect was located close enough to the parallel buckles.

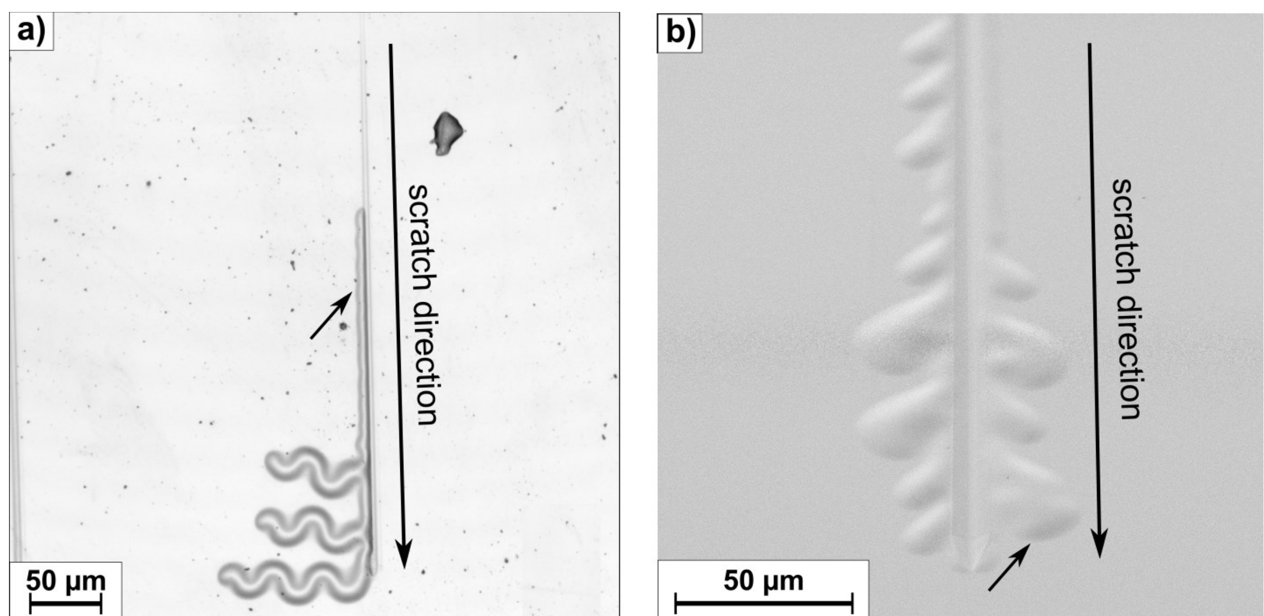

Figure 8: Buckles developed from scratch traces with maximum loads of 500 mN and with the sharp side of the pyramid as the scratch front. (a) CLSM laser image of a scratch with parallel buckles at the side of the trace (arrow) and spontaneous buckles. (b) SEM image of a scratch where the parallel buckles transition to spontaneous buckles and propagate along the trace indicated by the arrow.

The scratch distance-displacement (DD) and load-displacement (LD) curves of scratches made with loads of 300 to 500 mN are shown in Figure 2. The DD curve (Figure 2a) shows the increasing displacement into the surfaces over the scratch distance and the LD curves (Figure 2b) illustrate the displacement with increasing load. The 300-400 mN curves show no indication of buckling, such as pop-ins or load drops, which are common for indentation induced buckles [11,12]. Only the LD-curve of the 500 mN scratch shows a small change in the slope above 400 mN and could be an indication of a delamination or fracture event but are not always related to buckling.

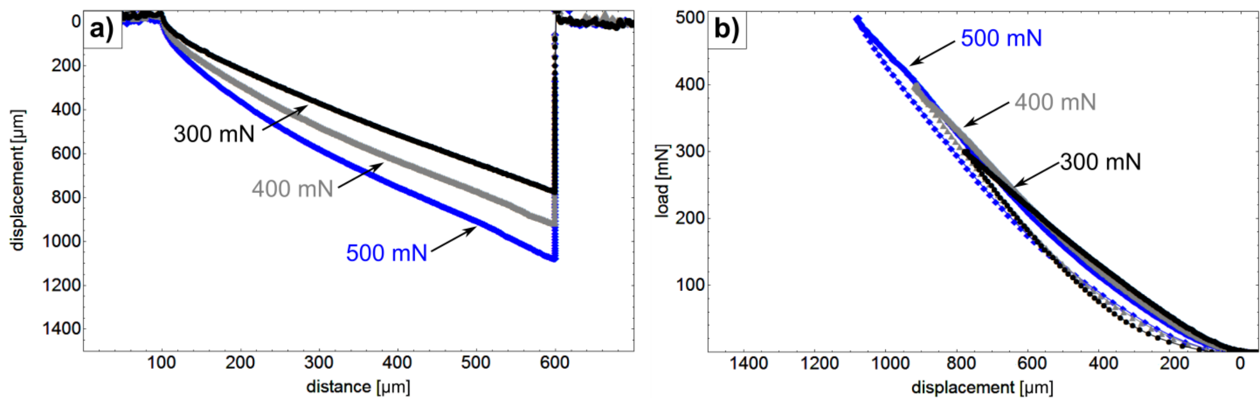

Figure 9: (a) Scratch distance-displacement curve and (b) load-displacement curve of the representative scratches with buckle development. No pop-ins or other indicators of delamination or fracture can be observed in the WTi/BPSG system.

The spontaneous buckles originating from the scratch trace are an ideal way to evaluate adhesion because these buckles develop without plastic deformation and are solely governed by film stress and adhesion to the substrate [26]. The parallel buckles, on the other hand, are heavily affected by the plastic deformation of the scratch trace which could impact their geometry. Due to the fact that the spontaneous buckles originate from the parallel buckles next to the scratch trace, it is imperative that the spontaneous buckles are measured far enough away from the scratch trace. This ensures that the dimensions of the buckle are measured at a location where the buckle is not influenced by the plastic deformation of the scratch. Presented in Figure 3 are FIB cross-sections of a spontaneous buckle and a parallel buckle, to illustrate how the interface crack propagated and is influenced by the scratch trace. The spontaneous buckle in Figure 3a propagated away from the trace and was no longer affected by the scratch trace deformation after about 5 µm from the scratch trace. The distance where the buckle has completely detached from the trace can be regarded as the location when the buckle bases are at the same level. This distance depends on many factors such as material properties of the film and substrate, distribution of film stress, adhesion and extension of the

scratch trace. The parallel buckle was always attached to the trace and the plastic deformation which occurred in the trace could affect its dimensions. Plastic deformation can be observed by the smoother film surface on the buckle flanks which face the trace, as seen in Figure 3b. Additionally it was observed that the BPSG (H = 5.3 GPa) densified [27] under the scratch trace due to the loading while the WTi (H = 14.1 GPa) was less affected. The difference in hardness of the two layers is most likely the cause for the different amounts deformation under the scratch tip. The interface crack between the BPSG and the WTi, visible in Figure 3b, kinks into the groove of the scratch trace and the buckle extends into the deformed scratch trace.

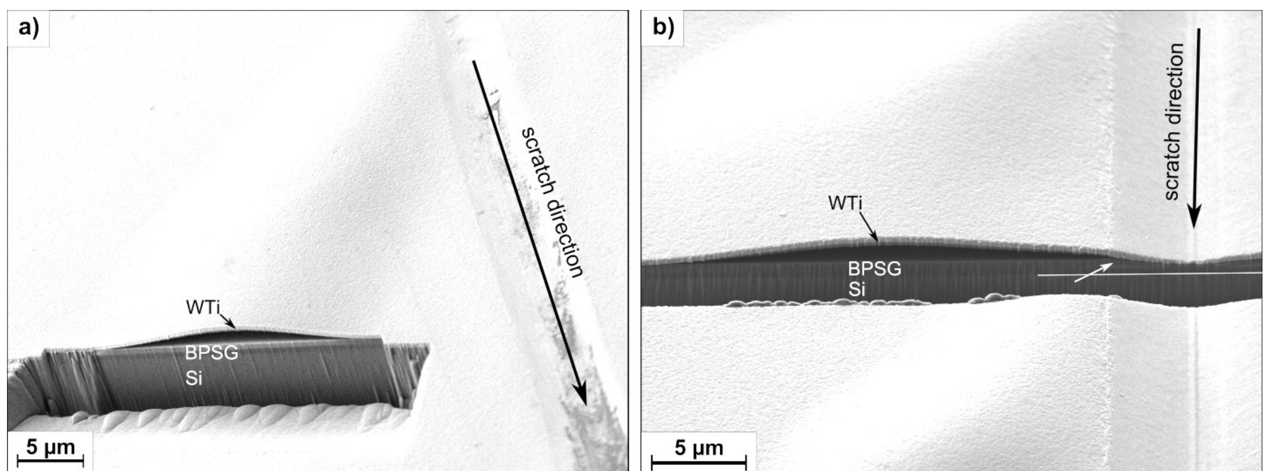

Figure 10: Cross-sections of (a) a spontaneous buckle originating from a scratch trace and (b) a parallel buckle along the scratch trace. The spontaneous buckle is completely detached from the trace. The parallel buckle stays attached to the scratch trace and the interface crack kinked into the plastically deformed trace (white arrow). The white line indicates the boundary between the Si and the BPSG to illustrate the densification of the BPSG under the trace.

An AFM height image used to measure the buckle dimension is shown in Figure 4a. Using the approach of Hutchinson and Suo (eqns. 1-3), the spontaneous buckles were modeled as unpinned straight sided buckles [19]. Their width and height were measured at the equilibrium positions as indicated in Figure 4b. The adhesion energy of WTi on BPSG was calculated as 2.7 ± 0.6 J/m² from spontaneous buckles originating from scratches and compare well to spontaneous buckles which developed solely due to film stress which to 2.6 ± 0.6 J/m² [24].

The cross-section of the parallel buckles in Figure 3b and the profile in Figure 4c suggests that the model of the pinned circular buckles can be applied to this kind of buckle (eqn. 4) [19]. The results of this approximation of the parallel buckles were calculated to 2.1 ± 0.2 J/m² which is slightly lower than the spontaneous buckles. It should be noted here, that for a

pinned blister its diameter has to be much larger than the residual indentation imprint to be used to avoid plastic deformation effects which can influence the adhesion calculation [11]. The same condition should be applied to the parallel buckles if modelled in this way and in the case of the WTi/BPSG system this condition is only minimally fulfilled, as seen in Figure 4c. However, a good agreement between the spontaneous and parallel buckles adhesion energies is observed.

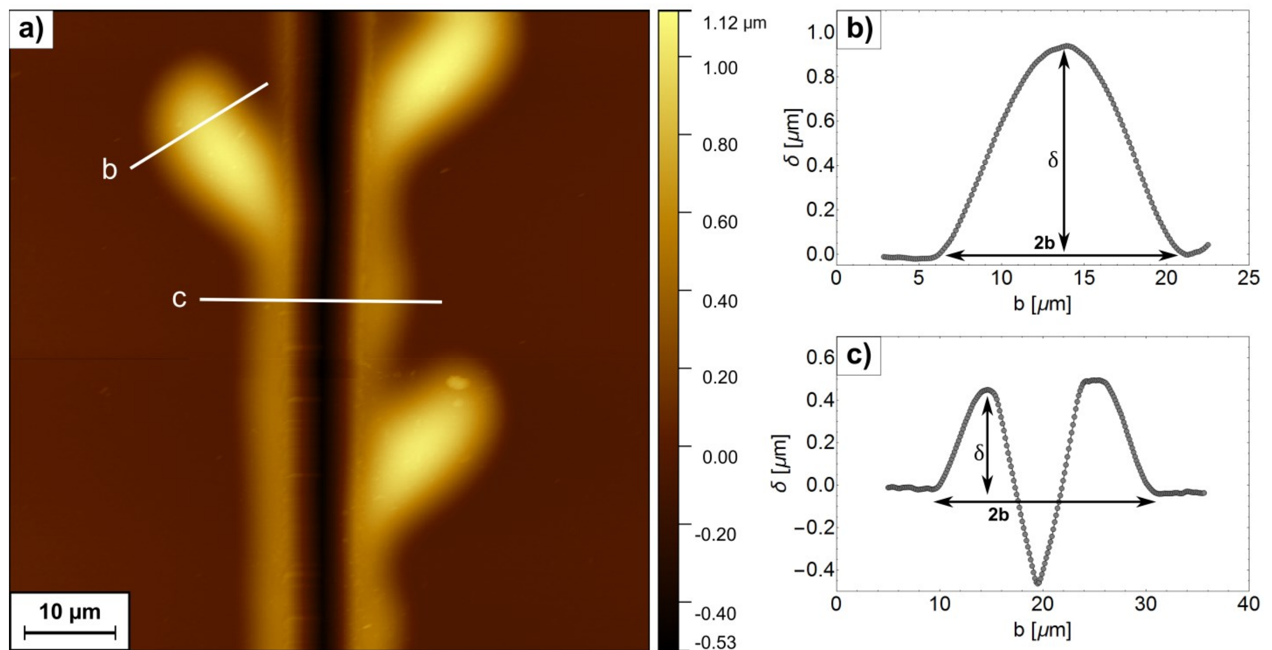

Figure 11: (a) AFM height image of scratch made with 500 mN load with parallel and spontaneous buckles. The white lines indicate where the profiles for (b) spontaneous and (c) parallel buckles have been taken.

3.2. WTi/Si_3N_4/BPSG system

On the WTi/Si_3N_4/BPSG system, the buckles developed in a similar way to the WTi/BPSG and in a similar load range (Figure 5). Buckles first developed at scratches made with maximum loads of 300 mN (Figure 5a) but only half of these scratches exhibited buckles. The scratches which delaminated formed parallel buckles that extended almost along the entire scratch distance. The spontaneous buckles then also propagated away from the parallel buckles in a straight or telephone cord pattern, similar to the case of the WTi/BPSG sample. As the maximum load was increased to 400 and 500 mN, all scratches produced buckles parallel to the trace with spontaneous buckles and spallation occurring after a certain scratch distance in the trace seen in Figure 5b. The parallel buckles developed immediately after the scratch was performed followed by the development of the spontaneous buckles. The further

propagation of the spontaneous buckles into telephone cords occurred over time. The spalled areas showed that the WTi and the Si_3N_4 film were removed from the BPSG film suggesting that the Si_3N_4/BPSG interface is the weakest interface as previously seen with nanoindentation experiments [12]. These areas also had mostly circular geometries which suggests a classical buckling failure of the film [13,14]. It should be noted that the majority of the buckle development on this system is governed by the stress in the WTi film because there was no significant stress in the Si_3N_4 film after annealing.

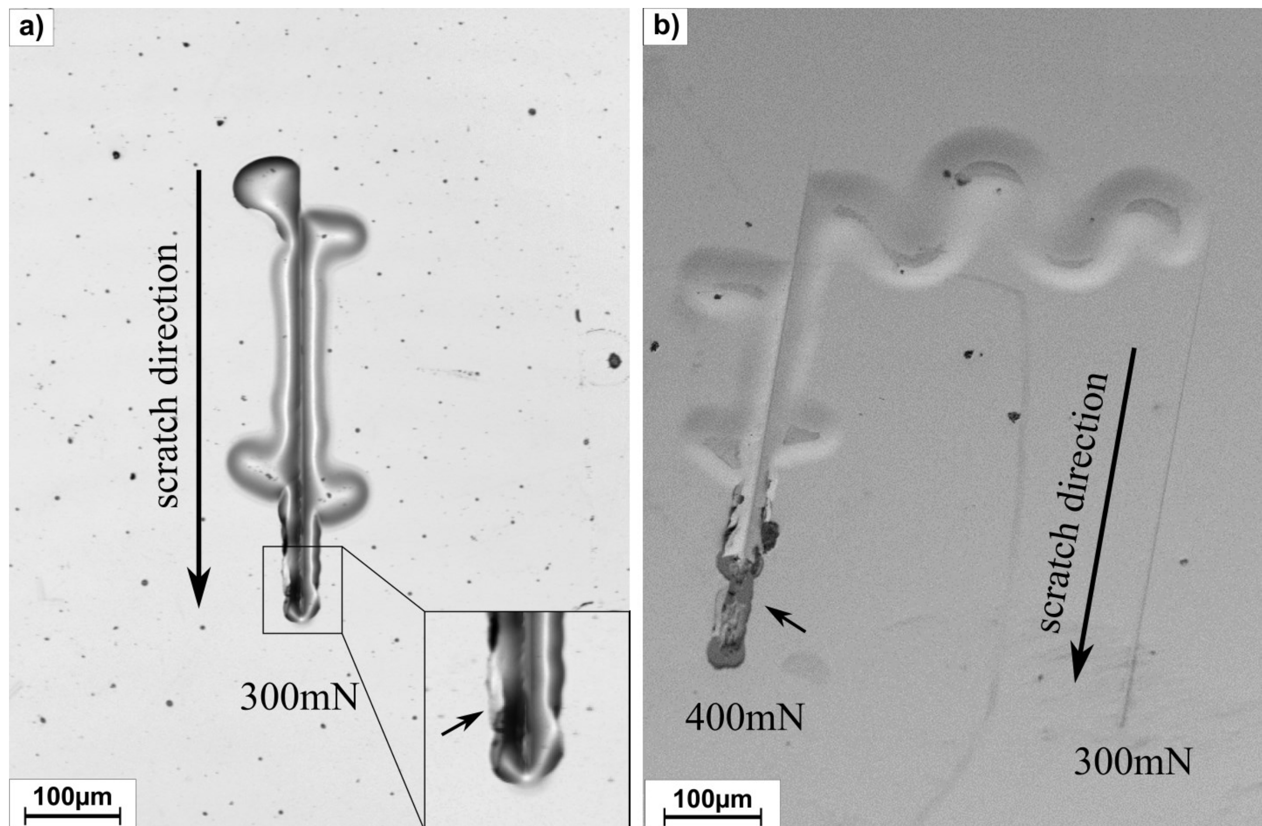

Figure 12: Buckles developed on a WTi/Si_3N_4/BPSG system after scratching with (a) 300 and (b) 400 mN, parallel to the scratch trace and as spontaneous buckles. The scratches made with 300 mN had, for the case of parallel buckling (a), signs of through thickness fracture at the end of the trace indicated by the arrow in the inset. Scratches made with higher loads (b) had this fracture earlier in the trace (arrow) which transitioned to spallation when the scratch is continued.

The DD and LD curves for scratches made with 300 to 500 mN are shown in Figure 6. In the case of the 300 mN scratch both curves show no indication of buckling or fracture, similar to the WTi/BPSG sample. However, fracture along the last 100 µm of the trace occurred at this load, as can be seen in the inset in Figure 5a, although it did not lead to spallation. For 400 and 500 mN of maximum load both curves illustrate spallation at loads between 262 and 276 mN and around about 1 µm of displacement into the surface. Analogous to indentation

induced delamination, reaching the fracture threshold of the Si_3N_4 film caused spallation (black arrow Figure 5b), but also triggered parallel buckle formation backwards along the scratch trace. A similar process was observed by Bahr et al. [28] and Moody et al. [18] for a tantalum nitride film on a sapphire substrate. This finding is supported by the fact that only scratches which exhibited fracture or spallation, as seen in the case of the 300 mN scratches in Figure 5a and b, generated parallel buckles. Scratches with loads of 300 mN did exceed the load required for spallation but the depth at the end of the scratch trace was less than 1 µm. As a consequence, most of these scratches produced no buckles. In the cases where buckles did develop, fracture in the form of through thickness cracking is visible at the end of the scratch trace which can be observed in the inset in Figure 5a, indicated by the arrow.

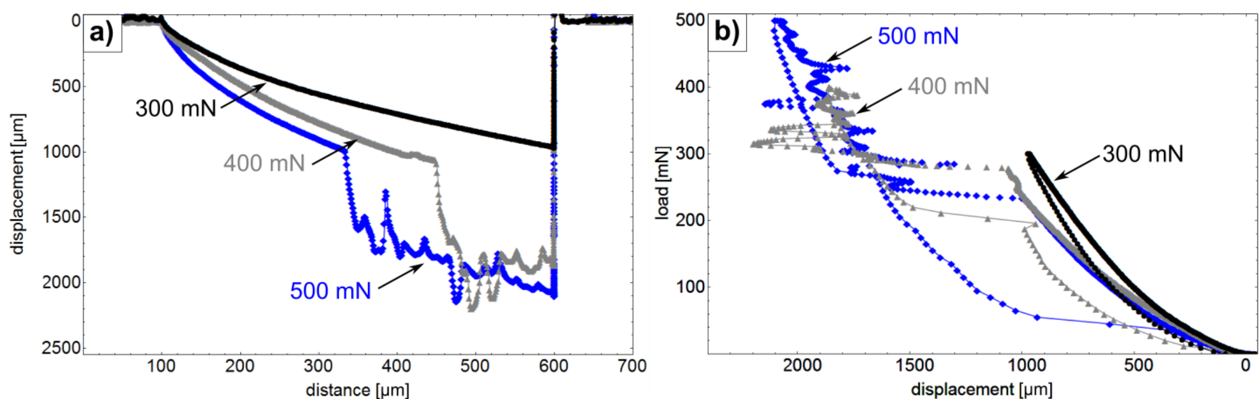

Figure 13: Scratch distance-displacement curve (a) and load-displacement curve (b) of scratches made with 300 to 500 mN. The curves for 300 mN scratches show no pop-in but also did not reach 1 µm of displacement. For scratches with higher loads the spallation can be seen in both curves occurring at depth of around 1 µm. This spallation occurs earlier in the trace, the higher the maximum scratch load.

The cross-sections of the spontaneous and parallel buckles in this system are shown in Figure 7a and b. In Figure 7c and d the white rectangles in 7a and b are magnified and show the base of the spontaneous buckle as well as the center of the parallel buckle. It can be seen that for both buckle types the Si_3N_4/BPSG-interface is separated which is in agreement with the observation of the spalled areas. The development and propagation of the spontaneous buckles is strongly affected by the Si_3N_4 because through thickness cracks form at the buckle base and arrest in the WTi film (Figure 7c). The cracks in the Si_3N_4 halt the spontaneous buckle propagation when it occurs at the front of the growing buckle and can also cause the buckle to spall off the substrate (Figure 5b), similar to indentation buckles [12]. The parallel buckles were not as severely influenced by the deformation of the trace as in the case of the WTi/BPSG system because their dimensions were much larger and the Si_3N_4 film prevents

deformation of the BPSG due to its high hardness (H = 21 GPa). It was observed that the BPSG again densified by the passing indenter tip and the Si_3N_4 and WTi films remained about the same thickness and that the interface crack again reached into the area of deformed substrate. Figure 7d shows that the plastic deformation is very small compared to the width and height of the parallel buckle. Additionally, the parallel buckles had little to no fracture at the base which might also aid spontaneous buckles development due to the fact that the interface crack did not kink through the Si_3N_4.

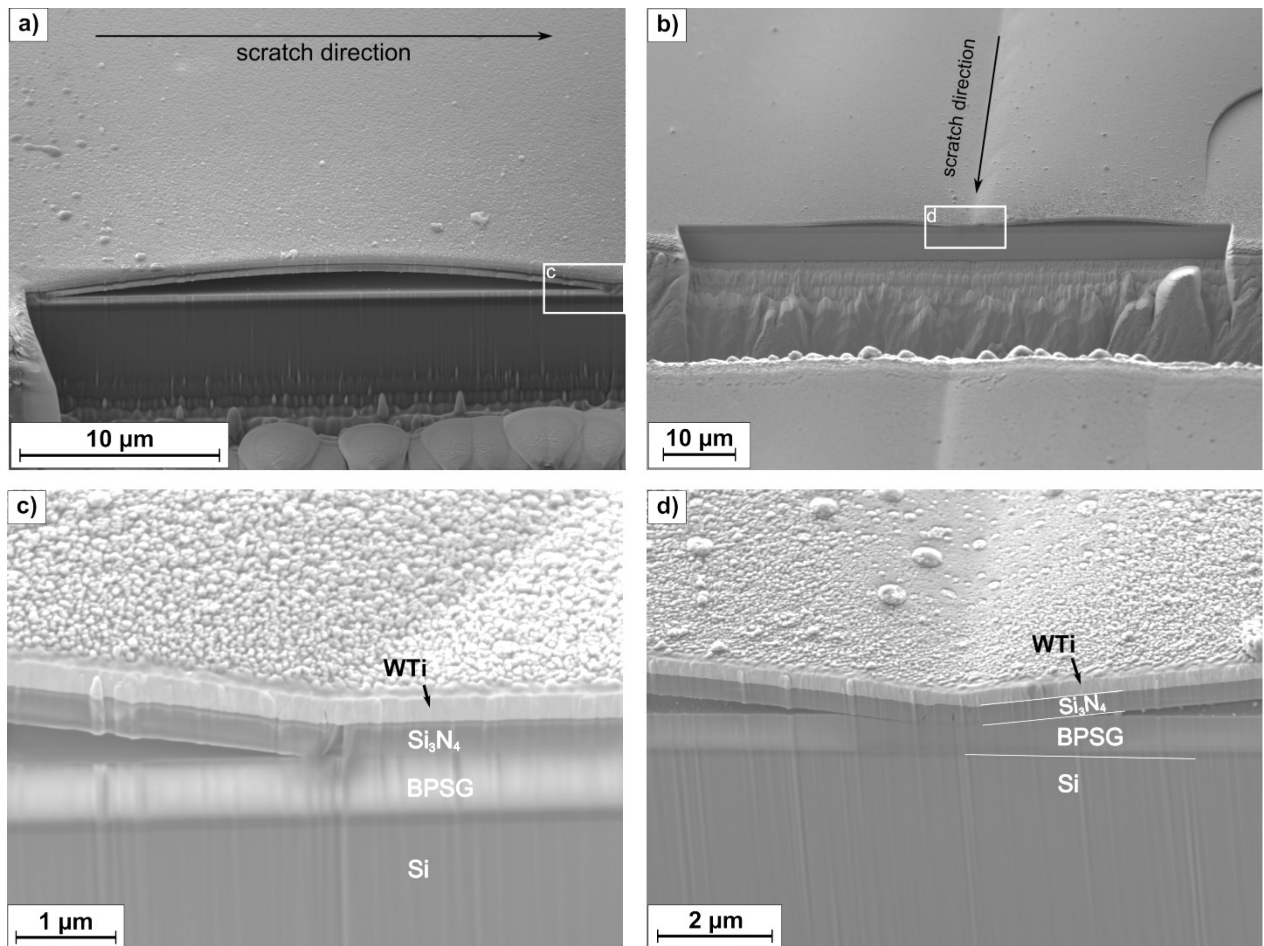

Figure 14: Cross-sections of (a) a spontaneous buckle originating from a scratch trace and (b) a parallel buckle along the scratch trace. (c) and (d) are the image sections indicated by the white rectangles which show the base of the spontaneous buckle and the center of the parallel buckle, respectively. The crack kinking through the Si_3N_4 can be seen in (c) and the densification of the BPSG can be observed in (d) and is indicated by the white lines.

A surface profile of the scratch buckles was measured using CLSM and is shown in Figure 8a. When using the spontaneous buckles for adhesion calculation on this system, it is also necessary to measure the buckles far enough away from the parallel buckles where they originated. The spontaneous buckles have a wider diameter at the point of origin from the

parallel buckles and are far enough away from the trace after a distance of about 10-20 µm, as shown in Figure 8a. The spontaneous buckles were again modelled as straight buckles according to Hutchinson and Suo and an example profile is shown in Figure 8b [19]. The adhesion energy of the Si_3N_4/BPSG-interface was calculated to be 1.54 ± 0.3 J/m² which agrees well with the value calculated from indentation buckles of 1.35 ± 0.3 J/m² [12].

The parallel buckles were again modelled as pinned buckles as the profile in Figure 8c would suggest. An adhesion energy of 1.54 ± 0.2 J/m² was calculated from them which is in good agreement with the values of the spontaneous and indentation buckles. The parallel buckles on this system fulfill the condition of the buckles being much larger than the imprint of the tip. The scratch buckles exhibit less fracture on the buckle surface compared to the indentation buckles which had radial cracking suggesting that less energy is dissipated by fracture on the scratch buckles and the calculated adhesion energy are more accurate.

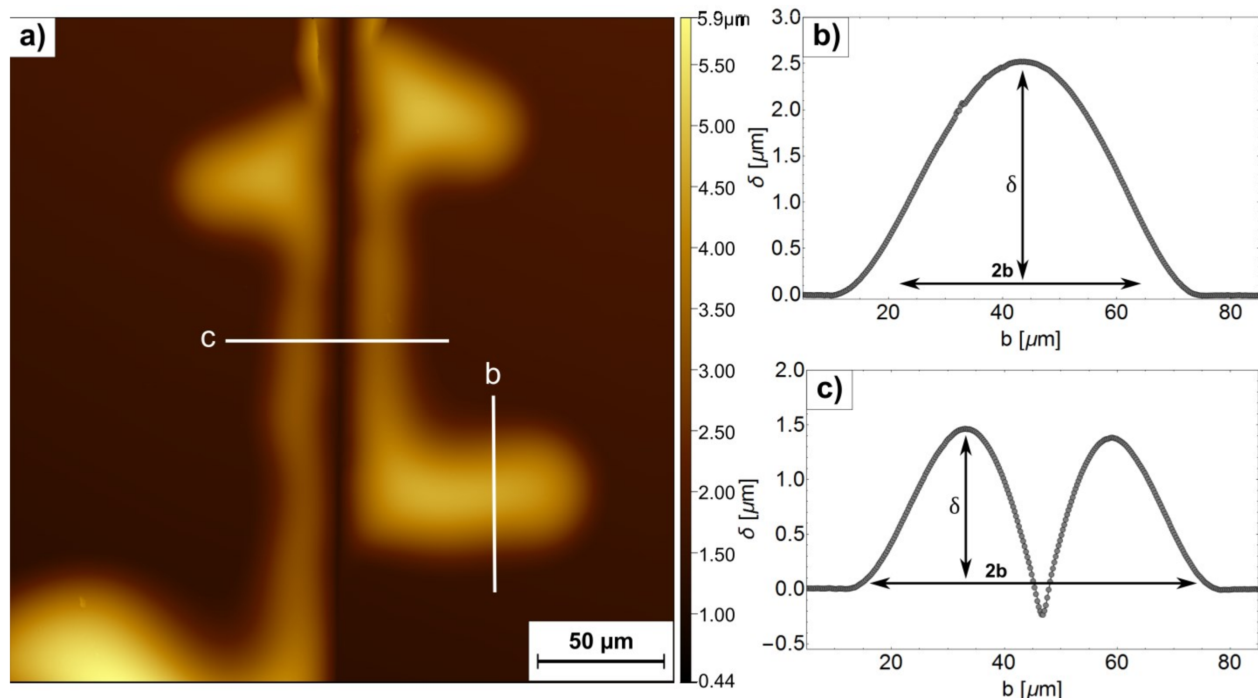

Figure 15: (a) AFM height image of scratch made with 400 mN load with parallel and spontaneous buckles. The white lines indicate the where the profiles for (a) spontaneous and (b) parallel buckles have been taken.

4. Discussion

The development of the parallel buckles in the investigated film systems is most likely a combination of many mechanisms. An important factor seems to be the deformation in the trace where the BPSG has been densified [27]. This densification, observed in the FIB cross-sections in Figure 3 and 7, affected the BPSG more than the other films in the stack. The

hardness of the BPSG is about three times lower than that of WTi and four times lower than Si_3N_4. The WTi and Si_3N_4 films were forced to bend or deflect into the groove left by the passing tip, shear stress between densified BPSG and the above films are created, leading to an additional stress concentration along the trace, causing the BPSG interfaces to be more susceptible to failure. On the WTi/BPSG system the parallel buckles started to occur at maximum scratch loads of 300 mN which suggested that a critical amount of densification was achieved at this load. At this critical amount of densification the shear forces where large enough to separate the two films and induce an interface crack. However, it is not possible to determine ex-situ exactly where this critical densification occurred because the buckles can propagate in both directions along the trace and the LD or DD-curves gave no indication of buckling. Additionally, a fracture event during the scratching or an interface defect lead to the formation of a buckle and propagation along the trace. Buckle development on the WTi/BPSG system is enhanced by the additional compressive stress that is generated at the front of the moving scratch tip. This compressive stress was described by Bull et al. [13,15] as the origin of the classical buckling failure mode during the scratch test, which can be a point of origin of the formation of a spontaneous buckle propagating away from the trace. This buckle is usually crushed by the passing tip and only residual marks on the side of the trace remain visible after the test. The buckling failure mode is also often accompanied by spallation which can cause the produced buckles to be spalled off the substrate again. On the WTi/Si_3N_4/BPSG system buckles seem to be dependent on the fracture of the Si_3N_4 film which triggers the delamination. But the deformation in the trace also has to be of importance since the buckles propagate along the trace in all observed tests. However, in both cases the high residual compressive stress in the WTi film (about 1.5 GPa) is the most critical factor. The models of Marshall and Evans [29,30] and Hutchinson and Suo [19] note that the induced stress is combined with the residual stress in the film and has to exceed the critical buckling stress necessary for delamination described by eqn. 1.

The tip orientation is also an important factor for scratch testing since the tip radius and shape determines the induced stress field [13]. Using a Berkovich tip, two orientations of the tip are frequently chosen, the sharp and the broad side. The results of the sharp side on the WTi/BPSG system were shown in Figure 1. Figure 9 shows a scratch made with a 500 mN load and using the broad side of the Berkovich tip as the scratch front. With this tip orientation it was possible to induce a larger amount of buckles, especially for better adhering films [31]. But it also resulted in more spallation of the film which can in turn lower the amount of buckles.

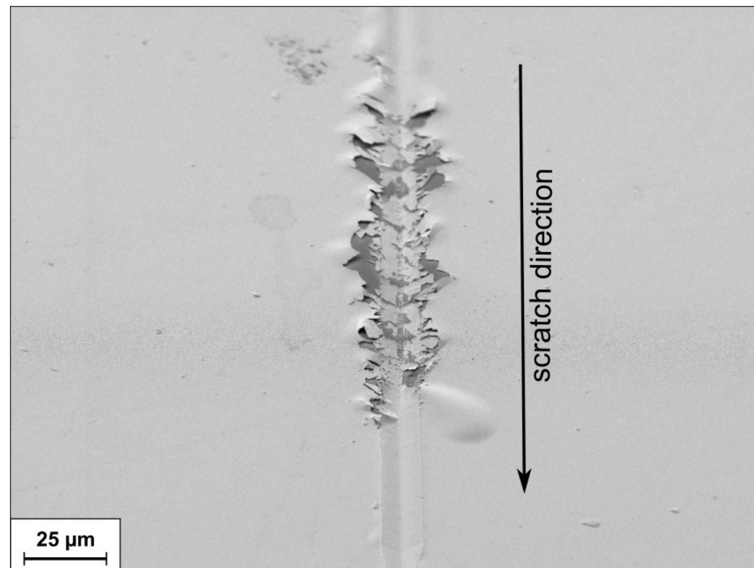

Figure 16: Scratch made with 500 mN and the broad side of the tip. This tip orientation results in more delaminations but also more spallation of the film.

Finally, the significant amount of wear the tip experiences during the scratch tests is another important factor to consider. Bull et al. [13] has demonstrated that the tip radius has large influence on the failure modes of the scratch test and Steinmann et al. [16] showed that a significant amount of wear of the scratch tip that changes the geometry will impact the critical load of coating detachment. Therefore, the form of the scratch groove will change when the tip becomes blunted with time causing a more shallow trace left in the samples, as shown in Figure 10, which would result in less shear stress at the interface. This is supported by the fact that the scratches exhibited a decreasing number of buckles after continuous use of a tip up to a point where the scratch tip was no longer able to produce parallel buckles on the same sample and under the same conditions. Further examination on tip wear and scratch testing is currently underway.

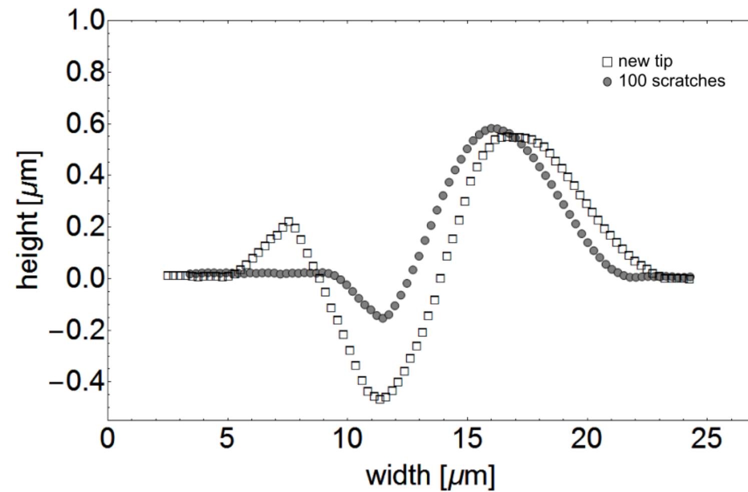

Figure 17: Comparison of profiles across a scratch trace and a parallel buckle on a WTi/BPSG sample. Profile 1 shows a trace made with a new Berkovich tip and profile 2 shows a trace made with the same tip and the same load after about 100 scratches (various loads between 100 and 500 mN) have been performed. Both profiles have been taken at the same scratch distance of 300 µm along the trace.

5. Conclusions

It has been demonstrated that the scratch test is a viable method for quantitative adhesion testing of compressively stressed thin films on rigid substrates. A high load nanoindenter is necessary in order to produce buckles and a minimum load of about 300 mN is needed to produce delaminations for the investigated systems. Two types of delaminations occurred from the scratch test: parallel buckles along the trace and spontaneous buckles originating from the parallel buckles. Delaminations parallel to the trace were produced as direct result of the scratching through a combination of the deformation and fracture of the films induced by the scratch and residual stresses. The initial parallel delaminations were the point of origin for spontaneous buckles which developed and propagated according to the stress distribution in the WTi film. Adhesion was calculated by modeling the spontaneous buckles as straight sided buckles and the parallel buckles as pinned blisters. The direct comparison of the two types of buckling revealed that the deformation in the scratch trace affects the dimensions of the parallel buckles and resulted in a lower adhesion energy compared to the spontaneous buckles for the WTi/BPSG interface. The adhesion energies calculated from the spontaneous buckles and the parallel buckles are in good agreement on the WTi/Si_3N_4/BPSG system. It should be noted that one scratch is able to induce a large amount of buckles on both systems which provide better statistics for adhesion calculations compared to other methods. The technique works well for thin films with a thickness range of a few hundred nanometers where nanoindentation has problems with substrate fracture. It was also shown that the scratch test

can be combined with stressed overlayers in order to produce buckles on brittle ceramic films (WTi/Si_3N_4/BPSG system).

Acknowledgements

The authors want to thank A. Leitner of the Erich Schmid Institute for experimental assistance and T. Pelisset of Infineon Technologies Austria AG for sample production. This work was jointly funded by the Austrian Research Promotion Agency (FFG: Project No. 846579) and the Carinthian Economic Promotion Fund (KWF, contract KWF-1521/26876/38867) further financial support by the Austrian Federal Government (837900) within the framework of the COMET Funding Program is appreciated.

References

[1] K.L. Mittal, The role of the interface in adhesion phenomena, Polym. Eng. Sci. 17 (1977) 467–473. doi:10.1002/pen.760170709.

[2] A.A. Volinsky, N.R. Moody, W.W. Gerberich, Interfacial Toughness Measurements for Thin Films on Substrates, Acta Mater. 50 (2002) 441–466. doi:10.1016/S1359-6454(01)00354-8.

[3] J. Chen, S.J. Bull, Approaches to investigate delamination and interfacial toughness in coated systems: an overview, J. Phys. D. Appl. Phys. 44 (2011) 1–19. doi:10.1088/0022-3727/44/3/034001.

[4] B. Völker, W. Heinz, K. Matoy, R. Roth, J.M. Batke, T. Schöberl, et al., Mechanical and chemical investigation of the interface between tungsten-based metallizations and annealed borophosphosilicate glass, Thin Solid Films. 583 (2015) 170–176. doi:10.1016/j.tsf.2015.03.047.

[5] B. Völker, W. Heinz, K. Matoy, R. Roth, J.M. Batke, T. Schöberl, et al., Interface fracture and chemistry of a tungsten-based metallization on borophosphosilicate glass, Philos. Mag. 6435 (2014) 1–15. doi:10.1080/14786435.2014.913108.

[6] Q. Ma, A four-point bending technique for studying subcritical crack growth in thin films and at interfaces, J. Mater. Res. 12 (1997) 840–845. doi:10.1557/JMR.1997.0122.

[7] K. Matoy, T. Detzel, M. Müller, C. Motz, G. Dehm, Interface fracture properties of

thin films studied by using the micro-cantilever deflection technique, Surf. Coatings Technol. 204 (2009) 878–881. doi:10.1016/j.surfcoat.2009.09.013.

[8] M.J. Cordill, D.F. Bahr, N.R. Moody, W.W. Gerberich, Adhesion measurements using telephone cord buckles, Mater. Sci. Eng. A. 443 (2007) 150–155. doi:10.1016/j.msea.2006.08.027.

[9] G. Parry, A. Cimetière, C. Coupeau, J. Colin, J. Grilhé, Stability diagram of unilateral buckling patterns of strip-delaminated films, Phys. Rev. E - Stat. Nonlinear, Soft Matter Phys. 74 (2006) 1–7. doi:10.1103/PhysRevE.74.066601.

[10] G. Parry, J. Faou, S. Grachev, E. Barthel, Towards interface toughness measurement in nanometric films, 13th Int. Conf. Fract. (2013) 1–4.

[11] M.J. Cordill, D.F. Bahr, N.R. Moody, W.W. Gerberich, Recent Developments in Thin Film Adhesion Measurement, IEEE Trans. Device Mater. Reliab. 4 (2004) 163–168. doi:10.1016/j.msea.2006.08.027.

[12] A. Kleinbichler, M.J. Pfeifenberger, J. Zechner, N.R. Moody, D.F. Bahr, M.J. Cordill, New Insights into Nanoindentation-Based Adhesion Testing, JOM. 69 (2017) 2237–2245. doi:10.1007/s11837-017-2496-2.

[13] S.J. Bull, E. G.-Berasetegui E., Chapter 7 An overview of the potential of quantitative coating adhesion measurement by scratch testing, in: Tribol. Interface Eng. Ser., 2006: pp. 99–114. doi:10.1016/S0167-8922(06)80043-X.

[14] S.J. Bull, Failure mode maps in the thin film scratch adhesion test, Tribol. Int. 30 (1997) 491–498. doi:10.1016/S0301-679X(97)00012-1.

[15] S.J. Bull, Failure modes in scratch adhesion testing, Surf. Coatings Technol. 50 (1991) 25–32. doi:10.1016/0257-8972(91)90188-3.

[16] P.A. Steinmann, Y. Tardy, H.E. Hintermann, Adhesion testing by the scratch test method: The influence of intrinsic and extrinsic parameters on the critical load, Thin Solid Films. 154 (1987) 333–349. doi:10.1016/0040-6090(87)90377-4.

[17] S. Venkataraman, D.L. Kohlstedt, W.W. Gerberich, Microscratch analysis of the work of adhesion for Pt thin films on NiO, J. Mater. Res. 7 (1992) 1126–1132. doi:10.1557/JMR.1992.1126.

[18] N.R. Moody, R.Q. Hwang, S. Venka-taraman, J.E. Angelo, D.P. Norwood, W.W. Gerberich, Adhesion and fracture of tantalum nitride films, Acta Mater. 46 (1998) 585–597. doi:10.1016/S1359-6454(97)00243-7.

[19] J.W. Hutchinson, Z. Suo, Mixed Mode Cracking in Layered Materials, Adv. Appl. Mech. 29 (1991) 63–191. doi:10.1016/S0065-2156(08)70164-9.

[20] M.D. Kriese, W.W. Gerberich, N.R. Moody, Quantitative adhesion measures of multilayer films: Part I. Indentation mechanics, J. Mater. Res. 14 (1999) 3007–3018. doi:10.1557/JMR.1999.0404.

[21] M.J. Pfeifenberger, M. Mangang, S. Wurster, J. Reiser, A. Hohenwarter, W. Pfleging, et al., The use of femtosecond laser ablation as a novel tool for rapid micro-mechanical sample preparation, Mater. Des. 121 (2017) 109–118. doi:10.1016/j.matdes.2017.02.012.

[22] D. Nečas, P. Klapetek, Gwyddion: an open-source software for SPM data analysis, Open Phys. 10 (2012) 181–188. doi:10.2478/s11534-011-0096-2.

[23] J.J. Vlassak, W.D. Nix, A New Bulge Test Technique for the Determination of Young Modulus and Poisson Ratio of Thin-Films, J. Mater. Res. 7 (1992) 3242–3249. doi:Doi 10.1557/Jmr.1992.3242.

[24] A. Kleinbichler, J. Zechner, M.J. Cordill, Buckle induced delamination techniques to measure the adhesion of metal dielectric interfaces, Microelectron. Eng. 167 (2017) 63–68. doi:10.1016/j.mee.2016.10.020.

[25] L.E.G. Hutchinson, J. W., Thouless M. D., Growth and configurational stability of circular, buckling-driven film delaminations, Acta Metall. Mater. 40 (1992) 295–308. doi:10.1016/S0020-7462(99)00038-4.

[26] J.-Y. Faou, G. Parry, S. Grachev, E. Barthel, How Does Adhesion Induce the Formation of Telephone Cord Buckles?, Phys. Rev. Lett. 108 (2012) 116102. doi:10.1103/PhysRevLett.108.116102.

[27] F.M. Ernsberger, Role of Densification in Deformation of Glasses Under Point Loading, J. Am. Ceram. Soc. 51 (1968) 545–547. doi:10.1111/j.1151-2916.1968.tb13318.x.

[28] D.F. Bahr, J.W. Hoehn, N.R. Moody, W.W. Gerberich, Adhesion and acoustic emission analysis of failures in nitride films with a metal interlayer, Acta Mater. 45 (1997) 5163–5175. doi:10.1016/S1359-6454(97)00180-8.

[29] A.G. Evans, D.B. Marshall, on the Mechanics of Delamination and, Int. J. Solids Struct. 20 (1984) 455–466.

[30] D.B. Marshall, A.G. Evans, Measurement of adherence of residually stressed thin films by indentation. I. Mechanics of interface delamination, J. Appl. Phys. 56 (1984) 2632–2638. doi:10.1063/1.333794.

[31] A. Kleinbichler, J. Todt, J. Zechner, S. Wöhlert, D.M. Többens, M.J. Cordill, Annealing effects on the film stress and adhesion of tungsten-titanium barrier layers, Surf. Coatings Technol. 332 (2017) 376–381. doi:10.1016/j.surfcoat.2017.07.087.